A comparison of similar aerosol measurements made on the NASA P3-B, DC-8, and NSF C-130 aircraft during TRACE-P and ACE-Asia

K. G. Moore II,[1] A. D. Clarke,[1] V. N. Kapustin,[1] C. McNaughton,[1] B. E. Anderson,[2] E. L. Winstead,[3] R. Weber,[4] Y. Ma,[4] Y. N. Lee,[5] R. Talbot,[6] J. Dibb,[6] T. Anderson,[7] S. Doherty,[7] D. Covert,[7] and D. Rogers[8]

Received 27 February 2003; revised 16 December 2003; accepted 24 December 2003; published 8 July 2004.

[1] Two major aircraft experiments occurred off the Pacific coast of Asia during spring 2001: the NASA sponsored Transport and Chemical Evolution over the Pacific (TRACE-P) and the National Science Foundation (NSF) sponsored Aerosol Characterization Experiment-Asia (ACE-Asia). Both experiments studied emissions from the Asian continent (biomass burning, urban/industrial pollution, and dust). TRACE-P focused on trace gases and aerosol during March/April and was based primarily in Hong Kong and Yokota Air Force Base, Japan, and involved two aircraft: the NASA DC-8 and the NASA P3-B. ACE-Asia focused on aerosol and radiation during April/May and was based in Iwakuni Marine Corps Air Station, Japan, and involved the NSF C-130. This paper compares aerosol measurements from these aircraft including aerosol concentrations, size distributions (and integral properties), chemistry, and optical properties. Best overall agreement (generally within RMS instrumental uncertainty) was for physical properties of the submircron aerosol, including condensation nuclei concentrations, scattering coefficients, and differential mobility analyzer and optical particle counter (OPC) accumulation mode size distributions. Larger differences (typically outside of the RMS uncertainty) were often observed for parameters related to the supermicron aerosols (total scattering and absorption coefficients, coarse mode Forward Scattering Spectrometer Probe and OPC size distributions/integral properties, and soluble chemical species usually associated with the largest particles, e.g., Na^+, Cl^-, Ca^{2+}, and Mg^{2+}), where aircraft sampling is more demanding. Some of the observed differences reflect different inlets (e.g., low-turbulence inlet enhancement of coarse mode aerosol), differences in sampling lines, and instrument configuration and design. Means and variances of comparable measurements for horizontal legs were calculated, and regression analyses were performed for each platform and allow for an assessment of instrument performance. These results provide a basis for integrating aerosol data from these aircraft platforms for both the TRACE-P and ACE-Asia experiments. *INDEX TERMS:* 0305 Atmospheric Composition and Structure: Aerosols and particles (0345, 4801); 0343 Atmospheric Composition and Structure: Planetary atmospheres (5405, 5407, 5409, 5704, 5705, 5707); 0345 Atmospheric Composition and Structure: Pollution—urban and regional (0305); 0365 Atmospheric Composition and Structure: Troposphere—composition and chemistry; 0394 Atmospheric Composition and Structure: Instruments and techniques; *KEYWORDS:* aerosols, special field campaigns, instrument comparison

Citation: Moore, K. G., II, et al. (2004), A comparison of similar aerosol measurements made on the NASA P3-B, DC-8, and NSF C-130 aircraft during TRACE-P and ACE-Asia, *J. Geophys. Res.*, *109*, D15S15, doi:10.1029/2003JD003543.

[1]School of Ocean and Earth Science and Technology, University of Hawaii at Manoa, Honolulu, Hawaii, USA.
[2]Chemistry and Dynamics Branch, Atmospheric Sciences Division, NASA Langley Research Center, Hampton, Virginia, USA.
[3]GATS, Inc., Hampton, Virginia, USA.
[4]School of Earth and Atmospheric Sciences, Georgia Institute of Technology, Atlanta, Georgia, USA.
[5]Brookhaven National Laboratory, Upton, New York, USA.
[6]Institute for the Study of Earth, Oceans, and Space, University of New Hampshire, Durham, New Hampshire, USA.
[7]Department of Atmospheric Sciences, University of Washington, Seattle, Washington, USA.
[8]National Center for Atmospheric Research, Broomfield, Colorado, USA.

0148-0227/04/2003JD003543$09.00

1. Introduction

[2] The NASA sponsored Global Tropospheric Experiment (GTE) and National Science Foundation (NSF) sponsored Aerosol Characterization Experiment (ACE) are ongoing research programs for studying tropospheric chemistry (GTE) [*McNeal et al.*, 1998] and aerosol properties (ACE) [*Bates et al.*, 1998; *Huebert et al.*, 2003] in the global atmosphere. Field missions from both research programs during the past two decades have sampled remote areas of the atmosphere, including over the Arctic, the Brazilian rain forest, the tropical Atlantic, the tropical Pacific, the southwestern Pacific near Australia, and the western Pacific. A major goal of these campaigns was to understand and characterize the concentration and variability in gas and aerosol species that influence properties of the global atmosphere and to assess the role of anthropogenic sources.

[3] The East Asia region is undergoing rapid population growth and economic/industrial development with fossil fuel combustion and energy use increasing at a brisk rate. Energy use has increased $\sim$5% yr^{-1} during the last decade; this increase is predicted to continue during the next 20 years (U.S. Department of Energy International Energy Outlook, Energy Information Administration, available at http://www.eia.doe.gov/oiaf/ieo/index.html). Along with this increase in economic activity and population, emissions from urban/industrial sources and biomass burning are expected to rise. These emissions include O_3, methane, CO and CO_2, NO_x, and aerosols (e.g., sulfates, nitrates, ammonium, black carbon, and organic carbon). Additionally, Asia is a significant source of dust aerosols to the Pacific atmosphere.

[4] The aerosol component of the Asian outflow can impact the atmosphere in several ways. It can be important in geochemical cycles (dust input/iron fertilization of oceans [*Duce and Tindale*, 1991] and the sulfur, nitrogen, and carbon budgets [*Galloway et al.*, 1984]). These aerosols can affect tropospheric chemistry by acting as sources/sinks for various chemically important gases through gas-to-particle conversion and cloud processes and providing reaction sites for both homogeneous and heterogeneous chemistry, especially the dust component [*Dentener et al.*, 1996]. Aerosols can also affect the hydrological cycle/precipitation [*Twomey et al.*, 1984; *Rosenfeld*, 1999; *Ackerman et al.*, 2000]. Additionally, aerosols have an impact on global/regional climate through their so-called "direct" and "indirect" radiative effects.

[5] The aerosol direct effect is due to the scattering and absorption of solar and terrestrial radiation by the particles themselves [*Penner et al.*, 1992; *Charlson et al.*, 1991]. The direct effect of sulfates in the atmosphere has been well characterized [*Charlson et al.*, 1991]; however, the direct effect of absorbing aerosols such as black carbon, organic and other carbonaceous aerosols, and dust is less well known. Overall, estimates of the direct effect of aerosols on the radiative balance of the Earth's atmosphere result in a negative "cooling" effect with a forcing term of approximately -1 W m^{-2} [*Kaufmann et al.*, 1997]. However, there are uncertainties in this forcing, due mostly to the role of absorbing aerosols. Even larger uncertainties are associated with the aerosol indirect effect that arises from the "activation" of aerosols in clouds to form cloud condensation nuclei and their resulting influence on cloud albedo, cloud lifetime and microphysics [*Andreae*, 1995; *Charlson and Heintzenberg*, 1995].

[6] The Transport and Chemical Evolution over the Pacific (TRACE-P) experiment focused on trace gases and aerosols in the Asian outflow during March/April and was based primarily in Hong Kong and Yokota Air Force Base, Japan. Two aircraft were involved: the NASA DC-8 and P3-B. The Aerosol Characterization Experiment-Asia (ACE-Asia) focused on aerosols and their radiative effects during April/May and was based in Iwakuni Marine Corps Air Station, Japan (southern portion of the main island of Honshu), and involved the NSF/National Center for Atmospheric Research (NCAR) C-130. The spring season was chosen to correspond to meteorological conditions that result in the maximum Asian outflow over the Pacific [*Merrill*, 1989].

[7] The unusual opportunity to combine the extensive data sets from these two major campaigns was long recognized as valuable in addressing some of the issues outlined above over greater spatial and temporal scales. Hence intercomparison flights were planned to ensure data sets were consistent and comparable. Five comparison flights (three between P3-B and DC-8, two between P3-B and C-130) were coordinated through interagency cooperation where time was devoted to flying "wingtip-to-wingtip" (within 500 m, typically less). The intercomparisons included 12 horizontal legs and 13 vertical profiles, allowing for comparison of data sampled in a variety of altitudes and conditions. The results of these intercomparisons provide a basis for integrating aerosol and gas phase data from the aircraft platforms for both the TRACE-P and ACE-Asia experiments. These links improve the spatial, temporal, and statistical characterization of the Asian aerosol and help to identify and constrain uncertainties when comparing different data sets.

2. Instrumentation to Be Compared

[8] The payloads of the three platforms discussed in this paper (P3-B, DC-8, and C-130) each had a suite of instruments for measuring a variety of gas phase species, aerosols, and their precursors [*Huebert et al.*, 2003; *Jacob et al.*, 2003]. Separate papers will focus on the TRACE-P gas phase comparison [*Eisele et al.*, 2003] and the ACE-Asia multiplatform surface measurements (S. J. Doherty et al., A comparison and summary of aerosol optical properties as observed from aircraft, ship and land during ACE-Asia, submitted to *Journal of Geophysical Research*, 2004). Here we focus on comparable instrumentation for measuring aerosol concentrations, size distributions and integral properties, optical properties, and aerosol chemical constituents. Each set of instruments has a different sampling frequency, but the data compared here have been merged into the same 1-min data set.

[9] With the exception of the complete high-resolution aerosol size distributions and associated aerosol thermal volatility discussed below, data are available through the NASA TRACE-P ftp site (ftp://ftp-gte.larc.nasa.gov/pub/TRACEP/merges) and the NSF/NCAR ACE-Asia Web site (http://www.joss.ucar.edu/ace-asia/dm/data_access_frame.html). Full aerosol size distributions and volatility

measurements are available upon request from the principle investigators of the relevant research groups.

2.1. Aerosol Concentrations

[10] Concentrations of condensation nuclei (CN) were measured with several CN counters: two TSI (Thermo-Systems, Inc., St. Paul, Minnesota) 3010s on the P3-B and two TSI 3760s on board the DC-8 and C-130. The CN counters' nominal 50% cut sizes depend on the temperature difference (ΔT) between the saturator and condenser and the absolute temperature of the condenser. The condenser temperature was not controlled and varied, depending on ambient and aircraft conditions. The cut sizes of the CN counters were reported as $\sim$0.015 μm for all three aircraft. The actual cut size can vary when environmental conditions (e.g., elevated instrument temperatures and/or changes in sample pressure) perturb normal condition required for saturation [*Hermann and Wiedensohler*, 2001]. The ΔT was set to 17°C on board the P3-B and C-130 but was set to 22°C on the DC-8, causing some variation in the actual cut size of the CN counters. Therefore we expect CN concentrations on the DC-8 (higher ΔT) to have been greater than on the other aircraft when there were significant quantities of small particles with diameters at or near the instrument cut size. On each platform, one CN counter was operated at aircraft cabin temperature ($\sim$30 ± 4°C), while the other sampled after heating the air stream to 350 ± 10°C, driving off any volatile components and leaving a residual, refractory aerosol (RCN) that is frequently combustion derived [*Moore et al.*, 2003; *Clarke*, 1991; *Clarke et al.*, 2001].

[11] Additionally, all three platforms had a TSI 3025 for counting ultrafine CN (UCN) with diameters greater than 0.003 μm. The P3-B UCN counter was modified to measure size distributions from 3 to 10 nm by replacing the laser light source with white light and adding a pulse height analyzer. This modification increased the detection volume, leading to coincidence counting (underestimating concentrations) when UCN were above several thousand numbers per cubic centimeter. This problem does not occur for normal operation of the standard UCN counter until $\sim$100,000 numbers cm^{-3}, and therefore we expect that often the P3-B UCN concentrations could have been less than those measured on the other platforms due to coincidence counting. This instrument was deployed to provide a measurement of the presence, or lack of, aerosols with diameters between 3 and 4 nm for studies of homogeneous nucleation in Asian plumes [*Weber et al.*, 2003]. Under cleaner conditions during the ACE-1 experiment, this modified UCN counter was in good agreement with other CN and UCN counters [*Weber et al.*, 1999].

[12] The DC-8 UCN and CN counters were operated downstream of a critical orifice in order to maintain a constant pressure of $\sim$213 mbar, whereas those on the C-130 and P3-B operated at near ambient sample pressure that varied with altitude. All CN measurements are reported after scaling to standard temperature and pressure (STP, T = 298.15 K and P = 1013 mbar).

2.2. Aerosol Optical Properties

[13] The aerosol light scattering coefficients (σ_{sp}) and hemispheric backscattering coefficients at three wavelengths (450, 550, and 700 nm) were measured with a TSI 3563 integrating nephelometer on all aircraft and corrected for size-dependent truncation errors as per *Anderson et al.* [1996]. The nephelometer relative humidity (RH) was typically below 45%, and therefore the reported scattering coefficients are considered "dry." Particle absorption coefficients (σ_{ap}) were measured on each platform with a Radiance Research particle/soot absorption photometer (PSAP) at a wavelength of 550 nm on board the C-130 and 565 nm on the other aircraft. PSAP data were corrected according to *Bond et al.* [1999], and the reported absorption coefficients are also considered dry. The dominant aerosol absorber in the visible wavelengths is black carbon (BC) [*Heintzenberg*, 1982] and the submicrometer aerosol absorption component, where the majority of coarse mode dust has been excluded, is usually directly related to BC concentrations [*Clarke et al.*, 2004].

[14] On the DC-8 a single nephelometer operated continuously, while on the P3-B a 30 L min^{-1} impactor (aerodynamic size cut of 1.0 μm, fabricated by National Oceanic and Atmospheric Administration Pacific Marine Environmental Laboratory, Seattle, Washington) was periodically switched in line to assess scattering and absorption by submicrometer aerosols. The C-130 had two nephelometers and two PSAPs, one set of which always had a 1.0-μm impactor in line, resulting in continuous measurements of both total and submicrometer scattering and absorption. Aerosol optical properties are reported at ambient pressure and temperature, not at STP. The measured dry scattering coefficients will often be greater at ambient RH due to hygroscopic growth [*Tang and Munkelwitz*, 1993; *Hagen et al.*, 1989]. The effect of hygroscopic growth on measured absorption coefficients is currently being debated. Some authors [*Chylek et al.*, 1996] have suggested an enhancement of absorption due to liquid water "focusing" light on the underlying soot, but recent modeling studies [*Fuller et al.*, 1999] have not predicted said enhancement.

2.3. Aerosol Size Distributions

[15] Aerosol size distributions were measured with a variety of instruments on each platform. The smallest aerosols ($0.007 < D_p < 0.25$ μm) were measured with a custom-made radial differential mobility analyzer [*Zhang et al.*, 1995] on the P3-B and C-130. The DC-8 used a TSI 3936 Scanning Mobility Particle Sizer (SMPS) for measuring size distributions for particles with $0.01 < D_p < 0.25$ μm. Larger particles ($0.1 < D_p < 20.0$ μm) were sampled on board the P3-B and C-130 with a custom-made laser optical particle counter (OPC) [*Clarke*, 1991]. Both the differential mobility analyzers (DMAs) and OPCs were operated inside the aircraft near ambient pressure, but at cabin temperatures. The size distributions were measured after mixing with desiccated air to achieve dry conditions with sample RH usually less than 35%. This reduced the impact of water uptake by the aerosol on the measured size so that the distribution better reflected the soluble and insoluble aerosol components. During horizontal legs the DMAs and OPCs operated with a thermal preconditioning unit that cycled the aerosol through 150°C and 350°C to drive off the volatile and semivolatile aerosol constituents, allowing inference of aerosol chemistry [*Moore et al.*, 2003; *Clarke*, 1991; *Smith and O'Dowd*, 1996]. Even though volatility measurements

were consistent on the P3-B and C-130, only the unheated size data are included in the comparisons discussed here. The DC-8 measured particle size distributions with a wing mounted Particle Measuring Systems (PMS) Passive Cavity Aerosol Spectrometer Probe (PCASP) for $0.11 <= D_p <= 3.0$ μm. The PCASP cavity was heated to an elevated but unmeasured temperature to result in somewhat dry size distributions. PMS Forward Scattering Spectrometer Probes (FSSP-300, Droplet Measurement Technologies modified) were mounted on the wings of each aircraft and measured "ambient" (RH, *P*, and *T*) size distributions for particles with $0.3 < D_p < 20.0$ μm. All of the optical particle sizing instruments (OPCs, PCASP, and FSSPs) were calibrated using polystyrene latex spheres (PSL, index of refraction of 1.59 at 589 nm) and glass beads (index of refraction of 1.56 at 589 nm). Therefore the particle diameters are effective optical sizes (size of a PSL sphere that scatters the same amount of light as the measured aerosol particle) under the sample conditions experienced.

[16] We have selected two size ranges for calculating aerosol integral properties corresponding to the aerosol accumulation and coarse modes. For the dry sizing instruments (OPCs and PCASP), these size ranges are from 0.1 to 0.75 μm for the accumulation mode and 0.75 to 20.0 μm for the coarse mode. The PCASP only measures up to 3.0 μm, so only PCASP accumulation mode integrals are presented. The 0.75 μm size cut was chosen to match the 1-μm aerodynamic cut size of the impactor. An aerodynamic diameter of 1.0 μm typically corresponds to an effective optical diameter of 0.75 μm, assuming a dry sulfate aerosol of typical density and index of refraction. Also, 0.75 μm effective optical diameter is near the minimum observed between the accumulation and coarse modes in the dry size distributions, although the actual position can vary. The FSSP separation between the accumulation and coarse modes was selected to be 1.0 μm since this was usually the observed position of the minimum between the two modes and the FSSPs are measuring at ambient RH and not dry. It should be noted that OPC and PCASP dry size distributions often swell to larger diameters at ambient RH due to hygroscopic growth [*Tang and Munkelwitz*, 1993]. Size distributions and integral properties are reported as measured at ambient pressure and temperature and not STP corrected, except when compared to aerosol chemistry measurements as noted below.

2.4. Aerosol Chemistry

[17] On board the C-130 and P3-B, soluble aerosol chemical constituents were measured with a new particle into liquid sampler (PILS) [*Lee et al.*, 2003; *Orsini et al.*, 2003; *Weber et al.*, 2001]. The PILS had a 50% size cut of ~1.3 μm and typically provided data between 3 and 5 min. Nominal integration times were 3 min 24 s and reported every 4 min. Aerosol chemical constituents were collected with bulk filters on the DC-8. Soluble aerosol species for sizes up to ~6 μm were measured after aqueous extraction and IC analysis [*Dibb et al.*, 2003]. The average filter collection time varied with altitude and was ~6 min below 1 km, 9 min between 1 and 6 km, 13.5 min between 6 and 9 km, and 16 min above 9 km. Additionally, a new technique was employed on board the DC-8 utilizing a mist chamber and a dual ion chromatography analytical system (MC/IC) that sampled trace acidic gases and measured "fine" aerosol sulfate every ~2–4 min [*Dibb et al.*, 2003]. The 50% size cut for the fine aerosol sulfate has yet to be determined, but preliminary analysis suggests that it is near 2.7 μm. Aerosol chemical constituent concentrations are reported at STP conditions, similar to mixing ratios.

[18] Because the DC-8 filter samples measured chemical constituent concentrations up to ~6 μm, while the PILS instrument had a 50% size cut of ~1.3 μm, discrepancies between aerosol chemical components associated with the largest, coarse mode aerosols are expected (i.e., Na^+, Cl^-, Mg^{2+}, and Ca^{2+}). It is also expected that disagreement between the PILS and filter samples for the aerosol chemical constituents normally associated with the accumulation mode (SO_4^{2-}, NH_4^+, and NO_3^-) will be relatively small. However, recent data from the ACE-Asia experiment have shown that these components can be associated with the larger aerosol sizes, particularly when in the presence of "aged" dust aerosol.

2.5. Inlet Losses

[19] Each aircraft had its own set of sample inlets and associated inlet efficiencies that are most severe for the largest, supermicron particles. All inlets were kept isokinetic during flight by adjusting flows as flight parameters changed. The P3-B aerosol measurements were made through a solid diffuser inlet (SDI), while the ACE-Asia C-130 measurements were made with a new low-turbulence inlet (LTI) that has been shown to pass coarse mode particles more efficiently, although corrections for size-dependent particle enhancements by the LTI still need to be made. Corrections to the size distributions sampled behind the SDI and LTI are reported by B. Huebert et al. (Passing efficiency of a low-turbulence inlet (PELTI), final report to NSF, 2000, available from http://raf.atd.ucar.edu/Projects) and at 3 μm, after accounting for inlet effects, volume concentrations should increase by 25% and 11% for the SDI and LTI, respectively.

[20] The DC-8 had several aerosol sampling inlets. Aerosol chemistry measurements were made through a forward facing tandem probe arrangement [*Dibb et al.*, 2003], while the other aerosol parameters were sampled through either a forward facing SDI similar to the P3-B (nephelometer and PSAP) or a "scoop" inlet (CN counters and SMPS system). The latter does not efficiently pass supermicron particles, but its advantage is in reducing droplet shatter for measurements within clouds. All of the various DC-8 inlets have different and uncharacterized passing efficiencies for the supermicron aerosol that will affect measurements of the coarse mode particles and are one of the largest sources of differences between some measurements.

2.6. Additional Parameters

[21] Most aerosol measurements are extensive parameters (σ_{sp}, σ_{ap}, RCN, CN, and UCN concentrations, aerosol integral properties, and chemical constituent concentrations) that vary with altitude, concentration, and other factors. We also report comparisons of several derived, intensive variables that vary with aerosol properties but not concentration. Significant changes in the latter generally reflect differing air mass characteristics.

[22] The aerosol single scatter albedo (ω_0) is the ratio of aerosol light scattering to aerosol total light extinction (scattering plus absorption) and defined by

$$\omega_0 = \sigma_{sp}/(\sigma_{sp} + \sigma_{ap}).$$

This quantity is of significant interest to those in the aerosol remote sensing and radiative transfer communities [*Russell et al.*, 2002]. Since variations in ω_0 are driven by absorption, we also report values of the aerosol coalbedo, defined as the ratio of aerosol absorption to aerosol extinction, or $1 - \omega_0$. The RCN ratio is the ratio of RCN to total CN and regions with elevated RCN ratios, in the absence of significant concentrations of dust or sea salt, are likely to have been influenced by combustion/continental emissions [*Moore et al.*, 2003; *Clarke et al.*, 1997]. Low values of this parameter indicate the dominant presence of a more volatile aerosol number. Ultrafine particle (UF) concentrations are operationally defined as the difference between the UCN and total CN concentrations (UF = UCN − CN) and are the number of particles with diameters between 0.003 μm and the CN cut size (~0.015 μm). Large UF concentrations often imply recent nucleation. We also calculate a derived average effective diameter to assess how well the OPC, PCASP, and FSSP instrumentation are sizing relative to each other. This quantity is defined by $(6V)/A$, where V is the integral volume and A is the integral surface area.

2.7. Instrument Uncertainties

[23] All of the instruments are prone to uncertainties due to errors in measured flow rates, pressures, temperatures, actual cut sizes, and calibrations, among other factors. (The NASA TRACE-P (both P3-B and DC-8) aerosol instrumentation and principal investigator (PI) provided instrument uncertainties are found online at http://www-gte.larc.nasa.gov/trace/TP_Investigator_Measurements.htm.) Table 1 contains instrument uncertainties as reported by each principle investigator (PI) and appropriate references for the measurements compared in this paper.

[24] Uncertainties in CN and UCN concentrations are due primarily to errors in flow rates and STP corrections and are listed as 5–10% for CN concentrations and 20–50% for the UCN data. We use 10% for the reported CN concentrations. When comparing two instruments with the same uncertainty that is not independent/random, the measured parameters should agree within the combined root-mean-square (RMS) uncertainty given by v ($\delta x_1^2 + \delta x_2^2$), where δx refers to the uncertainty in each instrument, and the subscript 1 and 2 refer to instruments 1 and 2, respectively. Hence, if both $\delta\sigma_1^2$ and $\delta\sigma_2^2$ equal 10% (e.g., the CN counters), then the total uncertainty would be equal to 0.14 (14%). When small particles are present at or near the nominal cut sizes, additional errors are expected. The modified UCN counter on board the P3-B also has additional uncertainty due to the aforementioned coincidence counting at concentrations above a few thousand numbers cm^{-3} and when there are significant numbers of particles with diameters between 3 and 10 nm [*Weber et al.*, 2003]. We use 20% for the estimated uncertainty in UCN concentrations from each instrument, suggesting the measurements should agree to within 28%.

[25] Aerosol scattering coefficients are prone to errors due to truncation correction, instrument noise, instrument drift, and errors in calibration. These can be propagated through a linear combination of the squares of each error term [*Anderson et al.*, 1996]:

$$\delta\sigma^2_{sp\ total} = \delta\sigma^2_{sp\ noise} + \delta\sigma^2_{sp\ drift} + \delta\sigma^2_{sp\ cal} + \delta\sigma^2_{sp\ trunc},$$

resulting in a concentration-dependent uncertainty (Table 1). Similarly, errors in aerosol absorption coefficients are found utilizing the uncertainties described by *Bond et al.* [1999] and

$$\delta\sigma^2_{ap\ noise} + \delta\sigma^2_{ap\ drift} + \delta\sigma^2_{ap\ K1} + \delta\sigma^2_{ap\ K2} + \delta\sigma^2_{ap\ flow}.$$

K1 and K2 are calibration coefficients and the above also results in a concentration-dependent uncertainty. The noise terms depend on averaging period and the reported uncertainties in Table 1 are appropriate for 1-min averaged data. On the basis of typical σ_{sp} and σ_{ap} values for the TRACE-P/ACE-Asia experiments, we use uncertainties of 15% and 25% for the aerosol scattering and absorption coefficients, respectively. These error estimates, when propagated, result in measurement uncertainties of 21% and 35% for the two parameters that will be utilized for both total and submicrometer optical properties. The uncertainty in the sizing instruments is more complicated due to a variety of factors. DMA errors are associated with measured flow rates, size-dependent particle losses in plumbing, and sizing. Sizing errors in this instrument are due to uncertainties in particle mobility that depend on pressure, temperature, and small differences between the actual and assumed voltage applied to the electrostatic classifier. We utilize the PI reported error of 20% (Table 1) for the DMA number concentration. When comparing two DMAs, this results in an uncertainty of 28%. Uncertainties in the number concentrations from the optical sizing instruments (OPCs, PCASP, and FSSPs) are due to flow rates and additional variables. Notably, composition (index of refraction) and RH-dependent errors will change the calibration curve, resulting in size-dependent errors that are not well quantified. The reported uncertainties in OPC accumulation and coarse mode number concentrations are 15% (Table 1), resulting in a combined uncertainty for two OPCs of 21%. PCASP number distributions have a reported uncertainty of 20% so that when comparing the OPC and PCASP integral numbers, a RMS uncertainty of 25% is appropriate. Integrated surface areas and volumes and their associated estimated errors would be larger due to the D_p^2 and D_p^3 terms utilized in converting number to surface area and volume, respectively. Also, at the largest sizes (coarse mode, $D_p >$ 0.75 μm), there are poor counting statistics and size-dependent inlet/plumbing losses that increase these uncertainties. For the FSSP, sizing errors arising from calibration and assumed index of refraction can be even larger since the FSSP measures forward scattered light, not side scatter like the PCASP and OPC. Forward scattering is more sensitive to changes in these parameters relative to the calibration aerosol. Also, the FSSP tends to oversize in the 3 to 10 μm diameter size range [*Reid et al.*, 2003]. For this reason, and that the FSSP measures at ambient conditions, differences are expected between FSSP data and the other sizing instruments. We use 20% for the FSSP coarse mode number concentration (B. Huebert et al., Passing efficiency

Table 1. Reported and Utilized Instrument Uncertainties[a]

Instrument	Measurement	Aircraft	Inlet	Reported Uncertainties, %	PI	References[b]
CN counter	CN concentrations	P3-B	SDI	5	Clarke (UH)	1, 7
		DC-8	"scoop"	10	Anderson (LARC)	
		C-130	LTI	5	Clarke (UH)	
UCN counter	UCN concentrations	P3-B	SDI	20–50[c]	Weber (GT)	1, 2, 7
		DC-8	"scoop"	20	Anderson (LARC)	
		C-130	LTI	20	Weber (GT)	
Nephelometer	total and submicron particle scattering coefficients	P3-B	SDI	10–15[d]	Clarke (UH)	3, 4, 7
		DC-8	DSDI		Anderson (LARC)	
		C-130	LTI		Covert (UW)	
PSAP	particle absorption coefficients	P3-B	SDI	10–25[e]	Clarke (UH)	5, 4, 7
		DC-8	DSDI		Anderson (LARC)	
		C-130	LTI		Covert (UW)	
DMA/SMPS	"dry" number size distributions	P3-B	SDI	20	Clarke (UH)	1, 7
		DC-8	"scoop"		Anderson (LARC)	
		C-130	LTI		Clarke (UH)	
OPC	"dry" number size distributions (accumulation and coarse modes)	P3-B	SDI	15	Clarke (UH)	1, 7
		C-130	LTI		Clarke (UH)	
OPC	"dry" surface area size distributions (accumulation and coarse modes)	P3-B	SDI	15	Clarke (UH)	1, 7
		C-130	LTI		Clarke (UH)	
PCASP	"dry" number size distributions	DC-8	none (wing probe)	20	Anderson (LARC)	1, 7
PCASP	"dry" surface area size distributions	DC-8	none (wing probe)	50	Anderson (LARC)	1, 7
FSSP	ambient number size distributions	P3-B	none (wing probe)	20	Clarke (UH)	1, 7
		DC-8			Anderson (LARC)	
		C-130			Rogers (NCAR)	
FSSP	ambient surface area size distributions	P3-B	none (wing probe)	20	Clarke (UH)	1, 7
		DC-8		50	Anderson (LARC)	
		C-130		20	Rogers (NCAR)	
PILS	aerosol soluble chemical concentrations	P3-B	SDI	20–30	Weber (GT)	1, 7
		C-130	LTI		Weber (GT)	
Bulk chemistry (filter measurements and MC/IC)	aerosol soluble chemical concentrations	DC-8	NHI	13–35[f]	Talbot (UNH)	6, 7

[a]These uncertainties are either given by the Principal Investigators (PIs) or calculated on the basis of references. When comparing two instruments, it is appropriate to use the RMS combined uncertainty and this number is given in the text. The SDI is a solid diffuser inlet flown on the P3-B, while the DSDI is a similar solid diffuser operated on the DC-8. The LTI is the low-turbulence inlet that was utilized to sample on board the C-130. NHI refers to the University of New Hampshire forward facing tandem probe inlet used to sample aerosol chemistry on the DC-8 and the DSDI refers to the DC-8 solid diffuser inlet. The "scoop" inlet was used on the DC-8 to sample CN concentrations and DMA distributions. The various inlets are described in the text. UH is the University of Hawaii, LARC is Langley Research Center, GT is Georgia Institute of Technology, NCAR is the National Center for Atmospheric Research, and UW is the University of Washington.

[b]References: 1, http://www-gte.larc.nasa.gov/trace/TP_Investigator_Measurements.htm; 2, *Weber et al.* [2003]; 3, *T. Anderson et al.* [1999]; 4, *Clarke et al.* [2002]; 5, *Bond et al.* [1999]; 6, *Hoell et al.* [1999]; 7, PI personal correspondence.

[c]For the modified UCN counter-, concentration-, and size-dependent; 50% for concentrations over 10,000 numbers/cm^3 and for particles in the 3–4 nm range and 20% for typical sizes and concentrations.

[d]Concentration-dependent; ~15% for σ_{sp} = 10 Mm^{-1}, ~10% for σ_{sp} = 100 Mm^{-1}; no STP correction and based on 1 min averages.

[e]Concentration-dependent; ~25% for σ_{ap} = 0.5 Mm^{-1}, ~10% for σ_{ap} = 10 Mm^{-1}; no STP correction and based on 1 min averages.

[f]Species-, filter blank-, and integration time (altitude)-dependent; Cl 30%, Na 35%, K 20%, Mg 10%, Ca 15%, NO_3 20%, NH_4 15%, SO_4 13%, NSS SO_4 15%.

of a low-turbulence inlet (PELTI), final report to NSF, available from http://raf.atd.ucar.edu/Projects, 2000), resulting in a combined 28% uncertainty. The PI reported uncertainties for OPC/PCASP and FSSP surface areas are listed in Table 1 and vary from 15% to 50% for the various groups. We believe that 20% is reasonable for the accumulation mode surface areas and 50% is more realistic for the coarse mode data. These result in RMS uncertainties of 28% and 71% when comparing the results from two instruments. Both estimates are utilized, however, in the scatterplots of integral areas presented later to provide an estimate of the range of expected uncertainty. It should be noted that despite having the same 1-min time stamp, DMA and OPC measurements on the aircraft are not "synchronous" due to the temperature cycling associated with these instruments (each DMA scan occurs every ~6 min, each OPC scan occurs every ~3 min). This adds an additional potential source for discrepancy, particularly when sampling in inhomogeneous air masses.

[26] The PI reported error estimates for the aerosol chemical composition instruments are also listed in Table 1. The listed uncertainties for the PILS measured species are given as 20–30%. The 30% value is for concentrations below 0.1 μg m^{-3}. Error estimates for the DC-8 bulk filter measurements are dependent on a variety of factors, including composition, filter blank concentrations, and integration time, and range from 10% to 35% [*Hoell et al.*, 1999]. Because of the difference in cut sizes between the PILS and filter sampler, the primary focus of the chemical composition comparison portion of this paper is for the aerosol constitu-

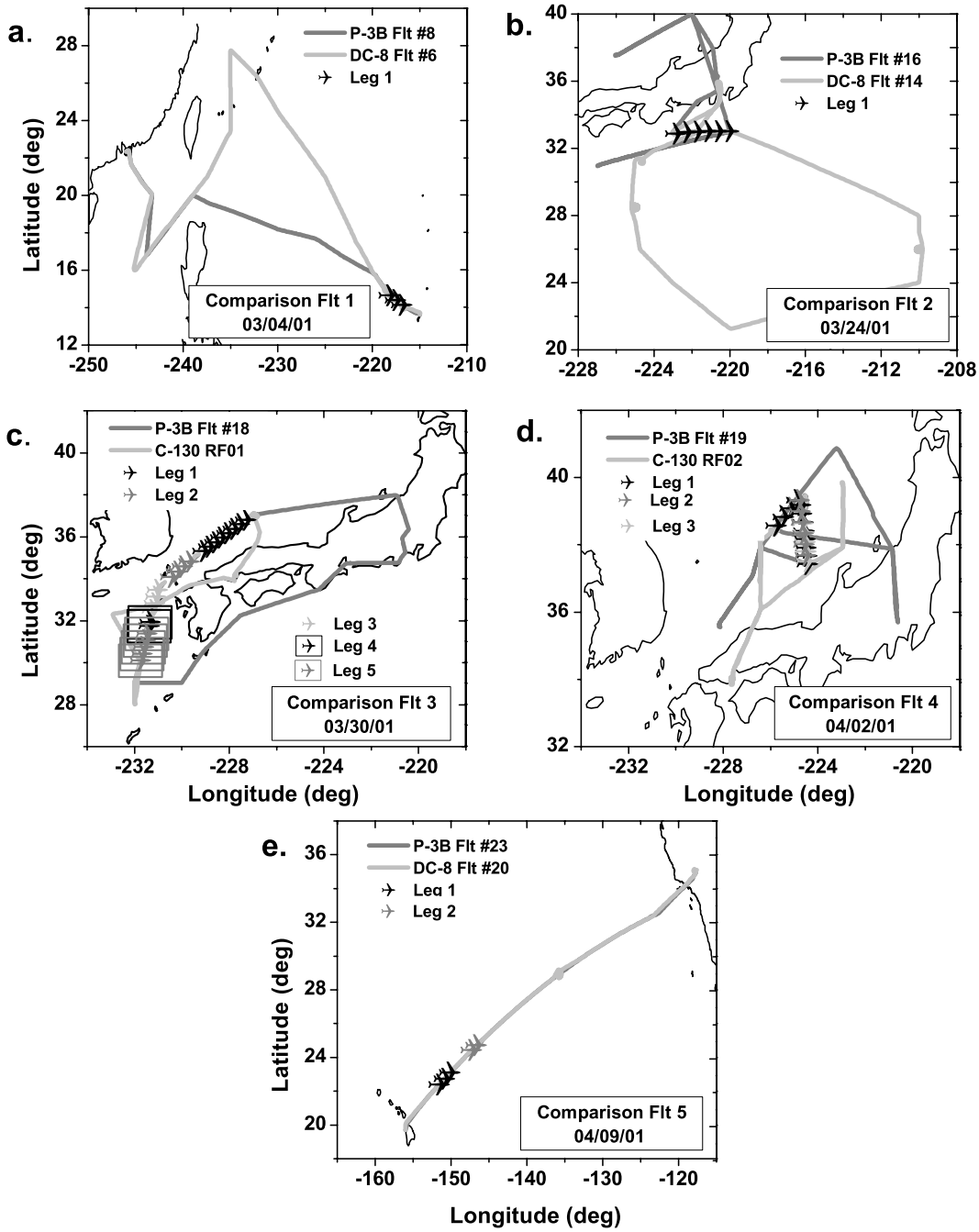

Figure 1. Flight tracks for the various aircraft during the intercomparison flights. Also shown are the comparison legs. (a) Flight tracks for the DC-8 and P3-B for flight 1. (b) Flight tracks for the DC-8 and P3-B for flight 2. (c) Flight tracks for the C-130 and P3-B for flight 3. (d) Flight tracks for the C-130 and P3-B for flight 4. (e) Flight tracks for the DC-8 and P3-B for flight 5.

ents usually associated with the accumulation mode (NH_4^+, SO_4^{2-}, and NO_3^-) and those uncertainties range from 10 to 20%. We utilize a value of 20% uncertainty for these species, resulting in a RMS estimated error of 28%.

3. Intercomparison Flights

[27] Figure 1 shows the flight tracks for the five intercomparison flights and the locations of the horizontal legs during the intercomparison time periods discussed here. Intercomparison flights 1, 2, and 5 (TRACE-P DC-8 and P3-B) are shown in Figures 1a, 1b, and 1e, respectively. Flight 1 occurred in the marine boundary layer (MBL) to the northwest of Guam on the ferry flight to Hong Kong and remote from the Asian continent, presumably in "clean" air. Flight 2 occurred downwind of the main Japanese Island of Honshu in a region of pollution outflow from the Asian continent. The flight 5 intercomparison legs were to the northeast of the Hawaiian Islands on the ferry flight to California in air that was remote from any continents

Table 2. Intercomparison Flights and Horizontal Leg Information

Aircraft Flight	Date	Location	Latitude, Longitude	Leg Times, GMT, hours	Leg Altitudes, km	Average Leg Ambient RH, %	Comments
			Intercomparison Flight 1				
TRACE-P P3-B Flight 08	4 March 2001	NW of Guam	14°N, 142°E	1.167–1.500	0.2	77	"clean" MBL
TRACE-P DC-8 Flight 06							
			Intercomparison Flight 2				
TRACE-P P3-B Flight 16	23 March 2001	SE of Japan	33°N, 138°E	24.017–24.500	5.2	24	pollution and dust, FT
TRACE-P DC-8 Flight 14							
			Intercomparison Flight 3				
TRACE-P P3-B Flight 18, ACE-Asia C-130 Flight 01	30 March 2001	west and SW of Japan	34°N, 130°E				pollution, dust, and sea salt, MBL and lower FT
Leg 1				0.900–1.550	0.2	53	
Leg 2				1.683–2.017	2.5	8	
Leg 3				2.150–2.450	0.9	64	
Leg 4				2.533–2.633	0.1	44	
Leg 5				3.000–3.400	0.9	70	
			Intercomparison Flight 4				
TRACE-P P3-B Flight 19, ACE-Asia C-130 Flight 02	2 April 2001	west of Japan	38°N, 135°E				pollution, dust, and sea salt, MBL and lower FT
Leg 1				2.200–3.167	0.2	70	
Leg 2				3.200–3.667	0.6	82	
Leg 3				4.500–4.850	1.7	15	
			Intercomparison Flight 5				
TRACE-P P3-B Flight 23	9 April 2001	NE of Hawaii	25°N, 148°W				"clean" FT and "semipolluted" MBL
TRACE-P DC-8 Flight 20							
Leg 1				6.050–6.417	5.2	12	
Leg 2				7.000–7.317	0.2	63	

and also presumably representative of clean conditions. Flights 3 and 4 (ACE-Asia C-130 and TRACE-P P3-B) are shown in Figures 1c and 1d, respectively, and occurred in strong Asian outflow near Japan. Table 2 contains a listing of all the comparison flights, which platforms were being compared, their locations, dates, number of horizontal legs, and leg information (altitude, ambient RH, leg times, and primary aerosol constituents).

[28] A time series of the ambient, nephelometer, and OPC RH and aircraft altitudes are shown in Figures 2a–2e for flights 1–5, respectively, and reveal the wide range of conditions encountered. The FSSP RH is ambient and the PCASP RH was not measured, although since the inlet is heated, it is presumed to be relatively dry. In all cases throughout this paper, the reported ambient RH is over water, not ice. The low and stable instrument RHs shown in Figure 2 confirm that measured optical properties and OPC size distributions were dry (instrument RH not over 40%, except in the warm MBL to the northeast of Hawaii, flight 5, and in the warm MBL to the northwest of Guam, flight 1). Therefore observed differences in measured parameters should not be due to differences in water uptake by the aerosol. Figure 2 also shows periods influenced by cloud penetrations that might affect the quality of the data comparison since various groups may have edited their data differently and both aircraft may not have flown through similar clouds.

4. Horizontal Leg-Averaged Data

[29] The majority of the continuous physical measurements (CN concentrations, scattering and absorption coefficients, and FSSP measurements) have means and variances calculated only when there were simultaneous measurements on both platforms, resulting in the same number of 1-min data for each aircraft. Time periods where there were no data from one or both of the platforms are not included. For the more intermittent OPC, DMA, and aerosol chemistry measurements, data were included in the averages regardless of whether or not there were coincidental measurements on both platforms since these instruments were neither simultaneous nor continuous, although this may introduce biases in the leg-averaged data. For these measurements, the number of data points from each platform is reported in Tables 3 and 4, with the P3-B number of data points being reported first. Intercomparison legs where data were not available from one of the platforms for the entire leg are marked by "no data"

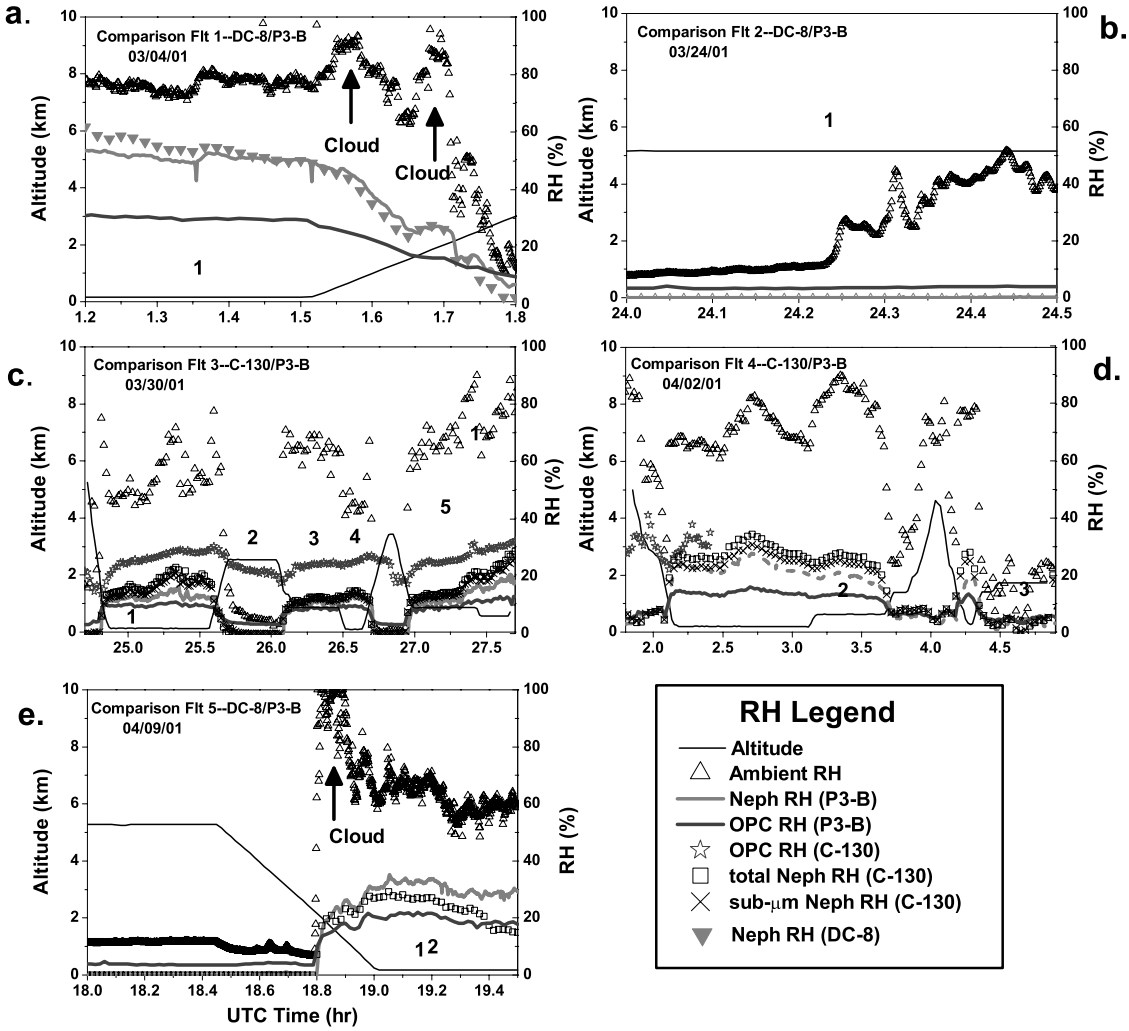

Figure 2. (a) Time series of altitude, ambient RH, and instrument RH (OPCs and nephelometers) for flight 1. (b) Same as Figure 2a, but for flight 2. (c) Same as Figure 2a, but for flight 3. (d) Same as Figure 2a, but for flight 4. (e) Same as Figure 2a, but for flight 5. Also shown in Figures 2a–2e are the locations of cloud penetrations that occurred during flights 1 and 5.

and corresponding "N/A" for the platform where data were available. There was no C-130 PILS data for flight 4; therefore this flight was omitted from Table 4.

[30] When the ratios of the means for compared measurements were within the combined RMS uncertainty, they are indicated by italics in Tables 3 and 4 and are considered here as reasonable agreement. Those legs where the ratios of the means are outside the uncertainties listed in Table 1 are also indicated.

5. Data Presentation Format

[31] We first discuss the comparison of the leg-averaged data measured on the comparison platforms. We then show time series of the compared measurements to see if trends in the data are duplicated despite any discrepancies in the absolute values. Following the time series, we present scatterplots of the various parameters and perform a regression analysis. In performing this analysis, we force the data to go through the origin and also allow the y intercept to vary. The regression lines shown in the scatterplots, however, will only be for the lines forced through the origin. We assert, especially when the same instrumentation is being compared, that these regressions are more appropriate. In the majority of cases, the regression slopes do not vary significantly between the two lines, and often the y intercepts for the nonforced lines are within the limit of detection of the measurements and not considered significant. Where the offsets are outside the instrumental limits of detection, outliers are often the driving force. The exception to this is for the comparison of aerosol chemistry, where significant offsets may in fact occur due to the difference in measurement cut size. Results from these regressions are listed in Table 5, both for the line forced through the origin and the line where the y intercept is allowed to vary. The scatterplots also include the combined RMS uncertainty limits from the ideal 1:1 line. Integral surface area scatterplots include both the 20% and 50% error estimates.

[32] In each data section, we present comparisons between the ACE-Asia C-130 and TRACE-P P3-B aircraft first since their payloads are more similar. Next, favorable comparisons between the TRACE-P DC-8 and P3-B plat-

Table 3. Intercomparison Legs, Means, and Variances of Aerosol Microphysical and Optical Properties[a]

	Flight 1	Flight 2	Flight 3				
	Leg 1	Leg 1	Leg 1	Leg 2	Leg 3	Leg 4	Leg 5
Aircraft	P3-B/DC-8	P3-B/DC-8	P3-B/C-130	P3-B/C-130	P3-B/C-130	P3-B/C-130	P3-B/C-130
Date	4 March 2001	24 March 2001	30 March 2001	30 March 2001	30 March 2001	30 March 2001	30 March 2001
			Heated CN Concentration, number/cm^3				
P3-B values	165 (41)	469 (180)	N/A	378 (111)	N/A	N/A	N/A
DC-8/C-130 values	D 167 (73)	D 595 (225)	no data	C 252 (54)	no data	no data	no data
Ratio	**1.01** (1.76)	1.27 (1.25)		*0.67* (0.48)			
Number of data points	20	28		19			
			Unheated CN Concentration, number/cm^3				
P3-B values	222 (48)	772 (253)	1830(341)	599 (267)	3472 (582)	2518 (187)	2053(145)
DC-8/C-130 values	D 259 (74)	D 972 (324)	C 1909 (385)	C 691 (556)	C 4651 (782)	C 4044 (306)	C 2717 (115)
Ratio	1.17 (1.53)	1.26 (1.28)	**1.04** (1.13)	**1.15** (2.08)	1.34 (1.34)	*1.61* (1.64)	*1.32* (0.79)
Number of data points	20	28	39	20	18	6	24
			RCN Ratio				
P3-B values	0.74 (0.02)	0.60 (0.05)	N/A	0.68 (0.11)	N/A	N/A	N/A
DC-8/C-130 values	D 0.61 (0.11)	D 0.60 (0.03)	no data	C 0.48 (0.11)	no data	no data	no data
Ratio	0.82 (4.71)	**1.01** (0.71)		*0.71* (1.07)			
Number of data points	20	28		19			
			Total Scattering Coefficient at 550 nm, Mm^{-1}				
P3-B values	30.98 (2.29)	11.95 (4.30)	49.28 (9.93)	14.52 (2.68)	78.70 (9.82)	61.99 (3.97)	49.02 (3.60)
DC-8/C-130 values	D 7.19 (1.04)	D 13.18 (3.79)	C 54.92 (11.67)	C 26.61 (14.61)	C 88.99 (10.02)	C 71.57 (3.12)	C 57.65 (1.97)
Ratio	*0.23* (0.46)	**1.10** (0.88)	*1.11* (1.18)	*1.83* (5.45)	*1.13* (1.02)	*1.15* (0.79)	*1.18* (0.55)
Number of data points	19	23	13	10	8	6	7
			Submicron Scattering Coefficient at 550 nm, Mm^{-1}				
P3-B values	no data	N/A	39.11 (8.75)	12.48 (1.49)	67.91 (6.69)	no data	43.20 (3.58)
DC-8/C-130 values	no data	no data	C 38.73 (8.72)	C 9.05 (1.48)	C 65.73 (6.60)	N/A	C 39.39 (2.57)
Ratio			**0.99** (1.00)	0.72 (0.99)	**0.97** (0.99)		**0.91** (0.72)
Number of data points			13	8	8		11
			Total Absorption Coefficient at 565 nm (550 nm for C-130), Mm^{-1}				
P3-B values	0.52 (0.00)	0.79 (0.24)	6.60 (0.91)	1.01 (0.00)	N/A	N/A	N/A
DC-8/C-130 values	D 0.35 (0.00)	D 1.71 (1.07)	C 7.51 (1.13)	C 1.79 (0.00)	no data	no data	no data
Ratio	**0.69** (0.00)	*2.16* (4.39)	**1.14** (1.25)	*1.77* (0.00)			
Number of data points	1	15	7	1			
			Total Coalbedo				
P3-B values	0.02 (0.00)	0.06 (0.01)	0.11 (0.01)	0.06 (0.00)	N/A	N/A	N/A
DC-8/C-130 values	D 0.06 (0.00)	D 0.11 (0.05)	C 0.12 (0.01)	C 0.06 (0.00)	no data	no data	no data
Ratio	*3.38* (0.00)	*1.84* (7.07)	**1.01** (1.20)	**0.96** (0.00)			
Number of data points	1	15	6	1			
			DMA Integral Number, number/cm^3				
P3-B values	N/A	N/A	549 (33.00)	117 (89.05)	935 (23.04)	671 (8.86)	571 (48.43)
DC-8/C-130 values	no data	no data	C 1041 (30.00)	C 92 (8.32)	C 907 (131.50)	C 633 (169.23)	C 500 (37.51)
Ratio			*1.90* (0.91)	**0.78** (0.09)	**0.97** (5.71)	**0.94** (19.10)	**0.88** (0.78)
Number of data points			P 5, C 7	P 3, C 3	P 2, C 3	P 2, C 2	P 5, C 4
			DMA Integral Surface Area, $\mu m^2/cm^3$				
P3-B values	N/A	N/A	5.98 (2.95)	1.52 (0.97)	13.72 (0.56)	9.84 (0.30)	7.76 (0.43)
DC-8/C-130 values	no data	no data	C 8.16 (3.93)	C 1.52 (0.05)	C 14.17 (1.77)	C 10.05 (3.14)	C 7.71 (0.59)
Ratio			1.37 (1.33)	**1.00** (0.05)	**1.03** (3.16)	**1.02** (10.42)	**1.00** (1.36)
Number of data points			P 5, C 7	P 3, C 3	P 2, C 3	P 2, C 2	P 5, C 4
			DMA Integral Volume, $\mu m^2/cm^3$				
P3-B values	N/A	N/A	0.08 (0.04)	0.02 (0.01)	0.18 (0.01)	0.13 (0.00)	0.10 (0.01)
DC-8/C-130 values	no data	no data	C 0.11 (0.05)	C 0.02 (0.00)	C 0.18 (0.02)	C 0.13 (0.04)	C 0.10 (0.01)
Ratio			1.38 (1.33)	**1.07** (0.08)	**1.05** (2.57)	**1.04** (9.32)	**1.01** (1.13)
Number of data points			P 5, C 7	P 3, C 3	P 2, C 3	P 2, C 2	P 5, C 4
			OPC (PCASP on DC-8) Accumulation Mode integral Number, number/cm^3				
P3-B values	105 (12.00)	115 (38.42)	1282 (228.06)	196 (46.44)	1817 (163.62)	1615 (0.00)	1091 (119.82)
DC-8/C-130 values	D 70 (5.69)	D 148 (38.90)	C 1264 (271.35)	C 216 (55.03)	C 1799 (298.99)	C 1423 (415.24)	C 1070 (120.45)
Ratio	0.67 (0.47)	**1.28** (1.01)	**0.99** (1.19)	**1.10** (1.19)	**0.99** (1.83)	**0.88** (NA)	**0.98** (1.01)
Number of data points	P 7, D 20	P 10, D 27	P 10, C 26	P 7,C 13	P 6, C 12	P 2,C 4	P 8, C 23
			OPC (PCASP on DC-8) Accumulation Mode Integral Surface Area, $\mu m^2/cm^3$				
P3-B values	15.46 (1.73)	14.42 (4.48)	154.92 (27.05)	26.02 (5.90)	227.29 (22.83)	193.29 (0.00)	133.71 (14.92)
DC-8/C-130 values	D 8.77 (0.81)	D 11.05 (2.86)	C 166.55 (36.48)	C 30.56 (7.79)	C 246.85 (43.28)	C 178.38 (52.22)	C 134.86 (13.67)

Table 3. (continued)

	Flight 1 Leg 1	Flight 2 Leg 1	Flight 3 Leg 1	Flight 3 Leg 2	Flight 3 Leg 3	Flight 3 Leg 4	Flight 3 Leg 5
Ratio	*0.57* (0.47)	**0.77** (0.64)	**1.08** (1.35)	**1.17** (1.32)	**1.09** (1.90)	**0.92** (NA)	**1.01** (0.92)
Number of data points	P 7, D 20	P 10, D 27	P 10, C 26	P 7,C 13	P 6, C 12	P 2, C 4	P 8, C 23
			OPC (PCASP on DC-8) Accumulation Mode Integral Volume, $\mu m^2/cm^3$				
P3-B values	0.83 (0.10)	0.69 (0.21)	6.37 (1.12)	1.13 (0.26)	9.55 (1.01)	8.00 (0.00)	5.59 (0.63)
DC-8/C-130 values	D 0.45 (0.06)	D 0.54 (0.14)	C 7.19 (1.64)	C 1.32 (0.35)	C 11.09 (2.05)	C 7.58 (2.37)	C 5.73 (0.59)
Ratio	*0.55* (0.57)	**0.79** (0.67)	**1.13** (1.47)	**1.16** (1.34)	**1.16** (2.03)	**0.95** (NA)	**1.02** (0.93)
Number of data points	P 7, D 20	P 10, D 27	P 10, C 26	P 7, C 13	P 6, C 12	P 2, C 4	P 8, C 23
			OPC Coarse Mode Integral Number, number/cm^3				
P3-B values	N/A	N/A	1.56 (0.28)	1.08 (0.16)	2.24 (0.13)	2.14 (0.27)	2.34 (0.16)
DC-8/C-130 values	no data	no data	C 1.18 (0.48)	C 2.07 (2.40)	C 1.42 (0.52)	C 1.33 (0.58)	C 1.80 (1.19)
Ratio			**0.76** (1.68)	*1.91* (15.50)	0.63 (3.88)	0.62 (2.13)	**0.77** (7.39)
Number of data points			P 10,C 26	P 7,C 13	P 6,C 12	P 2,C 4	P 8,C 23
			OPC Coarse Mode Integral Surface Area, $\mu m^2/cm^3$				
P3-B values	N/A	N/A	9.43 (2.03)	13.97 (4.42)	13.74 (1.39)	15.10 (2.19)	16.01 (2.85)
DC-8/C-130 values	no data	no data	C 12.52 (4.41)	C 14.96 (8.31)	C 15.40 (2.67)	C 20.12 (10.41)	C 15.05 (3.39)
Ratio			1.33 (2.18)	**1.07** (1.88)	**1.12** (1.93)	1.33 (4.76)	**0.94** (1.19)
Number of data points			P 10,C 26	P 7,C 13	P 6,C 12	P 2,C 4	P 8,C 23
			OPC Coarse Mode Integral Volume, $\mu m^2/cm^3$				
P3-B values	N/A	N/A	4.45 (1.87)	8.79 (3.89)	7.03 (1.92)	8.97 (2.74)	8.88 (4.70)
DC-8/C-130 values	no data	no data	C 6.61 (3.51)	C 9.79 (6.76)	C 8.31 (3.36)	C 19.92 (18.67)	C 7.49 (4.02)
Ratio			1.47 (1.88)	**1.11** (1.74)	**1.18** (1.75)	*2.22* (6.82)	**0.84** (0.86)
Number of data points			P 10,C 26	P 7,C 13	P 6,C 12	P 2,C 4	P 8,C 23
			FSSP Coarse Mode Integral Number, number/cm^3				
P3-B values	1.39 (0.17)	1.06 (0.40)	0.39 (0.14)	0.30 (0.09)	1.06 (0.10)	1.06 (0.10)	1.64 (0.34)
DC-8/C-130 values	D 3.44 (1.64)	D 0.43 (0.25)	C 0.73 (0.23)	C 0.46 (0.16)	C 1.07 (0.11)	C 1.07 (0.07)	C 1.64 (0.46)
Ratio	*2.46* (9.42)	*0.41* (0.62)	*1.85* (1.56)	1.50 (1.69)	**1.01** (1.20)	**1.01** (0.68)	**1.00** (1.35)
Number of data points	20	27	39	20	18	6	24
			FSSP Coarse Mode Integral Surface Area, $\mu m^2/cm^3$				
P3-B values	50.35 (7.92)	54.26 (25.62)	12.97 (17.67)	3.56 (0.78)	44.83 (6.04)	33.93 (7.63)	78.34 (26.02)
DC-8/C-130 values	D 97.99 (47.45)	D 6.08 (4.01)	C 23.51 (12.76)	C 10.99 (4.02)	C 29.97 (3.49)	C 31.26 (1.52)	C 56.88 (23.77)
Ratio	*1.95* (5.99)	*0.11* (0.16)	*1.81* (0.72)	*3.09* (5.15)	0.67 (0.58)	**0.92** (0.20)	**0.73** (0.91)
Number of data points	20	27	39	20	18	6	24
			FSSP Coarse Mode Integral Volume, $\mu m^3/cm^3$				
P3-B values	44.67 (10.02)	67.33 (36.14)	16.89 (38.03)	0.32 (0.07)	51.61 (10.26)	33.74 (13.42)	98.94 (43.86)
DC-8/C-130 values	D 83.02 (41.60)	D 4.34 (3.89)	C 28.09 (29.33)	C 8.08 (3.37)	C 31.12 (6.54)	C 27.90 (2.08)	C 66.09 (36.56)
Ratio	*1.86* (4.15)	*0.06* (0.11)	*1.66* (0.77)	*25.39* (45.44)	0.60 (0.64)	**0.83** (0.16)	0.67 (0.83)
Number of data points	20	27	39	20	18	6	24

	Flight 4 Leg 1	Flight 4 Leg 2	Flight 4 Leg 3	Flight 5 Leg 1	Flight 5 Leg 2
Aircraft	P3-B/C-130	P3-B/C-130	P3-B/C-130	P3-B/DC-8	P3-B/DC-8
Date	2 April 2001	2 April 2001	2 April 2001	9 April 2001	9 April 2001
			Heated CN Concentration, number/cm^3		
P3-B values	3537 (407)	3444 (386)	348 (61)	49 (7)	166 (24)
DC-8/C-130 values	C 3851 (385)	C 3574 (365)	C 332 (63)	D 163 (8)	D 196 (198)
Ratio	**1.09** (0.95)	**1.04** (0.95)	**0.95** (1.03)	*3.31* (1.06)	**1.18** (8.14)
Number of data points	58	30	21	17	19
			Unheated CN Concentration, number/cm^3		
P3-B values	4821 (445)	5256 (1198)	598 (47)	1763 (52)	271 (32)
DC-8/C-130 values	C 7127 (801)	C 7603 (2273)	C 636 (51)	D 2703 (126)	D 354 (268)
Ratio	*1.48* (1.80)	*1.45* (1.90)	**1.06** (1.09)	*1.53* (2.42)	1.31 (8.41)
Number of data points	58	30	21	17	19
			RCN Ratio		
P3-B values	0.73 (0.02)	0.67 (0.09)	0.58 (0.08)	0.03 (0.00)	0.61 (0.01)
DC-8/C-130 values	C 0.54 (0.02)	C 0.49 (0.09)	C 0.52 (0.09)	D 0.06 (0.00)	D 0.52 (0.02)
Ratio	**0.74** (0.68)	**0.74** (1.01)	**0.90** (1.14)	*2.16* (0.73)	**0.85** (1.18)
Number of data points	58	30	21	17	19
			Total Scattering Coefficient at 550 nm, Mm^{-1}		
P3-B values	104.47 (30.44)	108.29 (19.30)	6.00 (1.06)	0.61 (0.06)	24.52 (3.65)
DC-8/C-130 values	C 126.89 (30.80)	C 133.33 (21.74)	C 7.43 (1.18)	D 0.78 (0.23)	D 10.11 (0.81)

Table 3. (continued)

	Flight 4			Flight 5	
	Leg 1	Leg 2	Leg 3	Leg 1	Leg 2
Ratio	*1.21* (1.01)	*1.23* (1.13)	*1.24* (1.12)	1.27 (3.84)	*0.41* (0.22)
Number of data points	28	15	10	17	14
		Submicron Scattering Coefficient at 550 nm, Mm^{-1}			
P3-B values	93.32 (26.80)	77.67 (12.50)	6.07 (1.18)	no data	N/A
DC-8/C-130 values	C 95.39 (30.01)	C 75.24 (12.67)	C 4.75 (0.83)	no data	no data
Ratio	**1.02** (1.12)	**0.97** (1.01)	0.78 (0.71)		
Number of data points	21	15	5		
		Total Absorption Coefficient at 565 nm (550 nm for C-130), Mm^{-1}			
P3-B values	10.96 (4.05)	11.10 (1.84)	0.75 (0.45)	0.10 (0.04)	0.80 (0.29)
DC-8/C-130 values	C 12.88 (3.44)	C 13.62 (2.30)	C 1.08 (1.77)	D 0.22 (0.16)	D 1.11 (0.31)
Ratio	**1.18** (0.85)	**1.23** (1.26)	1.45 (3.94)	*2.22* (3.61)	1.39 (1.08)
Number of data points	20	9	5	10	10
		Total Coalbedo			
P3-B values	0.10 (0.02)	0.09 (0.01)	0.09 (0.07)	0.13 (0.07)	0.03 (0.01)
DC-8/C-130 values	C 0.10 (0.00)	C 0.09 (0.00)	C 0.07 (0.23)	D 0.21 (0.11)	D 0.10 (0.03)
Ratio	**0.99** (0.26)	**0.98** (0.19)	**0.77** (3.52)	*1.64* (1.63)	*3.03* (2.20)
Number of data points	20	9	5	10	10
		DMA Integral Number, number/cm^3			
P3-B values	1464 (599.46)	981 (1086.57)	112 (62.77)	N/A	N/A
DC-8/C-130 values	C 1041 (573.22)	C 861 (753.87)	C 125 (105.20)	no data	no data
Ratio	0.71 (0.96)	**0.88** (0.69)	**1.11** (1.68)		
Number of data points	P 7,C 9	P 5,C 5	P 3,C 3		
		DMA Integral Surface Area, $\mu m^2/cm^3$			
P3-B values	18.21 (8.86)	8.81 (9.15)	1.06 (0.83)	N/A	N/A
DC-8/C-130 values	C 16.55 (8.53)	C 13.30 (11.33)	C 1.74 (1.41)	no data	no data
Ratio	**0.91** (0.96)	*1.51* (1.24)	*1.65* (1.71)		
Number of data points	P 7,C 9	P 5,C 5	P 3,C 3		
		DMA Integral Volume, $\mu m^3/cm^3$			
P3-B values	0.23 (0.12)	0.08 (0.08)	0.01 (0.01)	N/A	N/A
DC-8/C-130 values	C 0.22 (0.11)	C 0.17 (0.15)	C 0.02 (0.02)	no data	no data
Ratio	**0.94** (0.94)	*2.17* (1.93)	*1.76* (1.74)		
Number of data points	P 7,C 9	P 5,C 5	P 3,C 3		
		OPC (PCASP on DC-8) Accumulation Mode Integral Number, number/cm^3			
P3-B values	N/A	N/A	N/A	10 (1.36)	172 (20.14)
DC-8/C-130 values	no data	no data	no data	D 25 (1.99)	D 122 (22.06)
Ratio				*2.44* (1.46)	0.71 (1.10)
Number of data points				P 6,D 22	P 6,D 19
		OPC (PCASP on DC-8) Accumulation Mode Integral Surface Area, $\mu m^2/cm^3$			
P3-B values	N/A	N/A	N/A	1.01 (0.18)	26.37 (2. 80)
DC-8/C-130 values	no data	no data	no data	D 1.04 (0.13)	D 17.14 (4.21)
Ratio				**1.03** (0.70)	0.65 (1.51)
Number of data points				P 6,D 22	P 6,D 19
		OPC (PCASP on DC-8) Accumulation Mode Integral Volume, $\mu m^3/cm^3$			
P3-B values	N/A	N/A	N/A	0.04 (0.01)	1.32 (0.14)
DC-8/C-130 values	no data	no data	no data	D 0.04 (0.01)	D 0.88 (0.27)
Ratio				**0.91** (0.69)	0.67 (1.97)
Number of data points				P 6,D 22	P 6,D 19
		OPC Coarse Mode Integral Number, number/cm^3			
P3-B values	N/A	N/A	N/A	N/A	N/A
DC-8/C-130 values	no data	no data	no data	no data	no data
		OPC Coarse Mode Integral Surface Area, $\mu m^2/cm^3$			
P3-B values	N/A	N/A	N/A	N/A	N/A
DC-8/C-130 values	no data	no data	no data	no data	no data
		OPC Coarse Mode Integral Volume, $\mu m^3/cm^3$			
P3-B values	N/A	N/A	N/A	N/A	N/A
DC-8/C-130 values	no data	no data	no data	no data	no data
		FSSP Coarse Mode Integral Number, number/cm^3			
P3-B values	3.67 (1.18)	4.55 (1.55)	0.10 (0.03)	N/A	N/A
DC-8/C-130 values	C 3.00 (1.06)	C 2.98 (0.97)	C 0.06 (0.02)	no data	no data

Table 3. (continued)

	Flight 4			Flight 5	
	Leg 1	Leg 2	Leg 3	Leg 1	Leg 2
Ratio	**0.82** (0.90)	0.65 (0.63)	0.59 (0.52)		
Number of data points	58	30	30		
	FSSP Coarse Mode Integral Surface Area, $\mu m^2/cm^3$				
P3-B values	117.62 (46.22)	181.58 (77.34)	2.50 (1.19)	N/A	N/A
DC-8/C-130 values	C 77.20 (31.35)	C 87.02 (36.12)	C 1.33 (0.75)	no data	no data
Ratio	0.66 (0.68)	0.48 (0.47)	0.53 (0.64)		
Number of data points	58	30	30		
	FSSP Coarse Mode Integral Volume, $\mu m^3/cm^3$				
P3-B values	114.37 (55.16)	202.53 (103.42)	1.81 (1.65)	N/A	N/A
DC-8/C-130 values	C 77.08 (34.61)	C 93.09 (44.80)	C 1.00 (0.93)	no data	no data
Ratio	0.67 (0.63)	0.46 (0.43)	0.55 (0.56)		
Number of data points	58	30	30		

[a]Means of the parameters were taken over time periods where there were measurements on both platforms. Variances are reported as standard deviations for the same time periods. P3-B and DC-8 (D) and C-130 (C) values of means and variances, the ratios of the means and variances (C-130/DC-8 data divided by P3-B data), and the number of data points utilized in calculating the means and variances are given for each parameter. For the majority of the physical measurements (CN concentrations, scattering and absorption coefficients, and FSSP measurements), the leg averages were calculated only when there were simultaneous measurements on both platforms resulting in the same number of data. OPC and DMA data were included regardless of whether or not there were coincidental measurements since these data were neither simultaneous nor continuous. For these entries, the P3-B number of data points is reported first. Intercomparison legs where data were not available from one of the platforms for the entire leg are marked by "no data" and corresponding "N/A" for the platform where data were available. Legs with the ratio of the means within the expected instrumental uncertainty are in bold. Legs with ratios well outside of the estimated errors (by >15%) or if the observed differences are systematic (e.g., C-130/P3-B total scattering coefficient comparison) are in italics and most are discussed in the text. If the compared data are outside the estimated instrumental errors by only a few percent, they are entered in normal font.

forms are shown, followed by presentation of data from the two TRACE-P aircraft where there is less agreement.

6. Aerosol Optics

6.1. ACE-Asia C-130 and TRACE-P P3-B: Intercomparison Flight 4

[33] Total and submicrometer aerosol light scattering coefficients (λ = 550 nm) for flight 4 shown in Figure 3a were measured continuously on the C-130, while the P3-B periodically switched between the two. The comparison time period covered a wide range of ambient relative humidity but nephelometer RH never exceeded 30% (Figure 2d). The submicrometer scattering coefficients (Table 3 and Figure 3a) trended together and generally agreed to within 5% of each other over an order of magnitude of values with no systematic difference observed between the two platforms. This is within the 15% instrument uncertainty for the nephelometer. In contrast, the total scattering coefficients (Table 3 and Figure 3a) on the P3-B were systematically between 20 and 25% lower than on the C-130, except in time periods when the aircraft were above the inversion and there were less coarse aerosol (submicrometer and total scattering nearly equal, e.g., profile at 4.0 hours and leg 3). Even though the differences in total scattering coefficients were only 5–10% higher than the reported instrument uncertainty, the discrepancy between P3-B and C-130 total scattering data was systematic and is addressed in section 10.

[34] The aerosol total absorption coefficients for this flight (Figure 3b, no submicrometer absorption measurement for the C-130) trended closely but were systematically lower by 17–44% on the P3-B than on the C-130 (Table 3 and Figure 3b). The values for two of the legs were within the reported 25% error estimate for the absorption coefficients; however, the observed differences were systematic. The P3-B total absorption was ~10% higher than the submicrometer absorption for the majority of data points, indicating some absorption from the coarse mode aerosol.

[35] Total ω_0 values were near ~0.9 (coalbedo ~0.1) for the majority of measurements and agreed within 5% of each other (Figure 3c). There were no submicrometer ω_0 values from the C-130 to compare to, but the values from the P3-B ranged from ~0.87 to 0.89. Total ω_0 values for leg 3 were highly variable on both aircraft due to scattering and absorption coefficients at or near instrumental noise levels of ~0.05 Mm^{-1} for scattering and ~0.2 Mm^{-1} for absorption.

[36] Plotting the data as scatterplots and performing regression analysis further illustrate the results of these comparisons. Total (squares) and submicrometer (triangles) σ_{sp} data for this flight and all legs are shown in Figure 4a. The solid black line is the result of the regression analysis for the total scattering coefficient after forcing the line to pass through the origin. The slope is 1.22 with a R^2 value of 0.96 (Table 5). While this 22% difference between the C-130 and P3-B data is near the uncertainty estimate for this parameter, the discrepancy is systematic and is addressed in section 10. The regression for the submicrometer σ_{sp} (gray solid line) was also forced through the origin and resulted in a slope of 0.99 and R^2 value of 0.98 and showed agreement within the specified instrument uncertainty. The comparison of total σ_{ap} data is shown in Figure 4b, and the slope of the regression line (solid black line) is 1.16, within the specified error estimate for PSAP absorption, with a R^2 of 0.92. However, this underestimation of total aerosol absorption as measured on the P3-B is systematic and is also discussed below.

6.2. TRACE-P DC-8 and P3-B Comparison

6.2.1. Intercomparison Flight 2

[37] Total and submicrometer light scattering coefficients (no submicrometer measurements on the DC-8) during comparison flight 2 (Figure 3d) from both aircraft showed

Table 4. Intercomparison Legs, Means, and Variances of Aerosol Chemical Constituents[a]

	Flight 1	Flight 2	Flight 3					Flight 5	
	Leg 1	Leg 1	Leg 1	Leg 2	Leg 3	Leg 4	Leg 5	Leg 1	Leg 2
Aircraft	P3-B/DC-8	P3-B/DC-8	P3-B/C-130	P3-B/C-130	P3-B/C-130	P3-B/C-130	P3-B/C-130	P3-B/DC-8	P3-B/DC-8
Date	4 March 2001	24 March 2001	30 March 2001	30 March 2001	30 March 2001	30 March 2001	30 March 2001	9 April 2001	9 April 2001
					Na, μg/stdm^3				
P3-B values	0.70 (0.03)	0.09 (0.04)	0.14 (0.07)	0.07 (0.05)	0.18 (0.02)	0.29 (0.01)	0.43 (0.10)	N/A	0.21 (0.04)
DC-8/C-130 values	D 2.84 (0.08)	D 0.26 (0.11)	C 0.04 (0.02)	C 0.03 (0.00)	C 0.05 (0.03)	C 0.08 (0.01)	C 0.16 (0.07)	no data	D 4.35 (0.69)
Ratio	*4.08* (3.11)	*2.85* (2.85)	*0.30* (0.33)	*0.45* (0.07)	*0.28* (1.12)	*0.26* (1.74)	*0.38* (0.68)		*20.58* (18.71)
Number of data points	P 18,D 20	P 26,D 26	P 39,C 26	P 26,C 10	P 18,C 18	P 6,C 6	P 24,C 24		P 19,D 19
					Ca, μg/std m^3				
P3-B values	no data	0.36 (0.13)	0.02 (N/A)	0.02 (N/A)	0.05 (0.01)	0.11 (N/A)	N/A	N/A	0.06 (0.01)
DC-8/C-130 values	N/A	D 1.44 (0.45)	C 0.06 (N/A)	C 0.08 (0.05)	C 0.05 (0.03)	C 0.04 (N/A)	no data		D 0.28 (0.07)
Ratio		*3.99* (3.34)	*2.61* (N/A)	*4.10* (N/A)	**1.02** (2.10)	*0.40* (N/A)		no data	*5.02* (10.53)
Number of data points		P 26,D 26	P 4,C 6	P 2,C 27	P 15,C 10	P 2,C 4			P 7,D 16
					Mg, μg/std m^3				
P3-B values	0.09 (0.01)	0.03 (0.01)	0.03 (0.01)	0.02 (0.01)	N/A	0.04 (0.00)	0.07 (0.02)	N/A	0.03 (0.01)
DC-8/C-130 values	D 0.29 (0.01)	D 0.23 (0.06)	C 0.04 (0.02)	C 0.04 (0.01)	no data	C 0.04 (0.00)	C 0.03 (0.01)	no data	D 0.50 (0.09)
Ratio	*3.19* (1.10)	*6.75* (4.21)	*1.69* (1.64)	*1.48* (1.01)		**1.09** (0.00)	*0.42* (0.44)		*15.75* (7.99)
Number of data points	P 18,D 20	P 18,D 26	P 12,C 27	P 8,C 19		P 6,C 2	P 24,C 12		P 7,D 19
					Cl, μg/std m^3				
P3-B values	2.38 (0.08)	0.05 (0.03)	0.15 (0.09)	0.10 (0.06)	0.25 (0.02)	0.35 (0.01)	0.61 (0.14)	N/A	0.31 (0.08)
DC-8/C-130 values	D 2.50 (0.12)	D 0.19 (0.08)	C 0.14 (0.06)	C 0.07 (0.05)	C 0.20 (0.02)	C 0.29 (0.01)	C 0.48 (0.10)	no data	D 7.56 (1.21)
Ratio	**1.05** (1.40)	*3.90* (3.13)	**0.91** (0.61)	0.69 (0.75)	**0.80** (1.02)	**0.83** (0.84)	**0.79** (0.68)		*24.54* (14.68)
Number of data points	P 18,D 20	P 24,D 26	P 39,C 39	P 12,C 31	P 18,C 18	P 6,C 6	P 24,C 24		P 19,D 19
					NH_4, μg/std m^3				
P3-B values	0.28 (0.02)	0.05 (N/A)	1.27 (0.34)	0.69 (0.77)	2.43 (0.31)	1.80 (0.12)	1.45 (0.20)	0.05 (N/A)	0.40 (0.09)
DC-8/C-130 values	D 0.14 (0.00)	D 0.24 (0.07)	C 1.72 (0.29)	C 0.87 (0.84)	C 2.73 (0.36)	C 1.97 (0.03)	C 1.70 (0.12)	D 0.02 (0.00)	D 0.70 (0.14)
Ratio	*0.50* (0.07)	*4.88* (N/A)	1.36 (0.85)	**1.26** (1.08)	**1.12** (1.18)	**1.10** (0.25)	**1.17** (0.61)	0.46 (N/A)	*1.77* (1.56)
Number of data points	P 18,D 20	P 4,D 26	P 39,C 35	P 30,C 31	P 18,C 18	P 6,C 6	P 24,C 24	P 3,D 22	P 19,D 19
					NO_3, μg/std m^3				
P3-B values	0.11 (0.02)	0.18 (0.04)	0.37 (0.20)	0.45 (0.46)	1.98 (0.73)	0.84 (0.09)	0.68 (0.09)	no data	0.05 (0.01)
DC-8/C-130 values	D 0.03 (0.02)	D 0.40 (0.09)	C 0.44 (0.27)	C 0.95 (0.66)	C 2.36 (0.82)	C 0.94 (0.05)	C 0.76 (0.10)	no data	D 0.29 (0.05)
Ratio	*0.26* (0.83)	*2.15* (2.05)	**1.19** (1.35)	*2.12* (1.44)	**1.19** (1.13)	**1.12** (0.58)	**1.12** (1.14)		*6.29* (6.37)
Number of data points	P 18,D 20	P 26,D 26	P 39,C 35	P 30,C 24	P 18,C 18	P 6,C 6	P 24,C 24		P 19,D 19
					SO_4, μg/std m^3				
P3-B values	0.49 (0.03)	0.56 (0.21)	4.44 (0.77)	1.85 (1.94)	6.19 (0.45)	5.23 (0.29)	4.72 (0.63)	N/A	1.05 (0.23)
DC-8/C-130 values	D 0.50 (0.01)	D 1.28 (0.34)	C 5.80 (0.87)	C 2.86 (2.43)	C 7.67 (0.57)	C 6.44 (0.18)	C 5.93 (0.33)	no data	D 2.12 (0.33)
Ratio	**1.01** (0.34)	*2.80* (2.89)	1.31 (1.13)	*1.55* (1.25)	**1.24** (1.26)	**1.23** (0.64)	**1.26** (0.52)		*2.02* (1.42)

Table 4. (continued)

	Flight 1	Flight 2	Flight 3					Flight 5	
	Leg 1	Leg 1	Leg 1	Leg 2	Leg 3	Leg 4	Leg 5	Leg 1	Leg 2
Number of data points	P 18,D 20	P 26,D 26	P 39,C 39	P 30,C 31	P 18,C 18	P 6,C 6	P 24, C 24		P 19,D 19
					"Fine" SO_4, μg/std m^3				
P3-B values	0.49 (0.03)	0.56 (0.21)	N/A	N/A	N/A	N/A	N/A	0.10 (0.02)	1.05 (0.23)
DC-8/C-130 values	D 0.22 (0.09)	D 1.28 (0.34)	no data	no data	no data	no data	no data	D 0.13 (0.02)	D 0.81 (0.17)
Ratio	*0.44* (2.93)	*2.31* (1.60)						1.30 (0.99)	**0.77** (0.75)
Number of data points	P 18,D 20	P 26,D 27						P 17, D 22	P 19,D 19

[a]Means of parameters were taken over time periods where there were measurements on both platforms. Variances are reported as standard deviations for the same time periods. P3-B and DC-8 (D) and C-130 (C) values of means and variances, the ratios of the means and variances (C-130/DC-8 data divided by P3-B data), the number of data points utilized in calculating the means and variances with the P3-B number of data points being reported first are given. Intercomparison legs where data were not available from one of the platforms for the entire leg are marked by "no data" and corresponding "N/A" for the platform where data were available. Legs with the ratio of the means within the RMS expected instrumental uncertainty (28%) are in bold. Legs with ratios well outside of the estimated errors (by >15%) or if the observed differences are systematic (e.g., C-130/P3-B total scattering coefficient comparison) are in italics and some discrepancies are discussed in the text. If the compared data are outside the estimated instrumental errors by only a few percent, they are entered in normal font. Flight 4 aerosol chemistry data are not listed since the C-130 PILS was not functioning during this flight.

a gradient in scattering with higher values near the end of the leg. Total σ_{sp} values were within ~10%, and this is within the reported nephelometer uncertainty. Ambient RH (Figure 2b) was very dry at ~9% initially and increased to 50% at the end of the leg, exhibiting the same structure as the total aerosol light scattering. However, both nephelometer RHs remained at ~1% for the entire leg (Figure 2b), confirming that the gradient in measured scattering was not related to water uptake. Submicrometer scattering was only ~60% of the total (Figure 3d) and implied a significant contribution to total scatter from supermicron aerosols. This implies that for the conditions sampled during this comparison leg (high altitude and dry), the DC-8 and P3-B had similar sampling efficiencies for supermicron particles. As shown in section 10.1, this was not always the case.

[38] Total and submicrometer absorption coefficients (Figure 3e) were about a factor of 10 lower than the previously discussed flight. The insignificant change between total and submicrometer absorption reflected absorption due to the presence of submicrometer BC. The P3-B absorption data also showed a steady increase over time consistent with the scattering data. The DC-8 absorption data were typically higher by a factor of 2 and more variable than on the P3-B, and there was less evidence of any trend.

[39] The total and submicrometer ω_0 values derived from P3-B data were ~0.94 and ~0.87 (coalbedos of 0.06 and 0.13), respectively, as shown in Figure 3f. This value of submicrometer ω_0 was similar to the ω_0 values from the previously discussed flight that had little coarse scattering. This suggests a similar pollution aerosol on both flights, but with less absorbing coarse aerosol on this one. The DC-8 values of ω_0 appeared to be unreasonably low and were more variable than on the P3-B due to the variability in DC-8 absorption (see section 10).

[40] The scatterplot shown in Figure 4c for the total σ_{sp} data for this flight resulted in a regression line with a slope of 1.09, within the 15% reported uncertainty, and a R^2 of 0.79 (Table 5). The comparison of total σ_{ap} data is shown in Figure 4d, and the slope of the regression line is 2.09 with a R^2 of 0.16. The total σ_{sp} data show agreement between the P3-B and the DC-8 within stated uncertainties, but the absorption comparison is well outside of the reported PSAP error estimates.

6.2.2. Intercomparison Flight 1

[41] Flight 1 occurred in the clean MBL, providing an opportunity to compare DC-8 and P3-B measured aerosol optical properties under different conditions than the data presented for flight 2. The ambient and nephelometer RH were relatively high on this flight at ~80% and ~50%, respectively (Figure 2a) with more coarse sea salt sampled (see section 9) than during flight 2.

[42] After the MBL leg and above the inversion (~2.0 km), the air was dry with ambient RH ~20%, aerosol scattering was low, and there was agreement within ~5% between the two platforms (Figure 3g). However, within the MBL where the RH was higher at ~75%, DC-8 scattering was only ~23% of the P3-B data (Table 3 and Figure 3g), although both sets of data trend together. This large discrepancy is well outside of the reported instrument uncertainty in Table 1 and appears to be related to poor inlet performance on the DC-8 at low altitudes with higher ambient RH and concentrations of sea salt as discussed in more detail in section 10.1.

Table 5. Results From Regression Analysis From Scatterplots of the Aerosol Data Presented in Figures 4, 6, 9, and 13[a]

					y Intercept = 0		Best Fit Line		
Measurement	Platforms/Instruments	Intercomparison Flight	Leg	Figure	Slope	R^2	Slope	*y* Intercept	R^2
Aerosol total scattering coefficient (at 550 nm)	C-130, P3-B/ Nephelometer	4	all legs included	4a	1.221	0.960	1.144	8.613	0.968
	DC-8, P3-B/ Nephelometer	2	1	4c	1.086	0.790	0.698	5.112	0.820
	DC-8, P3-B/ Nephelometer	1	1	4e	0.235	0.617	0.178	0.752	0.649
Aerosol sub-(m scattering coefficient (at 550 nm)	C-130, P3-B/ Nephelometer	4	all legs included	4a	0.993	0.978	1.004	−1.040	0.981
Aerosol absorption coefficient (at 565/550 nm)	C-130, P3-B/ PSAP	4	all legs included	4b	1.161	0.920	1.107	0.683	0.925
	DC-8, P3-B/ PSAP	2	1	4d	2.091	0.157	1.605	0.419	0.161
	DC-8, P3-B/ PSAP	1	1	4f	1.196	0.116	0.918	0.211	0.201
CN concentrations	C-130, P3-B/ CN counters	4	all legs included	6a	1.525	0.925	1.520	25.174	0.953
	DC-8, P3-B/ CN counters	1	1	6c	1.230	0.496	1.075	37.482	0.602
	DC-8, P3-B/ CN counters	5	1	6e	1.538	0.548	1.762	−396.946	0.583
		5	2	6e	1.078	0.889	0.774	82.680	0.921
RCN concentrations	C-130, P3-B/ CN counters	4	all legs included	6b	1.070	0.953	1.064	19.197	0.963
	DC-8, P3-B/ CN counters	1	1	6d	1.126	0.486	1.223	−15.271	0.524
	DC-8, P3-B/ CN counters	5	1	6f	3.344	0.123	0.405	142.872	0.354
		5	2	6f	0.800	0.895	0.601	37.448	0.952
Accumulation mode "dry" surface area	C-130, P3-B/ OPCs	3	all legs included	9a	0.947	0.835	0.963	−2.662	0.851
	DC-8, P3-B/ PCASP, OPC	2	1	9c	0.836	0.648	0.502	4.721	0.759
	DC-8, P3-B/ PCASP, OPC	1	1	9e	0.576	0.086	0.112	6.551	0.386
Coarse mode "dry" surface area	C-130, P3-B/ OPCs	3	all legs included	9b	1.133	0.046	0.598	7.783	0.374
Coarse mode "ambient" surface area	C-130, P3-B/ FSSPs	3	all legs included	9b	0.730	0.663	0.501	10.226	0.738
	DC-8, P3-B/ FSSPs	2	1	9d	0.118	0.832	0.137	−1.230	0.835
	DC-8, P3-B/ FSSP's	1	1	9e	1.988	0.557	1.818	8.308	0.583
NH_4 concentrations	C-130, P3-B/ PILSs	3	all legs included	13a	1.198	0.893	1.030	0.289	0.902
	DC-8, P3-B/ PILS, filters	5	all legs included	13d	1.721	0.767	1.300	0.167	0.803
	DC-8, P3-B/ PILS, filters	2	1	13g	3.753	NA[b]	NA	NA	NA[b]
SO_4 concentrations	C-130, P3-B/ PILSs	3	all legs included	13b	1.281	0.939	1.097	0.920	0.953
	DC-8, P3-B/ PILS, filters	5	all legs included	13e	2.006	0.787	1.521	0.471	0.846
	DC-8, P3-B/ PILS, filters	2	1	13h	2.772	0.815	2.615	0.101	0.838
NSS SO_4 Concentrations	DC-8, P3-B/ PILS, filters	5	all legs included	13e	0.827	0.743	0.595	0.221	0.804
	DC-8, P3-B/ PILS, filters	2	1	13h	2.076	0.36	0.920	0.761	0.574
NO_3 concentrations	C-130, P3-B/ PILSs	3	all legs included	13c	1.224	0.955	1.191	0.046	0.971
	DC-8, P3-B/ PILS, filters	5	all legs included	13f	3.716	0.317	0.240	0.220	0.461
	DC-8, P3-B/ PILS, filters	2	1	13i	2.135	0.839	1.884	0.049	0.875

[a]Data for aerosol optics, CN concentrations, integral surface areas, and NH_4^+, SO_4^{2-} and NO_3^- concentrations are presented. We have presented the results both for when the regression line is forced through the origin and when the y intercept is allowed to vary.
[b]Only one data point.

[43] The absorption data on the two platforms were quite low at ~0.75 Mm^{-1}, suggesting clean conditions with low BC, and approached the noise limit for 1-min averages (Figure 3h). Even so, the absorption values were similar over the comparison period, and leg-averaged values (see above and Table 3) were within 30% of each other, despite the spike (~1.4 hours) observed in the P3-B absorption data. This spike corresponded to enhancements in CN and RCN, NO and NO_y, and SO_2, suggesting that the aircraft flew through a ship plume. This was confirmed by visible observations from the cockpit. After removing this data point, the absorption coefficients were within 20% and were within the reported errors for this measurement.

[44] Total ω_0 values for both aircraft are shown in Figure 3i, and the DC-8 values were systematically lower than those on the P3-B. Values measured on the P3-B were generally ~0.99 (corresponding to a coalbedo of 0.01), in line with other values in the clean MBL reported in the literature [*Russell et al.*, 2002; *Dubovik et al.*, 2002]. In this case, the lower aerosol single scatter albedo and corresponding higher coalbedo measured on the DC-8 were due to the much lower scattering values and are not consistent with clean MBL air.

[45] The scatterplot and regression line shown in Figure 4e for the total σ_{sp} data resulted in a slope of 0.24, well outside of the reported uncertainty, and a R^2 of 0.62 (Table 5) This discrepancy is significant and is discussed further. Total σ_{ap} data are plotted in Figure 4f, and the regression analysis resulted in a slope of 1.20 and a R^2 of 0.12. The absorption data are uncorrelated due to low signals on this leg.

7. CN Concentrations

7.1. ACE-Asia C-130 and TRACE-P P3-B: Intercomparison Flight 4

[46] RCN concentrations exhibited agreement within the reported uncertainty of 10% between the C-130 and the P3-B on all legs (Table 3 and Figure 5a). However, both the total CN and UCN concentrations on the P3-B were systematically lower than those on the C-130 during legs 1 and 2 (Figures 5a and 5b). Despite the disagreement in absolute concentrations, the measurements trended together and exhibited the same

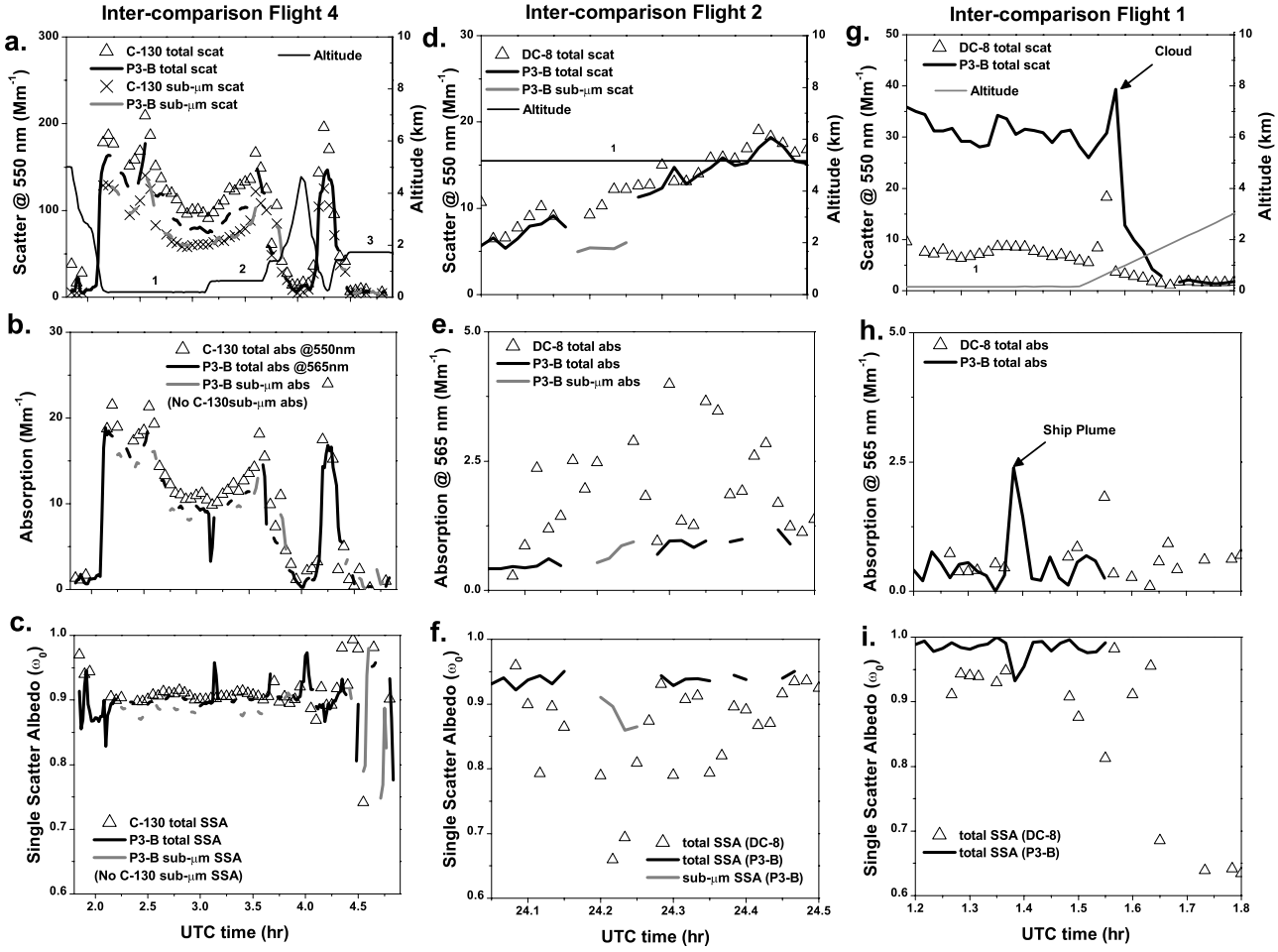

Figure 3. Time series of aerosol optical properties (non-STP corrected) for selected comparison flights. See Figure 1 and Table 2 for a complete listing of intercomparison locations. (a) Altitude and total and submicrometer scattering coefficients for flight 3 (ACE-Asia C-130/TRACE-P P3-B). (b) Total and submicrometer absorption coefficients for the same flight. (c) Total and submicrometer single scatter albedo for the same flight. (d) Same as Figure 3a, but for flight 2 (TRACE-P DC-8/P3-B). (e) Same as Figure 3b, but for flight 2. (f) Same as Figure 3c, but for flight 2. (g) Same as Figure 3a (no submicrometer data for either platform), but for flight 1 (TRACE-P DC-8/P3-B). (h) Same as Figure 3b (no submicrometer data for either platform), but for flight 1. A ship plume was encountered during this flight and is labeled. (i) Same as Figure 3c (no submicrometer data for either platform), but for flight 1.

structure. At higher altitudes, all similar measurements were in better agreement (e.g., 0400 UT and leg 3); leg 3 CN concentrations were within 3% and less than the proscribed uncertainty. Ultrafine (UCN-CN) concentrations were essentially zero for both platforms during leg 3, suggesting no particles below 15 nm.

[47] Since the C-130 CN concentrations were much higher and the RCN concentrations were virtually the same as on the P3-B, the C-130 RCN ratio (Figure 5c) was lower than measured on the P3-B for legs 1 and 2, but leg 3 values are more comparable. RCN ratios on both aircraft trended together and showed the same structure. The discrepancies in RCN ratio observed during legs 1 and 2 were due to errors in the total CN concentrations on either the P3-B or C-130.

[48] Scatterplots and regression lines for the CN concentrations are shown in Figure 6a. The CN data resulted in a slope of 1.53, outside of the reported uncertainty, but trended together as evidenced by the R^2 value of 0.93 (Table 5). The observed discrepancy for this flight is significant and is discussed in section 10.2. RCN concentrations for this flight are plotted in Figure 6b, and the regression analysis resulted in a slope of 1.07 and a R^2 of 0.95, within the stated RMS uncertainties.

7.2. TRACE-P DC-8 and P3-B Comparison

7.2.1. Intercomparison Flight 1

[49] A time series of the RCN and CN concentrations for the DC-8 and P3-B is shown in Figure 5d, and leg-averaged mean values agreed to within 1% to 17%, respectively (Table 3). Some variability in the measurements on the two aircraft was a result of clouds at ~1.57 and 1.68 hours (Figure 2a) and a ship plume near 1.4 hours (see discussion of absorption data for this flight in section 6.2.2). Small-scale features like these could have been intrinsically different as measured on both platforms. Although the CN

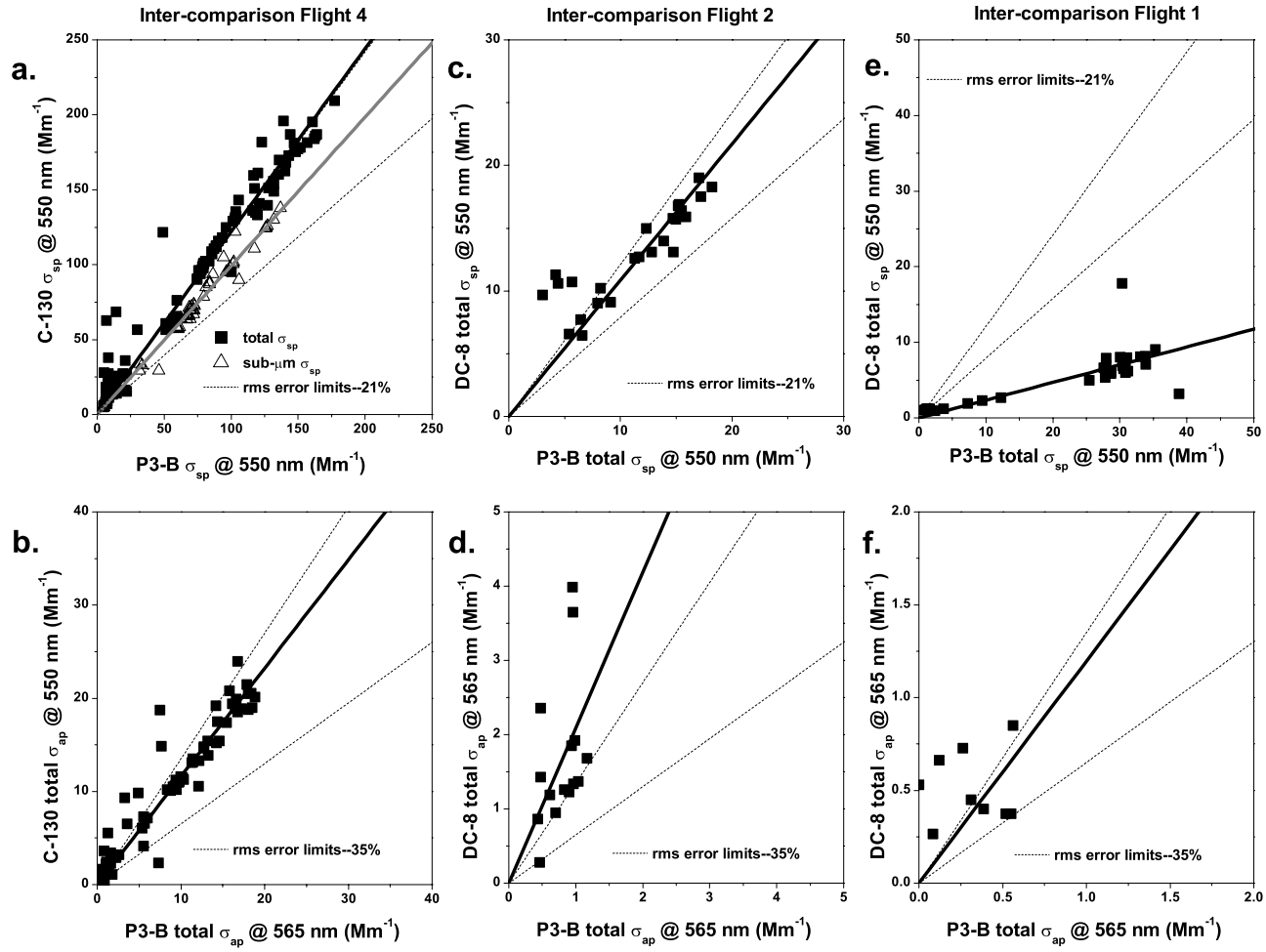

Figure 4. Scatterplots and regression analysis of the aerosol scattering and absorption coefficients for the comparison flights/legs shown in Figure 3. The *x* axes correspond to P3-B data. The *y* axes are for the other compared platform. Estimated RMS uncertainties based on the ideal 1:1 line are shown. Regression lines forced to pass through the origin are also plotted. Results from this analysis are presented in Table 5. (a) Total (black squares) and submicrometer scattering (triangles) coefficients at 550 nm for flight 4. (b) Total absorption coefficients for flight 4 (note that the wavelengths of the absorption measurements are not identical for this comparison). (c) Same as Figure 4a, but for flight 2 and without submicrometer scattering. (d) Same as Figure 4b, but for flight 2 and PSAP wavelengths are the same. (e) Same as Figure 4c, but for flight 1. (f) Same as Figure 4d, but for flight 1.

concentrations differ by more than the estimated error, these features likely caused the observed discrepancies. Figure 5e shows the DC-8 and P3-B UCN concentrations for the same time period, and there was agreement between these two measurements to within 5%, which is less than the reported UCN RMS uncertainties. UF concentrations were negligible for both aircraft indicating the absence of significant numbers of small particles.

[50] Although differences were variable between the RCN ratios on the two aircraft (Figure 5f), there was a tendency for larger differences at lower concentrations. The RCN ratios indicated that significant fractions (50–75%) of the total CN were refractory during this MBL leg. Also, the structure in RCN ratio observed on the climb out of the MBL starting at ~1.5 hours was represented in both measurements, even though the absolute values disagree.

[51] Figure 6c shows the scatterplot for the CN measurements. The regression analysis of the CN data resulted in a slope of 1.23, outside of the reported uncertainty, with considerable scatter in the data with an R^2 value of 0.50 (Table 5). The observed discrepancy is significant, but it is believed that the majority of the differences between the two platforms are due to the presence of clouds and the aforementioned ship plume. RCN concentrations for this flight are plotted in Figure 6d, and the regression line has a slope of 1.13 and a R^2 of 0.49. The RCN data comparison between the P3-B and the C-130 for this flight are greater than the stated uncertainties, but the observed differences are probably not significant given the nature of the air mass sampled, and the low R^2 is due primarily to the cloudy conditions and ship plume.

7.2.2. Intercomparison Flight 5

[52] Figure 5g shows the RCN and CN concentrations for the DC-8 and P3-B for flight 5. There were two comparison legs during this flight, with a descent profile between them (Figure 2e). The vertical profile had a cloud penetration

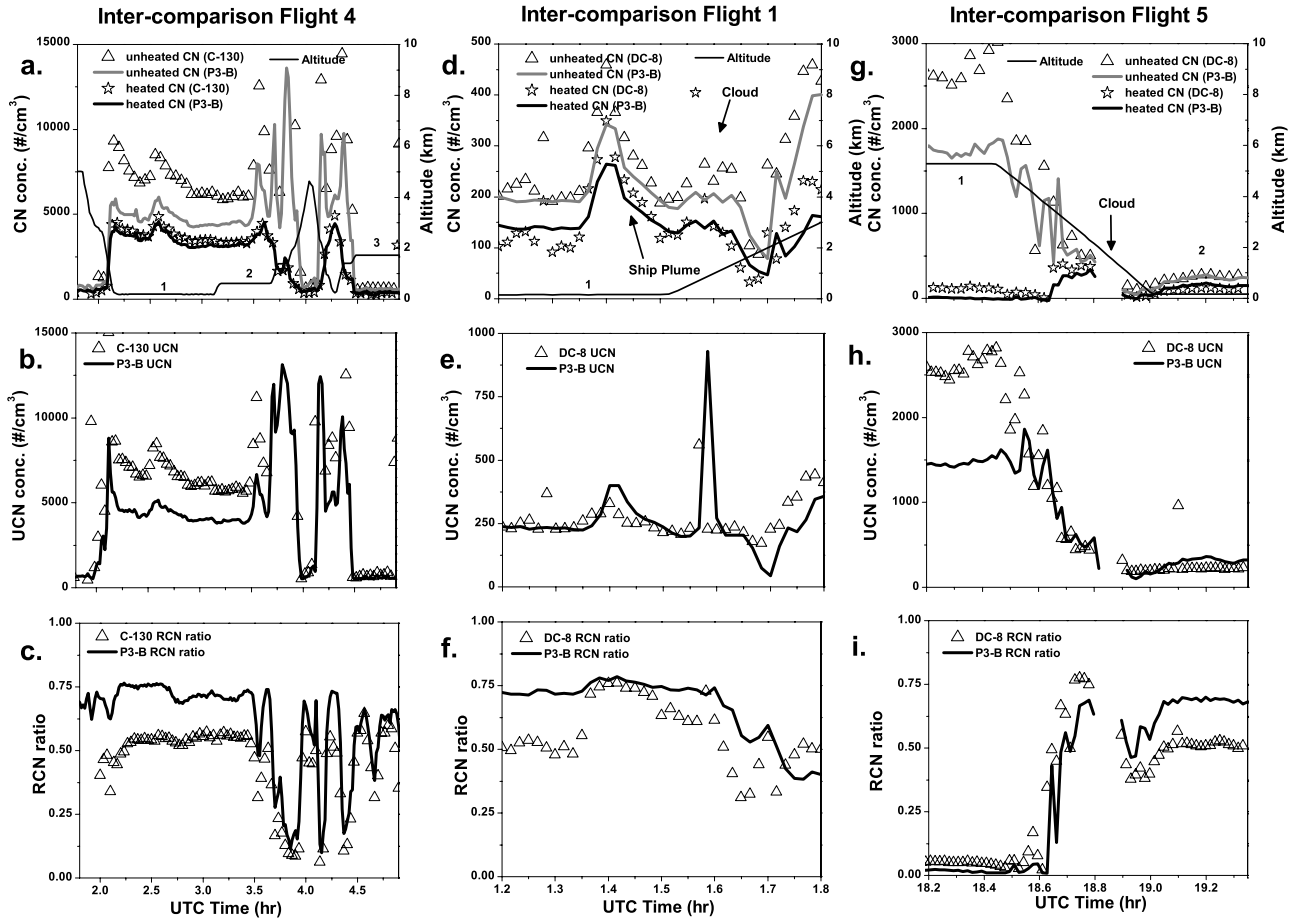

Figure 5. Time series of refractory, total, and ultrafine CN concentrations and RCN ratios for selected comparison flights. Note that these concentrations have been STP corrected. See Figure 1 and Table 2 for a complete listing of intercomparison locations. (a) Altitude and refractory and total CN for flight 4 (ACE-Asia C-130/TRACE-P P3-B). (b) UCN concentrations for the same flight. (c) RCN ratio for the same flight. (d) Same as Figure 5a, but for flight 1 (TRACE-P DC-8/P3-B). A ship plume was encountered during this flight and is labeled. (e) Same as Figure 5b, but for flight 1. (f) Same as Figure 5c, but for flight 1. (g) Same as Figure 5a, but for flight 5 (TRACE-P DC-8/P3-B). (h) Same as Figure 5b, but for flight 5. (i) Same as Figure 5c, but for flight 5.

from 1 to 2 km altitude, and data from that time period have been removed. Within the MBL (leg 2, 18.7–19.4 hours), mean CN and RCN concentrations agreed to within 30% and 5%, respectively (Table 3), and their structure was generally replicated on both platforms. UCN concentrations were within 10% on the two aircraft and also trended together (Figure 5h). The agreement in the above parameters started at ~18.6 hours, corresponding to an altitude of ~4 km (Figure 2e). Above this altitude (including the 5.2 km leg), the P3-B CN and UCN concentrations were systematically lower by up to ~65% than those measured on the DC-8; these differences are discussed in section 10.2. P3-B UCN values were also less than CN by 10–15% but within the reported errors. P3-B RCN concentrations were lower by a factor of 3 when compared to the DC-8 measurements. UF concentrations (UCN − CN) were negligible for both aircraft during the two legs.

[53] During leg 1 (5.2 km altitude), the DC-8 RCN ratio was approximately twice the P3-B value (Figure 5i), but both values were less than 0.1 and revealed a large volatile aerosol fraction. This is frequently observed in the clean free troposphere (FT) over the remote Pacific Ocean. RCN ratios for both aircraft in the MBL were above 0.5, indicating a much less volatile aerosol. On the descent profile between the two legs (from 18.5 to 19.0 hours), there was considerable variability in both RCN ratios, but in general, the two trended together. The large difference in RCN ratios at high-altitude was driven by the differences in RCN and CN concentrations.

[54] This difference in measured CN and RCN behavior between the high- and low-altitude legs is further illustrated in the scatterplots and regression analyses shown in Figures 6e and 6f. The CN data for leg 1 (black squares and line) resulted in a slope of 1.54, outside of the reported uncertainty, and considerable scatter in the data with an R^2 value of 0.55 (Table 5). The observed discrepancy is significant and is addressed in section 10. Leg 1 RCN concentrations for this altitude (black squares and line) had a slope of 3.34 and a R^2 of 0.12 and indicate major disagreement between the two platforms well outside of the listed uncer-

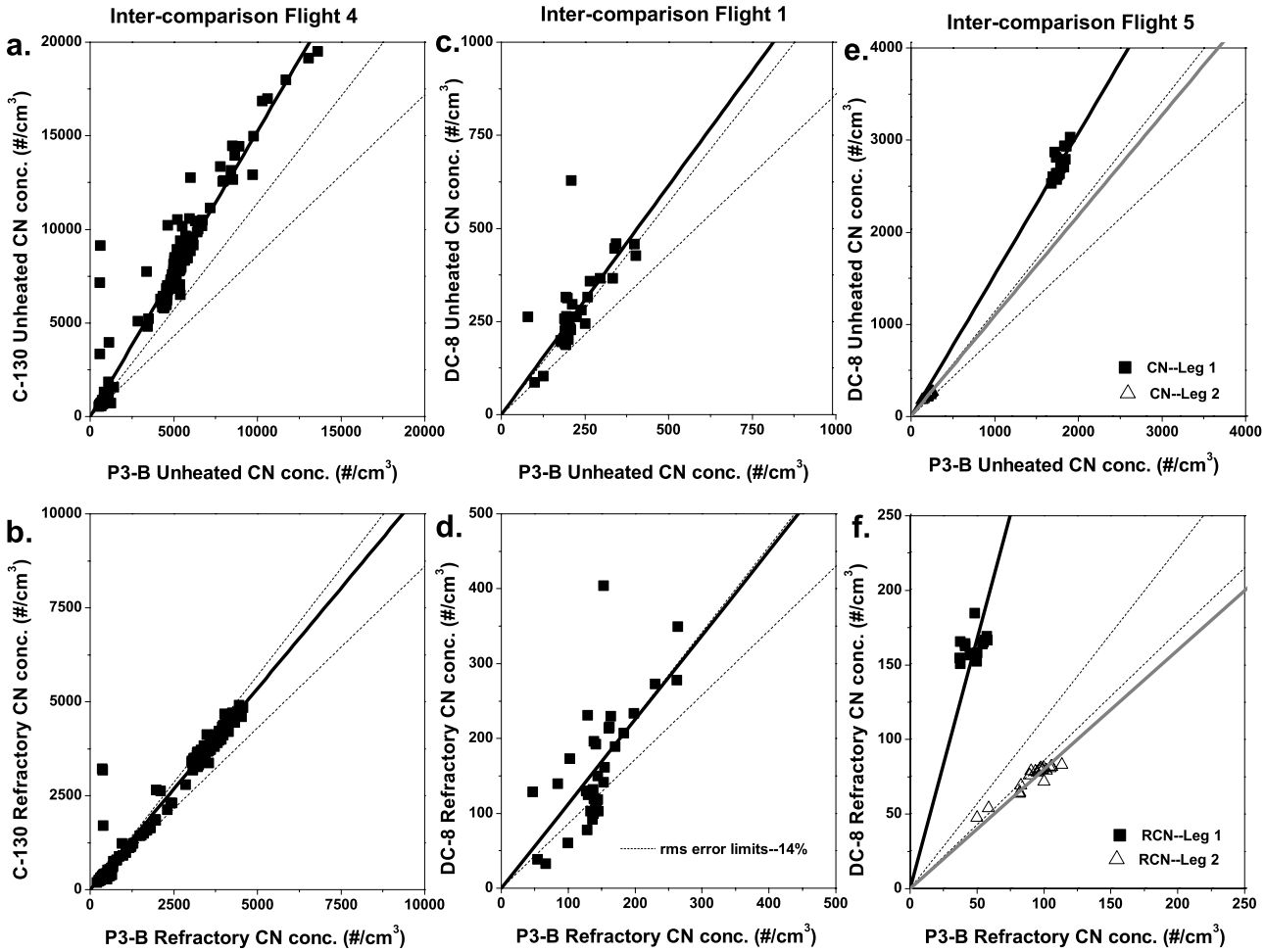

Figure 6. Scatterplots and regression analysis of the CN concentrations for the comparison flights/legs shown in Figure 5. The *x* axes correspond to P3-B data. The *y* axes are for the other compared platform. Estimated RMS uncertainties based on the ideal 1:1 line are shown. Regression lines forced to pass through the origin are also plotted. Results from this analysis are presented in Table 5. (a) CN data for flight 4. (b) RCN data for flight 4. (c) Same as Figure 6a, but for flight 1. (d) Same as Figure 6b, but for flight 1. (e) Same as Figure 6a, but for flight 5. The FT leg (leg 1, 5.2 km, black squares) and MBL leg (leg 2, 0.2 km, triangles) have been separated. (f) Same as Figure 6e, but for the RCN concentrations.

tainty. However, the leg 2 CN and RCN data (triangles and gray lines) are in much better agreement between the two platforms, with regression parameters of 1.08 and 0.8 (slopes) and 0.89 and 0.90 (R^2), respectively. The CN and RCN values between the DC-8 and P3-B during the MBL leg agreed to within the specified uncertainties. The slope of the regression analysis of RCN concentrations suggested disagreement of 20%, within the reported RMS errors (28%).

8. Aerosol Size Distributions and Integral Properties

8.1. ACE-Asia C-130 and TRACE-P P3-B: Intercomparison Flight 3

[55] Figure 7 shows the combined unheated number distributions from the DMAs and OPCs from both aircraft. Figure 7 shows the distributions with the concentrations on a log scale that allow the distributions to be viewed for the full range of diameters; the inset show concentrations on a linear scale, allowing for a more direct visual comparison between the four instruments. The distributions showed agreement in both shape and concentration between the DMA and OPC on each platform and between the two aircraft. Lognormal fits were performed on the combined OPC/DMA accumulation mode distributions. The number geometric mean diameters for the two distributions were 0.181 μm for both aircraft with standard deviations (σ_g) of 0.564 and 0.511 for the P3-B and C-130, respectively. Fitted amplitudes were 780 and 772 numbers cm^{-3} for the P3-B and C-130. In both cases the fits were good, with R^2 values of 0.988 (P3-B) and 0.982 (C-130). The differences in larger sizes are the greatest for this case (Table 3, flight 3, coarse volume) due to short sample times (Figure 2c) and nonsynchronous measurements (see instrument section).

[56] OPC accumulation mode integral surface areas for the C-130 and P3-B (Figure 8a) exhibited agreement within the stated 20% uncertainty (28% RMS error) over the wide range of surface areas measured from ~10 to ~300 μm^2 cm^{-3}

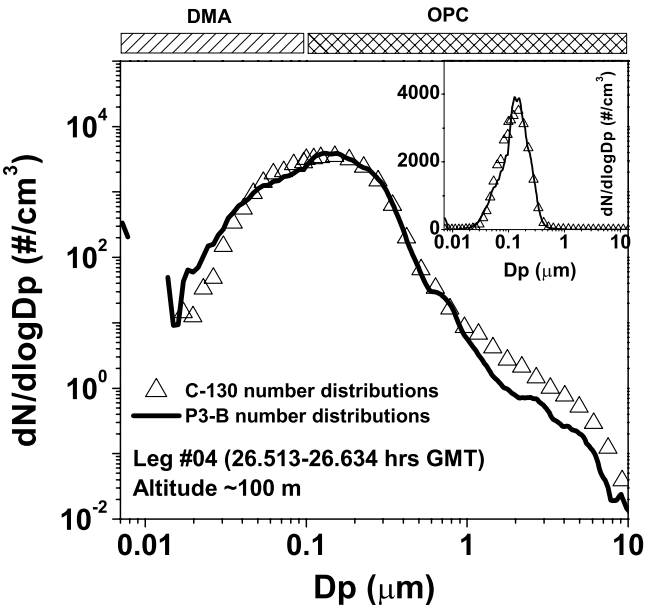

Figure 7. Leg-averaged combined DMA and OPC number distributions for comparison leg 4 during flight 3. Plot is on a log-log scale in order to observe the number distribution out to the largest sizes. Inset shows the same distributions but with a linear *y* axis (concentration). Note that these data are not STP corrected.

and over significant gradients. The highest surface areas were found on legs 1, 3, 4, and 5 in the MBL below 1.5 km altitude (Figure 2c). The average effective diameters for the two OPCs (not shown) were both ~0.25 μm with differences less than 5% over the entire comparison period in spite of the gradients observed in the data.

[57] Generally, greater variability was evident in the measured coarse particle surface areas (Figure 8b) due to the much lower count statistics for the larger sizes, especially over short timescales and expected differences in the inlet passing efficiencies. The C-130 OPC coarse mode surface area values were frequently higher than the P3-B data. This difference was consistent with the observed discrepancy between the total aerosol light scattering measured on the aircraft during flights 3 and 4, where P3-B values were between ~10% and 25% lower (Table 3). The higher C-130 values were probably due to enhancement in the largest aerosol due to the LTI and losses in the P3-B SDI.

[58] The FSSPs are wing-mounted probes and not affected by inlet and plumbing losses. Also, since the FSSP size distributions are measured at ambient RH and are not dry like the OPCs, FSSP integral properties should be greater than corresponding OPC measurements when the ambient RH is "high," especially when more than 45%. The actual RH at which we expect the dry and "wet" measurements to diverge is strongly dependent upon aerosol composition [*Tang and Munkelwitz*, 1993]. Portions of this flight where FSSP coarse mode surface areas were higher than the OPC measurements (Figure 8b) occurred predominately during periods where the ambient RH was above 55% (Figure 2c), with the greatest differences corresponding to the highest RH.

[59] P3-B FSSP coarse mode surface areas during the first two legs were lower than both the C-130 FSSP measurements and the OPC data, suggesting that P3-B FSSP data for these two legs were not accurate. There was a lot of variability in the coarse mode average effective diameter for all four instruments (not shown). However, this parameter was generally around 2.5 μm for both OPCs, and agreement was within ~15%. The P3-B FSSP average effective diameter was also ~2.5 μm until ~26.0 hours when it increased to ~4.9 μm when the ambient RH increased to 64% (Figure 2c) where we would expect hygroscopic growth to play a role. At ~26.5 hours when the aircraft entered drier air, the P3-B FSSP effective diameter decreased until ~26.9 hours, where the RH increased and it is again ~4.9 μm. The C-130 FSSP coarse mode surface area and average effective diameter were highly variable throughout but generally exhibited the same behavior as the P3-B FSSP (growth to larger sizes during legs with higher ambient RH).

[60] Figure 8c shows leg-averaged surface area distributions for leg 5 where ambient RH was ~70%, and the distributions exhibited good agreement between the two OPCs for both the accumulation and coarse modes (below 8.0 μm, counting statistics get progressively worse at larger sizes). The FSSP coarse mode distributions revealed modest agreement with each other, except below 1.0 μm. Both FSSP distributions had greater amplitudes and were at larger sizes in the coarse mode than the corresponding OPC distributions, consistent with the higher instrument RH. The P3-B FSSP distribution was clearly not capturing the majority of the accumulation mode.

[61] Figure 9a shows the scatterplot and regression line for the OPC dry accumulation mode surface area. Also shown in Figure 9 are both the 28% and 71% RMS uncertainty estimates for these measurements as reported in Table 1. The slope of the regression line for the C-130 and P3-B measurements is 0.95 with a R^2 value of 0.84 (Table 5). While there is some scatter in the data as evidenced by the intermediate values of R^2, the agreement is within the reported uncertainties for the OPC accumulation mode measurements.

[62] Figure 9b shows the coarse mode surface area data comparison between the OPC dry and FSSP ambient data for the C-130 and P3-B. For the OPC comparison, the slope of the regression line is 1.13, within the reported estimated errors, but had considerable scatter with a R^2 of 0.05. This value is low but not necessarily unexpected due to the difficulty in making coarse mode measurements on an aircraft and associated poor counting statistics. The low R^2 is also driven by several outliers, and after their removal, the R^2 value increased to 0.55. The FSSP coarse mode surface areas have relatively low correlation with a R^2 of 0.66 but have a slope of 0.73 that is within the reported 71% RMS uncertainty. The scatterplot for the FSSP comparison reveals a difference in instrument performance, with two separate "clusters" in the data. For P3-B data below 20 $\mu m^2\ cm^{-3}$, the P3-B FSSP appears to underestimate the coarse mode surface area relative to the C-130 data. After performing a regression analysis on this portion of the data, we obtain a slope of 1.60 and a R^2 of 0.66. For the data above this cutoff, we find a lower slope of 0.69 with much more scatter (R^2 equal to 0.25). These measurements agreed within the expected 71% RMS uncertainty, and considering the difficulties in measuring large particles on an aircraft,

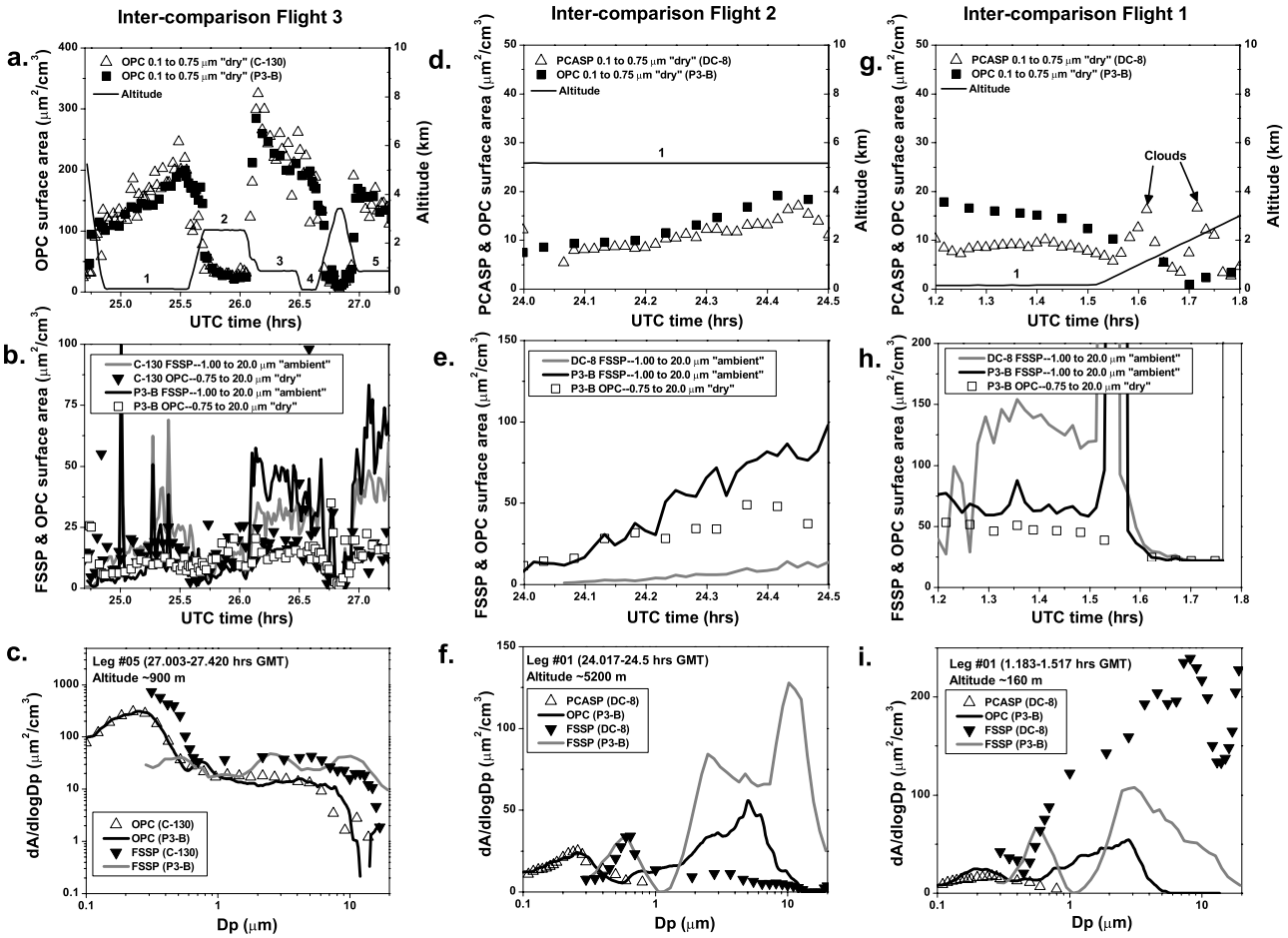

Figure 8. (a) Time series of altitude and OPC accumulation mode integral surface areas for flight 3 (ACE-Asia C-130/TRACE-P P3-B). (b) Time series of OPC and FSSP coarse mode integral surface areas for the same flight. (c) Log-log plot of the leg-averaged OPC and FSSP surface area distributions for comparison leg 5 (log-log was chosen since the accumulation mode surface area dominates the coarse mode). (d) Same as Figure 8a, but for flight 2. (e) Same as b), but for flight 2. (f) Same as Figure 8c, but for flight 2. These distributions are on a linear concentration scale since the accumulation and coarse mode distributions are of similar amplitudes. (g) Same as Figure 8a, but for flight 1. (h) Same as Figure 8b, but for flight 1. (i) Same as Figure 8c, but for flight 1 (concentration also on linear scale). Note that these data are not STP corrected. See Figure 1 and Table 2 for a complete listing of intercomparison locations.

these data seem reasonable. Some of this disagreement in slopes and low R^2 values is artificial since we forced the regression to go through zero.

8.2. TRACE-P DC-8 and P3-B Comparison

8.2.1. Intercomparison Flight 2

[63] The P3-B OPC and DC-8 PCASP accumulation mode surface areas exhibited agreement within 25% (Figure 8d) and trended toward higher values toward the end of the leg, consistent with aerosol optical properties (Figures 3d and 3e). This trend was not due to the rise in ambient RH and associated hygroscopic growth since the OPC instrumental RH was relatively constant (Figure 2b). The average effective diameter derived from the PCASP and OPC agree within 1% (not shown) at ~0.26 μm and remained constant over the leg, indicating that the increases in accumulation mode surface area are due to increases in concentration rather than aerosol size.

[64] Coarse mode surface areas from the OPC (P3-B) and FSSPs (P3-B and DC-8) are shown in Figure 8e. During the first portion of the leg from 24.0 to 24.225 hours where the ambient RH was less than 10% (Figure 2b), the OPC and FSSP coarse mode integral surface areas from the P3-B agreed, but the FSSP data increased relative to the OPC measurement after ambient RH increased above 25% (Figure 2b), and the differences grew larger as the humidity continued to climb. However, the DC-8 FSSP coarse mode integral surface area was only ~20% of the P3-B values throughout the entire leg, although the DC-8 data did exhibit the same trend to larger values.

[65] The OPC-derived coarse mode effective diameter (not shown) was relatively constant at ~4.0 μm, while the FSSP effective diameters for both the P3-B and DC-8 showed a gradual increase presumably due to the increase in ambient RH and water uptake. Leg-averaged surface area distributions for the four instruments (DC-8 PCASP and FSSP and

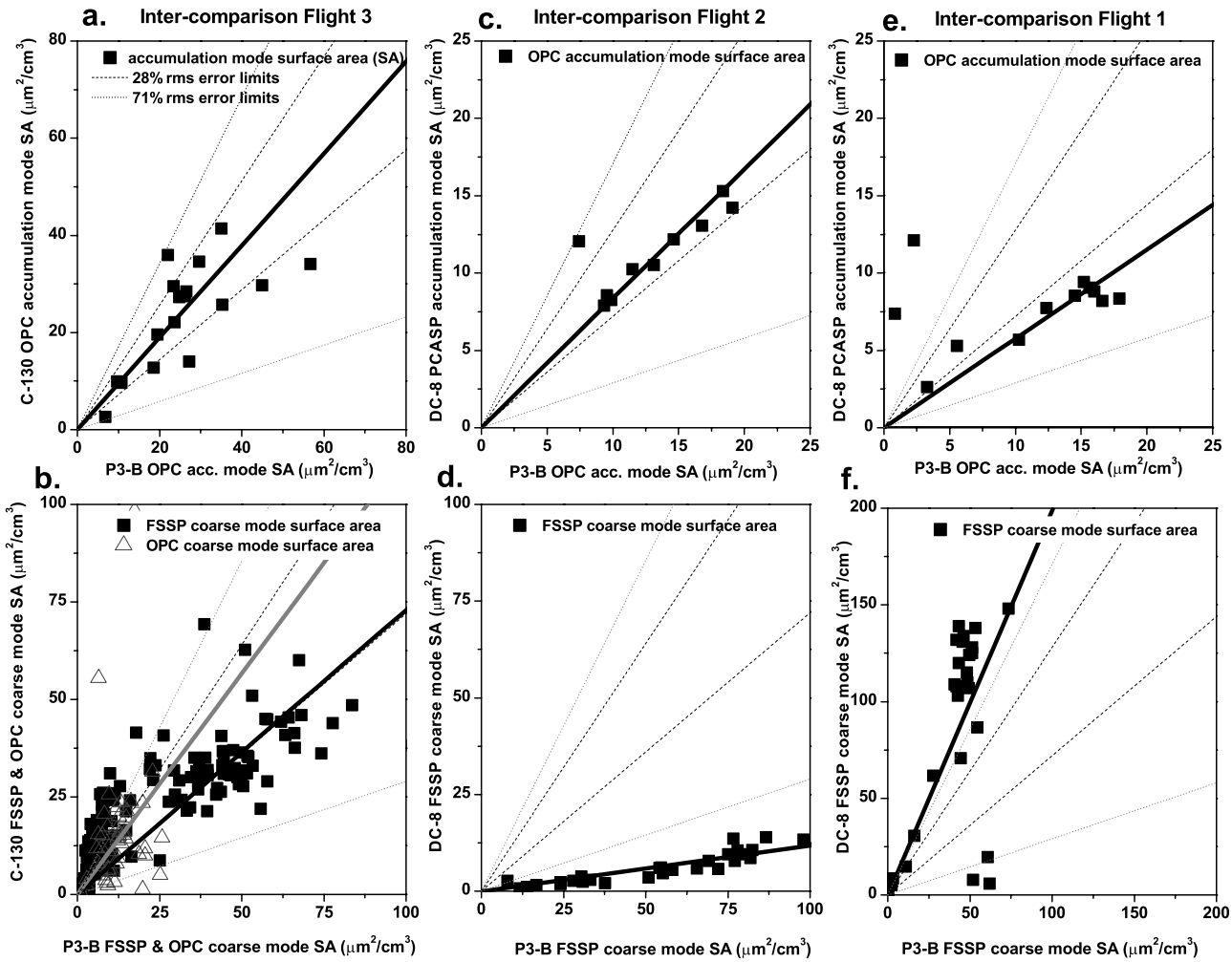

Figure 9. Scatterplots and regression analysis of the integral surface areas for the comparison flights/legs shown in Figure 8. The *x* axes correspond to P3-B data. The *y* axes are for the other compared platform. Estimated uncertainties based on the ideal 1:1 line are shown. One set of lines is based on an estimated 28% uncertainty; the other set is based on 71%. Regression lines forced to pass through the origin are also plotted. Results from this analysis are presented in Table 5. (a) OPC accumulation mode data for flight 3. (b) Coarse mode data for flight 3. The black squares are for the FSSP data; the triangles are for the OPC. (c) Same as Figure 9a, but for flight 2. On this flight, the instruments compared are the OPC and PCASP. (d) Same as Figure 9b, but for flight 2 (only FSSP data). (e) Same as Figure 9c, but for flight 1. (f) Same as Figure 9d, but for flight 1.

P3-B OPC and FSSP) are shown in Figure 8f, and the dry accumulation mode distributions (OPC and PCASP) exhibited good agreement in both shape and concentration. Again, the DC-8 FSSP distribution showed much less surface area in the coarse mode than either the P3-B OPC or FSSP, consistent with the integral values. The P3-B FSSP coarse mode distribution revealed more surface area and the presence of larger aerosols than the OPC, consistent with both hygroscopic growth and the loss of the largest particles due to plumbing/inlet losses as measured by the OPC.

[66] The OPC/PCASP dry accumulation mode surface areas are shown in Figure 9c as well as the 28% and 71% RMS uncertainty estimates for these measurements as reported in Table 1. The slope of the regression line for the DC-8 and P3-B accumulation mode surface areas is 0.84, within the estimated 28% error, and had a R^2 value of 0.65 (Table 5). The low R^2 is driven by one point; after removing this point the value is increased to 0.92.

[67] The poor agreement between the DC-8 and P3-B FSSP instruments are confirmed in Figure 9d. Although the R^2 of 0.83 shows that the FSSP coarse mode surface areas trend together on the two aircraft, the slope of this regression line is only 0.19 and reveal major problems in one or both of the FSSPs. Because of the relatively good agreement between the C-130 and P3-B FSSPs discussed in section 8.1 and that the P3-B FSSP is more consistent with the OPC coarse mode measurements on this flight (Figure 8e), we conclude that the DC-8 values of FSSP surface area are unrealistically low and represent an unidentified instrumental bias.

8.2.2. Intercomparison Flight 1

[68] The DC-8 integral PCASP accumulation mode surface areas (Table 3 and Figure 8g) were lower than OPC

values measured on the P3-B after excluding cloud affected time periods (~1.6–1.75 hours, Figure 2a). For most of this MBL leg, the ambient RH was ~75%, and the OPC RH was near 30%, but the PCASP RH was unknown. Hence we cannot assert that hygroscopic effects can be used to explain the PCASP and OPC differences, although this is possible. Also, the P3-B measurements showed a general trend toward lower values during the MBL leg (1.2 to 1.65 hours) while the PCASP surface area was relatively constant. The average effective diameters (not shown) were similar at ~0.33 μm for both PCASP and OPC and persisted throughout the MBL leg. The ship plume evident in Figures 3h and 5d is not as apparent in the surface area measurements since these instruments measure the larger particles and ship plumes are predominantly composed of aerosols with diameters less than the size range of these instruments.

[69] In contrast to flight 2 where the DC-8 FSSP measurements were systematically lower than on the P3-B, the DC-8 FSSP coarse mode surface areas were about twice the P3-B values (Figure 8h). This difference in the DC-8 FSSP behavior between the wet MBL on this flight and the dry FT during flight 2 is not well understood at present. The OPC coarse mode surface area was ~2/3 of the P3-B FSSP measurement while the aircraft were in the MBL (~1.2–1.6 hours) and agreed to within 2% after climbing to ~3 km in dry air. This is consistent with hygroscopic growth from dry to ambient conditions in the MBL with ambient conditions aloft being drier and growth is not expected (Figure 2a). Both the P3-B OPC and FSSP coarse mode measurements showed a general trend to smaller values from the beginning to the end of the MBL leg, while trends in the DC-8 FSSP surface area data are less apparent.

[70] The coarse mode average effective diameters (not shown) exhibited agreement within 20% between the two FSSPs with average values of ~5.0 μm, despite the discrepancy in integral surface areas (Figure 8h). The OPC coarse mode averaged effective diameter was less than this at ~2.5 μm, again consistent with water uptake by the ambient aerosol. Figure 8i plots the DC-8 PCASP and FSSP and P3-B OPC and FSSP leg-averaged surface area distributions for the MBL leg. PCASP and OPC distributions revealed good agreement below 0.6 μm. However, the FSSPs exhibited large differences between the two aircraft. The P3-B FSSP surface area distribution appeared to be more consistent with the OPC after allowing for hygroscopic growth of the aerosol.

[71] The scatterplots of the OPC/PCASP dry accumulation mode surface areas are shown in Figure 9e and include the RMS uncertainty estimates (Table 1). The slope of the regression line for the DC-8 and P3-B measurements is 0.58. This is outside of the 20% uncertainty estimated by the P3-B group but close to the 50% error reported for the DC-8. Propagating these two uncertainties results in a combined RMS error of 54%, and the slope of the regression line is close to this value. The regression had considerable scatter of the data and resulted in a R^2 value of 0.06 (Table 5). Two outliers associated with cloud penetrations were primarily responsible for the low R^2. After removing these points, R^2 increased to 0.89. We are not confident as to the cause of the larger difference observed between the OPC and PCASP measurements on this flight relative to the other intercomparison flights, although hygroscopic effects may be playing a role.

[72] The DC-8 and P3-B FSSP coarse mode surface area measurements are shown in Figure 9f. The slope of the plotted regression line is 1.99 and revealed a significant difference in FSSP performance for this flight compared to the previously discussed DC-8/P3-B intercomparison flight (flight 2) where DC-8 FSSP data were lower rather than higher than the P3-B surface areas. The R^2 was 0.56, but after removing three outliers associated with the cloud penetration data, the FSSP coarse mode surface areas resulted in a R^2 value of 0.84. Once again, the P3-B FSSP is more consistent with the OPC coarse mode measurements on this flight (Figure 8h), indicating instrumental issues with the DC-8 FSSP measurements.

9. Aerosol Chemistry

9.1. ACE-Asia C-130 and TRACE-P P3-B: Intercomparison Flight 3

[73] The soluble aerosol chemical concentrations for the C-130 and P3-B are shown in Figure 10 for comparison flight 3 (Na^+, Ca^{2+}, Mg^{2+}, Cl^-, NH_4^+, SO_4^{2-}, and NO_3^- are shown in Figures 10a, 10b, 10c, 10d, 10e, 10f, and 10g, respectively), and leg-averaged concentrations are contained in Table 4. Similar PILS instruments with the same impactor cut sizes showed good agreement for the majority of species [*Orsini et al.*, 2003; *Weber et al.*, 2001]. The aerosol constituents usually associated with the coarse mode (e.g., Na^+, Ca^{2+}, Mg^{2+}, and Cl^-) in general trended together and with the OPC coarse mode surface area (Figure 8b) and suggested the presence of sea salt and a nearly equal amount of Ca, indicating dust. Since soluble Ca^{2+} is only a small fraction of dust (3–4% (R. Arimoto, personal communication)), this implies that there was relatively more dust than sea salt sampled. The chemical species usually associated with accumulation mode aerosols (i.e., NH_4^+, SO_4^{2-}, and NO_3^-) agree to within ~30% (Table 4) between the two aircraft over a wide range of concentrations and also trended together and with the measured OPC accumulation mode surface areas (Figure 8a).

9.2. TRACE-P DC-8 and P3-B Comparison

9.2.1. Intercomparison Flight 5

[74] The aerosol chemical constituent concentrations measured on the DC-8 and P3-B are shown in Figures 11 and 12, and leg averages are contained in Table 4. Since the PILS instrument (P3-B) had a 50% size cut of 1.3 μm and the filter samples (DC-8) were bulk aerosol measurements ($D_p <$ ~6.0 μm), the large discrepancies for Na^+, Ca^{2+}, Mg^{2+}, and Cl^- are not surprising (Figures 11a, 11b, 11c, and 11d, respectively). Sodium concentrations in the MBL were ~3–5 μg m^{-3} (standard cubic meters) as measured on the DC-8, much higher than in the previously discussed flight and suggested the presence of significant sea salt. DC-8 Ca^{2+} concentrations were ~0.25 μg m^{-3}. Assuming that soluble Ca^{2+} composed ~3–4% of the dust concentration (R. Arimoto, personal communication), this implies ~8 μg m^{-3} of dust during the MBL leg, roughly the same concentration as Na^+. At ~18.8 hours during the descent profile, a layer of elevated Na^+ and Ca^{2+} concentrations was observed between 2.0 and 3.0 km. This layer was located

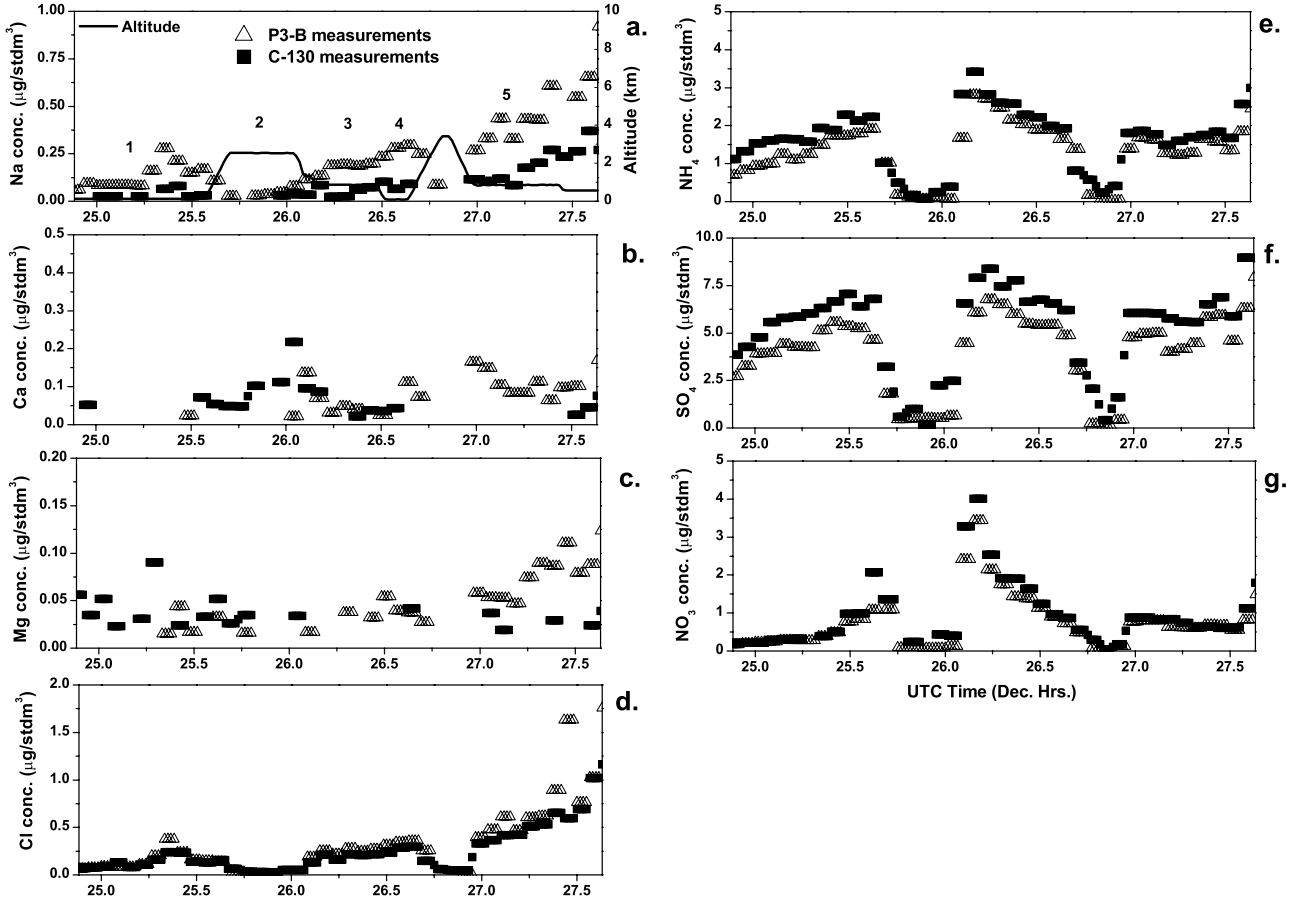

Figure 10. Soluble aerosol chemical constituent concentrations measured with identical PILS instruments (50% cut size of 1.3 μm) during flight 3 (ACE-Asia C-130/TRACE-P P3-B). These data have been corrected to STP. Time series of (a) altitude and Na^+, (b) Ca^{2+}, (c) Mg^{2+}, (d) Cl^-, (e) NH_4^+, (f) SO_4^{2-}, and (g) NO_3^- concentrations.

just above the inversion and cloud top level and in very dry air (Figure 2e). The Ca^{2+} concentrations were higher than in the MBL, and Na^+ concentrations were ~1/2 those observed below, indicating a higher relative fraction of the coarse aerosol was mineral dust.

[75] The time series of NH_4^+, SO_4^{2-}, and NO_3^- concentrations (Figures 11e, 11f, and 11g, respectively) displayed the same trends on board both aircraft, although the DC-8 values were systematically higher than on the P3-B, especially for SO_4^{2-} and NO_3^-. This was most likely due to the association of these species with the larger coarse mode aerosol (i.e., dust and sea salt) and the PILS cut size (see section 10.4). The MC/IC fine sulfate concentrations measured on the DC-8 exhibited agreement close to the stated 28% uncertainty with the PILS measured SO_4^{2-} (Figure 11f and Table 4).

[76] Scatterplots for the comparison of DC-8 filter and P3-B PILS measured NH_4^+, SO_4^{2-}, and NO_3^+ concentrations are shown in Figures 13d, 13e, and 13f, respectively, and include the 28% RMS uncertainty estimates (Table 1). Also included in Figure 13e is the DC-8 MC/IC measured fine sulfate versus the PILS SO_4^{2-}. The slope of the regression line for the NH_4^+ concentrations for this flight is 1.72 with a R^2 value of 0.77. This slope is outside the reported 28% uncertainty. The SO_4^{2-} comparison between the bulk filter sample and the PILS instrument (solid black line) results in a slope of 2.01 and R^2 of 0.79, while the DC-8 fine sulfates (triangles) have a slope of 0.83 and R^2 of 0.74. The NO_3^- comparison results give an even higher regression slope of 3.72 and more scatter, with R^2 equal to 0.32. These differences between the P3-B PILS and DC-8 filter measurements of aerosol chemical compositions are significant even though this subset of soluble constituents is thought to be predominantly associated with the accumulation mode and, if that were the case, should not be significantly different between the two methods despite the different size cuts. The fact that the DC-8 fine sulfate is within the estimated uncertainty for the measurements is a strong indicator that the observed systematic differences are due to these species also being associated with the larger, coarse mode aerosol and is addressed in section 10.4.

9.2.2. Intercomparison Flight 2

[77] Aerosol soluble chemical concentrations for this flight are shown in Figure 12, and leg-averaged values are listed in Table 4. The ratios of the DC-8 to the P3-B measurements for a given species are also shown (black lines) in Figure 12. The Na^+, Ca^{2+}, Mg^{2+}, and Cl^- concentrations (Figures 12a, 12b, 12c, and 12d, respectively) appeared enhanced by a factor of 3–5 on the DC-8 when compared to those on the P3-B due to the PILS cut size. The

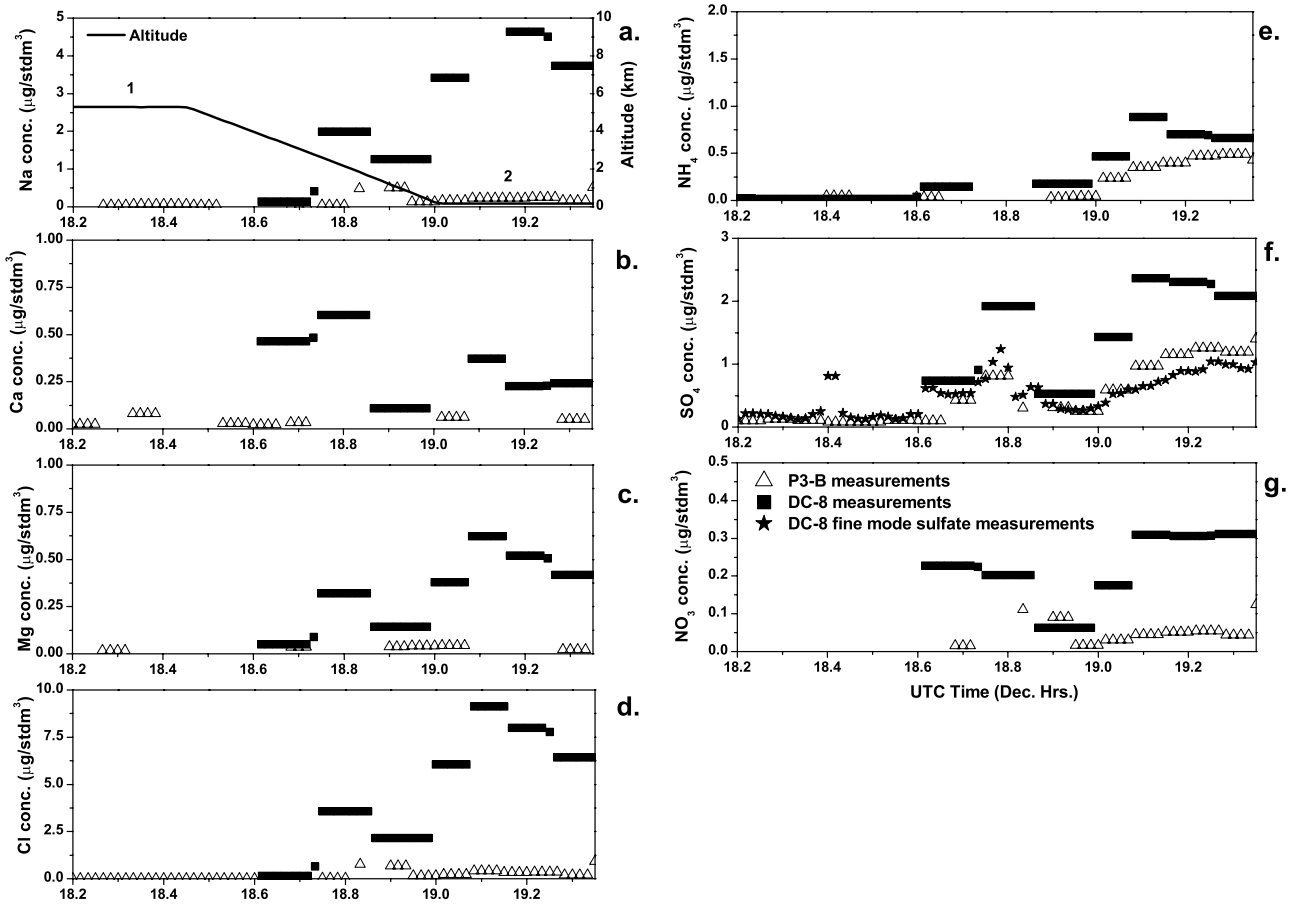

Figure 11. Soluble aerosol chemical constituent concentrations measured with bulk filters (DC-8) and PILS instrument (P3-B) during flight 5 (TRACE-P). These data have been corrected to STP. Time series of (a) altitude and Na^+, (b) Ca^{2+}, (c) Mg^{2+}, (d) Cl^-, (e) NH_4^+, (f) SO_4^{2-}, and (g) NO_3^- concentrations. Also included in Figure 11f is the DC-8 MC/IC fine sulfate.

DC-8 measurements indicated concentrations of Na^+ and Cl^- over a factor of 10 less than on flight 5, but Ca^{2+} concentrations were $\sim$2.0 μg m^{-3}, much higher than on flight 3 or 5, implying a greater concentration of dust aerosol.

[78] NH_4^+, SO_4^{2-}, and NO_3^- concentrations (Figures 12e, 12f, and 12g, respectively) exhibited much higher concentrations on the DC-8 than on the P3-B by approximately the same amount as those species usually associated with the coarse mode at $\sim$2–4 times the P3-B values. This is true even for the MC/IC fine and PILS sulfate concentrations (see section 10). Soluble aerosol species measured on both platforms exhibited a gradient from smaller to larger values near the end of the leg, consistent with aerosol light scattering and absorption coefficients (Figures 3d and 3e) and aerosol integral accumulation and coarse mode surface areas (Figures 8d and 8e).

[79] Figures 13g, 13h, and 13i show the scatterplots and regression lines for the DC-8 filter and P3-B PILS measured NH_4^+, SO_4^{2-}, and NO_3^- concentrations, respectively, and also include the 20% uncertainty estimates (Table 1). Also included in Figure 13h is the DC-8 MC/IC measured fine sulfate versus the PILS SO_4^{2-}. The regression line for the NH_4^+ concentration comparison results in a slope of 3.75. There is no R^2 value since there was only one set of P3-B PILS measurement to compare. The DC-8 total SO_4^{2-} data (black squares) comparison results in a slope of 2.77 and R^2 of 0.82, while the DC-8 fine sulfate (triangles) had a slope of 2.08 and R^2 value of 0.36, respectively (Figure 13g). The NO_3^- regression analysis had a slope of 2.14 and R^2 value of 0.84. These differences between the P3-B PILS and DC-8 filter measurements are addressed in section 10.4.

10. Discussion

[80] Some measurements reported above often showed agreement within the stated instrument uncertainties in aerosol concentrations, size distributions, integral surface areas, effective diameters, optical properties, and chemical components. However, several systematic and/or large differences were observed and highlighted in the data. In sections 10.1–10.5, we explore likely reasons for these discrepancies.

10.1. Aerosol Optics

[81] Total aerosol scattering and absorption coefficients measured on the P3-B were systematically lower than on the C-130 by 11–25% during comparison flights 3 and 4 as is evident from the time series and tabulated leg averages,

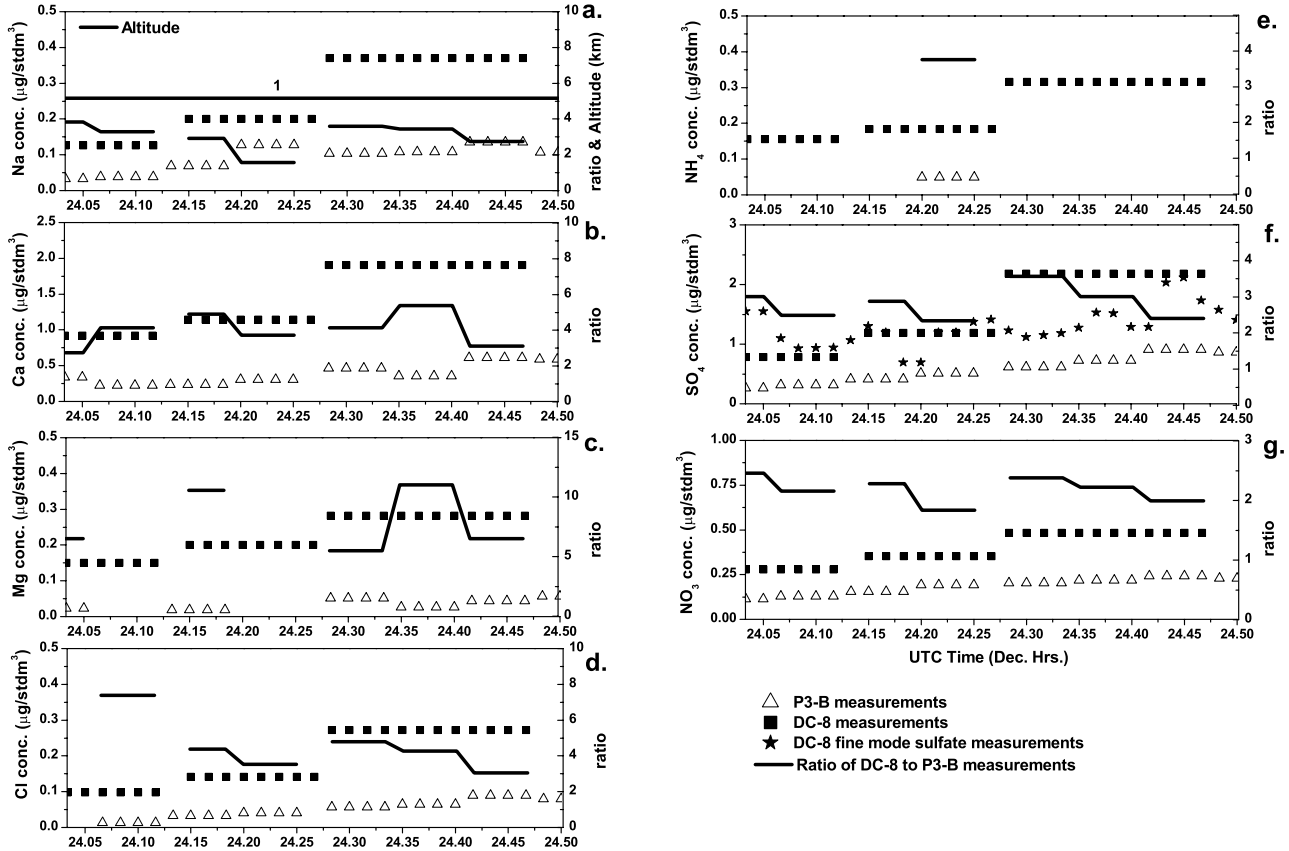

Figure 12. Same as Figure 11, except for flight 2 (TRACE-P DC-8/P3-B). Also included are the ratios (black lines) of the DC-8 to the corresponding P3-B measurements.

while submicrometer scattering coefficients (no submicrometer absorption measurements on the C-130) agreed within 5–10% for most legs between the two aircraft. These two observations suggest that the differences in total optical properties observed were due to the probable enhancement of coarse particles seen by the LTI and/or losses in the SDI.

[82] During the Passing Efficiency of a Low-Turbulence Inlet (PELTI) experiment where the LTI (C-130) and SDI (P3-B) were flown on the same aircraft, total aerosol scattering measured behind the LTI was higher than SDI measurements by ~10–20% for dry dust and wet sea salt cases, respectively. This is reported in the PELTI NSF final report by B. J. Huebert et al. (2000, available online at http://raf.atd.ucar.edu/Projects/PELTI/). The C-130/P3-B total scattering difference generally ranges between the two cases measured during PELTI, not surprising since these flights frequently sampled air that contained both sea salt and dust with intermediate values of ambient RH. There were no aerosol absorption measurements during PELTI, but the enhancements observed for the C-130 data during ACE-Asia are consistent with enhanced dust (mildly absorbing) concentrations due to the LTI. Single scatter albedos were generally within 5% from the two aircraft (resulting coalbedos were generally within 50%). The systematic ~20% lower P3-B total scattering values were offset by the same systematic differences in total absorption.

[83] Results for the DC-8/P3-B comparison of total optical properties (no submicrometer measurements on the DC-8) revealed different behavior under different sampling regimes. The DC-8 and P3-B scattering coefficients agreed within 10% aloft in the FT in dry air and in the presence of coarse dust aerosol. However, total scattering coefficients measured on the DC-8 were lower than on the P3-B by a factor of 2 or more when sampling in the clean MBL with high-ambient RH and relatively high-concentrations of sea salt.

[84] Comparison flight 5 provided an opportunity to sample in both dry FT air with dust and in the wet MBL with relatively more sea salt during the same flight. The aircraft altitude and total scattering for the DC-8 and P3-B and submicrometer scattering for P3-B are shown in Figure 14a. During the high-altitude leg, scattering coefficients on both aircraft were low (~0.7 Mm^{-1}, Table 3) and measurements from the two platforms are within 27%. However, the DC-8 leg-averaged values during the MBL run were only 40% of those measured on the P3-B (Table 3), similar to the MBL comparison during flight 1. Here the DC-8 scattering values were approximately equal to the P3-B submicrometer scattering coefficients, implying that virtually no coarse mode particles were making it into the DC-8 nephelometer during this leg. A layer of enhanced total scattering was encountered between 2 and 4 km altitude (~18.6–18.8 hours) in very dry air (Figure 2e) during the descent profile. Here, the DC-8 and P3-B total scattering coefficients were very nearly equal. Figure 14b shows the P3-B OPC accumulation mode, coarse mode, and

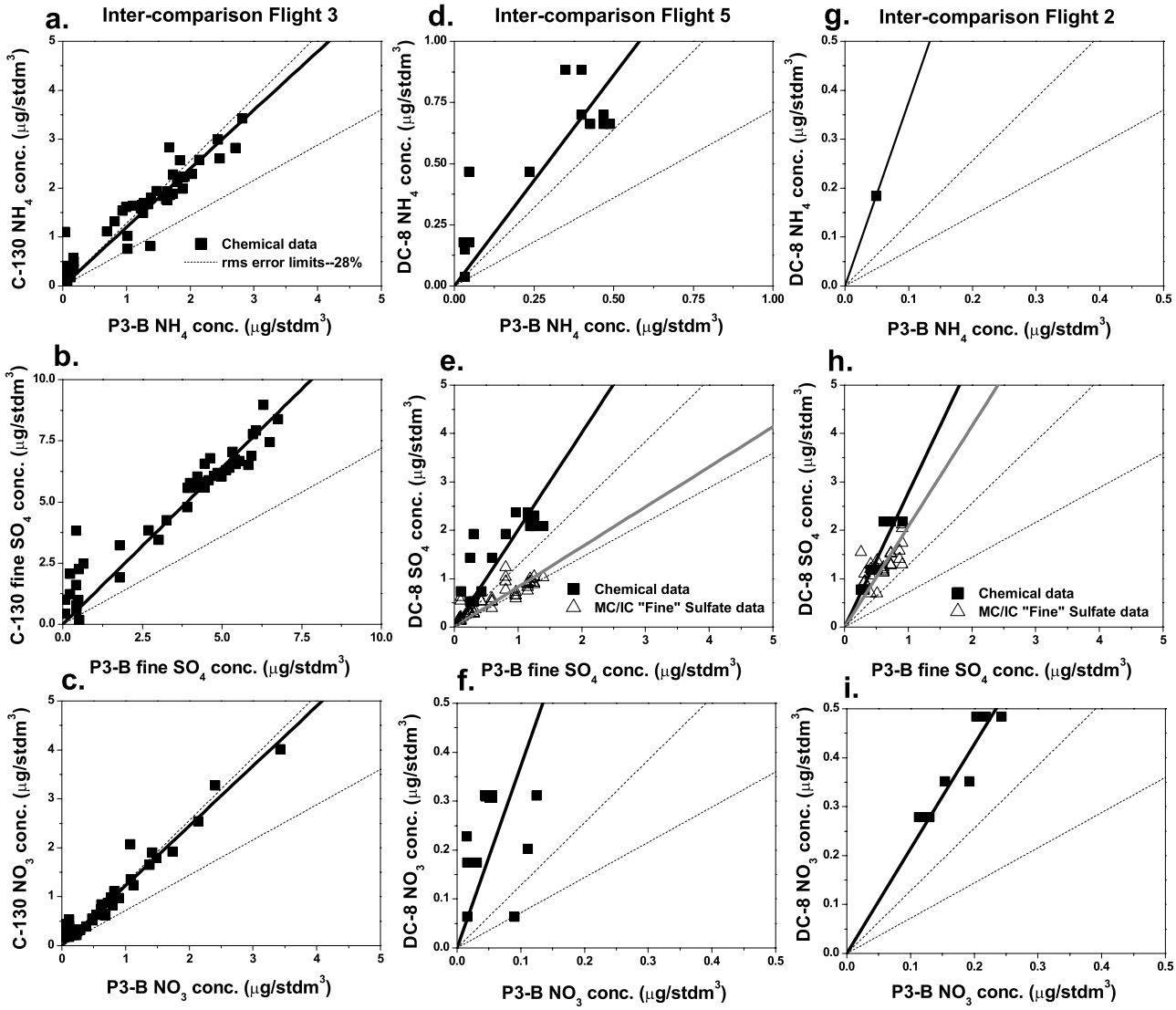

Figure 13. Scatterplots and regression analysis of the aerosol chemical constituents for the comparison flights/legs shown in Figures 10, 11, and 12. The *x* axes correspond to P3-B data. The *y* axes are for the other compared platform. Estimated uncertainties based on the ideal 1:1 line are shown. Regression lines forced to pass through the origin are also plotted. Results from this analysis are presented in Table 5. (a) NH_4^+ data for flight 3. Both sets of measurements are for the PILS instrument. (b) Same as Figure 13a, but for SO_4^{2-}. (c) Same as Figure 13a, but for NO_3^-. (d) Same as Figure 13a, but one set of data for PILS and the other for bulk filter measurements. (e) Same as Figure 13d, but for SO_4^{2-}. The black squares are for total SO_4^{2-}, the triangles are for the DC-8 fine SO_4^{2-}. (f) Same as Figure 13d, but for NO_3^-. (g) Same as Figure 13d, but for flight 2. (h) Same as Figure 13e, but for flight 2. (g) Same as Figure 13f, but for flight 2.

total dry aerosol surface areas for this period. About 2/3 of the total aerosol surface area was due to coarse mode particles in both the 2–4 km layer as well as the MBL, suggesting that there should be a similar relationship of total to submicrometer scattering at both altitudes.

[85] Aerosol Na^+ and Ca^{2+} mass concentrations for this flight are shown in Figures 11a and 11b, respectively, and from the discussion in section 8.2.1, it appears that there is more dust relative to sea salt in the dry 2–4 km layer than in the MBL. Combining this information with the scattering data from comparison flights 1 and 2 (sections 5.2.2 and 5.2.1), it appears that the DC-8 scattering data were representative of total aerosol scattering in the dry FT, even with coarse mode dust present. In the wet MBL with sea salt present, the DC-8 scattering data appear to be representative of submicrometer scattering.

[86] We believe that this difference in behavior is due primarily to two factors. The first is that despite attempts to keep the sample inlet isokinetic, the DC-8 SDI was super-isokinetic during MBL legs but closer to isokinetic sampling aloft. This would exclude some of the coarse aerosol in the MBL and also enhance turbulence within the inlet, increasing the loss of coarse aerosol to the inlet walls. The second is that wet sea salt is more likely to stick to the inlet

walls after a collision when compared to dry mineral dust that is more likely to bounce.

[87] Aerosol absorption coefficients measured on the DC-8 were within ~30% of the P3-B data when sampling in the MBL (flight 1). The agreement was within ~12% if one removed the large spike associated with a ship plume observed in the P3-B data on this flight. Aloft, DC-8 absorption was more variable and systematically higher than on the P3-B by as much as a factor of 2. We therefore tentatively conclude that within the MBL, the DC-8 absorption data may have been representative, but in the FT, the DC-8 absorption measurements were systematically high due to unknown causes.

10.2. CN Concentrations

[88] For the majority of comparison flight legs, RCN concentrations agreed within 5–10% between all three aircraft. The exceptions to this were a high-altitude P3-B/DC-8 leg during flight 5 and an individual P3-B/C-130 comparison during leg 2 of flight 3. The C-130 RCN counter experienced several failures during flight 3, hence the lack of data for the remaining legs, and we attribute this discrepancy between RCN concentrations to poor RCN counter performance on the C-130 for this flight. During the first three flights, RCN data should be removed from the ACE-Asia database. The RCN concentrations measured on the DC-8 and P3-B displayed different behaviors during the two high-altitude intercomparisons, although both were at 5.2 km altitude. During flight 2, RCN concentrations were within 27% while during leg 1, flight 5, P3-B values were ~1/3 the DC-8 concentrations.

[89] CN concentrations revealed that the C-130 data were systematically higher from 30% to a factor of 2 than the P3-B measurements, although some legs did reveal reasonable agreement (Table 3). However, the P3-B CN concentrations were within 15% to a second CN counter on the C-130 that was operated by NCAR for all comparison legs, suggesting that the C-130 CN counter (utilized in Figure 5 and Table 3) was over counting. After the comparison flights, this CN counter was tested, and detector adjustments were made that resulted in better agreement between the two C-130 CN measurements.

[90] DC-8/P3-B comparisons of CN concentrations exhibited agreement within ~25% for the majority of flight legs. Low-level MBL runs showed agreement within 1% and 30% for flight 1 and leg 2, flight 5, respectively (Table 3). After removing an outlier in the DC-8 data at ~19.1 hours (Figure 5g), the agreement between the two platforms was ~15%. Results from high-altitude comparisons of total CN were mixed. CN concentrations during comparison flight 2 agreed to within ~27% on the two aircraft, while DC-8 CN measurements were ~50% higher than P3-B values for leg 1, flight 5 (Table 3). These two legs were both at 5.2 km altitude and involved the same two aircraft, but the results showed a significant difference for both the RCN and CN concentrations.

[91] This difference in high-altitude DC-8/P3-B CN behavior is evident in DC-8/P3-B CN and RCN concentrations measured during the descent profile on flight 5 (Figure 15a). Near the surface, the CN concentrations were similar, but differences increased above 3 km altitude. Combined OPC and DMA number distributions as a function of diameter versus altitude are shaded to concentration and plotted in Figure 15b. For altitudes below 3.2 km, the size distributions revealed insignificant concentrations of the smallest particles. At the higher altitudes, the distributions showed a shift to smaller sizes with large numbers of particles with diameters below 0.02 μm. Above 4 km altitude where the differences between CN concentrations were greatest, the distributions showed that the number of particles with diameters below 0.015 μm, which is the nominal 50% cut size for the CN counters, was a significant fraction of the total number of aerosol. During flight 2 (also 5.2 km), DC-8/P3-B CN and RCN concentrations showed much better agreement and were within 27%. Size distributions for this leg (not shown) revealed no significant concentrations of the smallest aerosols. The P3-B CN counter appears to have been undercounting in "clean air" aloft compared to the DC-8 when there were large concentrations of small aerosol. This discrepancy is probably due to the differences between actual detection limits for the CN counters on the two aircraft. Note that minimum detection sizes can depend upon the saturator characteristics, the absolute temperature of the saturator, and the temperature difference between saturator and condenser. Unfortunately, the condenser and saturator temperatures were recorded only for the P3-B CN counters. Thus, if the P3-B CN and RCN counters had cut sizes just slightly larger than 0.015 μm (or if the DC-8 counters had cut sizes smaller than this), we would have expected large differences in reported CN concentrations. The DC-8 ΔT was set to 22°C and its actual cut size should have been smaller than the 0.015 μm listed as nominal. The P3-B CN counters ΔT was set to 17°C.

[92] In Figure 15c, we show combined DMA and OPC integral number concentrations after correcting to STP conditions for two different cut sizes; one integral number is for $D_p > 0.01$ μm and the other is for $D_p > 0.017$ μm. The first cut size was selected to most closely represent the CN concentrations for the DC-8 where the ΔT was set to 22°C. We selected the 0.017 μm cut size after allowing this diameter to change and selecting the cut size that best reproduced the concentrations observed on the P3-B. These results show that the integrated numbers from the sizing instruments accurately captured not only the relative behavior of the CN counters but also the absolute concentrations as observed in Figure 15a. We assert that the observed discrepancies between the DC-8 and P3-B CN data are due to the differences in the CN counter size cuts and that the actual size cuts are 0.01 μm for the DC-8 and 0.017 μm for the P3-B even though the nominal size cuts are listed as 0.015 μm for both.

[93] P3-B UCN concentrations were systematically lower than measurements on the other platforms when UCN concentrations were above several thousand numbers per cubic centimeter [*Weber et al.*, 2003]. This was due to modifications of the instrument to obtain size distributions for particles with $0.003 <= D_p <= 0.01$ μm. These modifications effectively lowered the threshold for coincidence counting due to the increased sampling volume.

10.3. Aerosol Size Distributions and Integral Properties

[94] There were not any DC-8 DMA data, so only DMA comparisons between the C-130 and P3-B were presented.

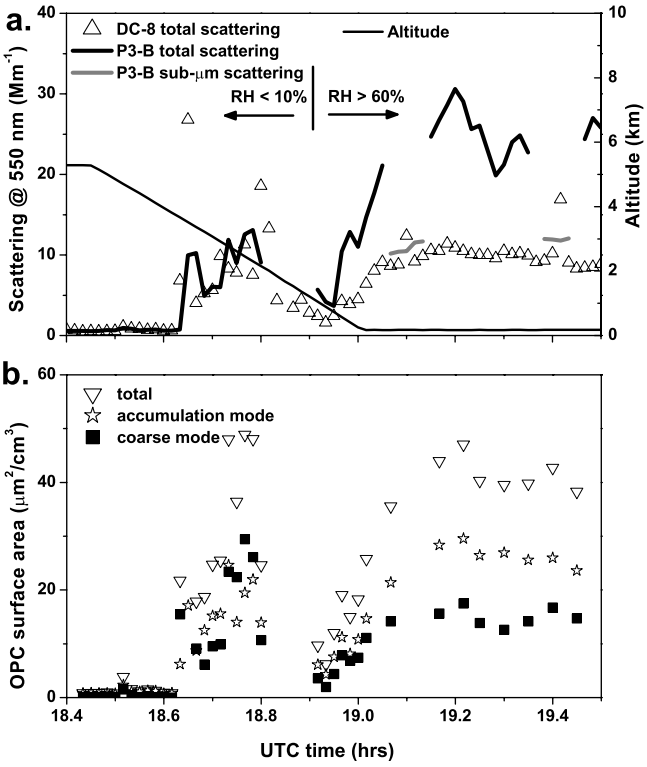

Figure 14. (a) Time series of altitude and total and submicrometer scattering coefficients for flight 5 (TRACE-P DC-8/P3-B). (b) Time series of P3-B OPC total, accumulation mode, and coarse mode integral surface areas for the same flight. Note that none of these measurements are STP corrected.

During these comparisons, average DMA integral properties (Table 3) displayed agreement within 25% for most legs. Several comparison legs had greater discrepancies, but this was not surprising given the nonsynchronous nature of the measurement due to temperature cycling and the high-degree of variability of aerosol properties during these legs. DMA number distributions displayed agreement in sizing and concentration, both with each other and the corresponding overlap region of the OPC size distribution.

[95] OPC (C-130/P3-B) and PCASP (DC-8) accumulation mode size distributions and integral properties also revealed agreement within 25% and frequently to within 10% and tracked each other over large gradients and range of values. The average effective diameters derived from these measurements demonstrated that the instruments were sizing properly, relative to each other. Exceptions to this were for PCASP/OPC comparisons made at low altitudes where size distributions showed that the PCASP was underestimating the concentration of particles with diameters between 0.5 and 0.8 μm relative to the OPC. This may have been related to hygroscopic effects, but without a PCASP RH measurement this cannot be assessed.

[96] OPC coarse mode measurements on the C-130 were consistently higher than those made on the P3-B by ~7% to ~30%. Size distributions revealed that the differences between the two aircraft only became significant for particles with diameters greater than 2–3 μm. This is consistent with the results reported by B. Huebert et al. (Passing efficiency of a low-turbulence inlet (PELTI), final report to NSF, available from http://raf.atd.ucar.edu/Projects/PELTI/, 2000), leading us to conclude that the observed systematic differences in coarse mode OPC measurements made on the C-130 and P3-B were due to probable enhancements of larger particles by the LTI and losses in the SDI. The average effective diameters derived from the OPC coarse mode data were also shown to be in agreement with differences generally not more than 15% between the two aircraft.

[97] Results from the comparisons of FSSP coarse mode measurements between the three platforms were less clear. During the C-130/P3-B intercomparisons, the FSSP integral coarse mode surface areas from the C-130 were systematically lower than those made on the P3-B for most flight legs by ~50–70%, but data from the two instruments trended together. Two of the C-130/P3-B comparison legs showed the P3-B FSSP data to be less than the C-130 FSSP and also the two OPCs. This is not realistic, and we take this as evidence that the P3-B FSSP was not functioning properly, for unknown reasons, during these two legs.

[98] DC-8 FSSP data were not consistent with the P3-B FSSP or OPC measurements. DC-8 size distributions, integral properties, and average effective diameters all showed lower concentrations or values than P3-B data when sampling in dry air aloft that had a significant coarse dust component. DC-8 FSSP data were lower than the OPC data under these sampling conditions, and this is unrealistic. DC-8 data when sampling in the wet MBL with a higher relative concentration of sea salt exhibited much higher concentrations and integral values than the P3-B measurements. Despite this, the average effective diameters derived from the two FSSPs were in good agreement under these conditions. As in the previous case, the P3-B FSSP data appear to be consistent with the OPC coarse mode measurements after allowing for hygroscopic growth. One would have to assume unrealistic growth factors for the DC-8 data to be consistent. Currently, we do not understand this difference in DC-8 FSSP behavior (undercounting in dry dust aloft, overcounting in wet sea salt in the MBL) evident during the two DC-8/P3-B comparison flights, and we are unable to suggest a method for consistent interpretation of DC-8 FSSP performance for the remainder of the TRACE-P field campaign.

10.4. Aerosol Chemistry

[99] C-130/P3-B aerosol chemical concentrations were measured with identical PILS instruments (50% cut size of 1.3 μm), and the comparisons of chemical constituents between the two aircraft were at or near the reported uncertainty for the majority of species. Comparisons of aerosol chemical concentrations between the DC-8 bulk filter samples and the P3-B PILS showed that for the species normally associated with the coarse mode (Na^+, Ca^{2+}, Mg^{2+}, and Cl^-), the PILS data were systematically low as expected since the bulk filters collected particles for sizes less than ~6 μm while the PILS only effectively measured concentrations for aerosol diameters less than 1.3 μm. However, the PILS data were also systematically lower than the DC-8 data for the species we normally associate with the accumulation mode (SO_4^{2-}, NH_4^+, and NO_3^-) where

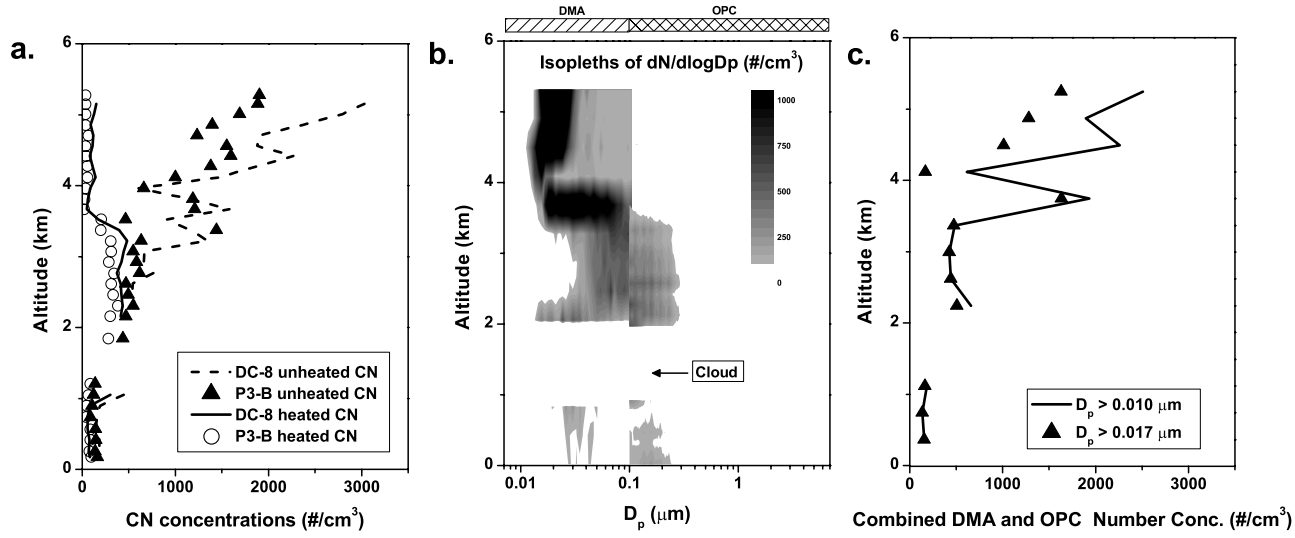

Figure 15. (a) Total and refractory CN concentrations (STP corrected) versus pressure for vertical descent profile during flight 5 (TRACE-P DC-8/P3-B). (b) Profile of the combined DMA and OPC number distributions (STP corrected). The y axis is pressure, and the x axis is aerosol diameter. The distributions are shaded to aerosol concentration (at each diameter). (c) Profile of the combined integrated DMA and OPC number distributions (STP corrected). The solid line is for the integrated number with $D_p > 0.01$ μm, and the triangles are for the integrated number with $D_p > 0.017$ μm.

we would not have expected significant differences between the two techniques. PILS sulfate concentrations agreed much better with the DC-8 MC/IC fine sulfate measurements for which the cut size was estimated to be ~2.7 μm, suggesting that the differences for these species between PILS and the filter samples were due primarily to a significant fraction of these constituents being associated with the larger aerosol. Some of this coarse sulfate and nitrate may have been associated with sea salt or dust; the presence of both was suggested by the chemistry data.

[100] To explore this possibility, we have combined the NH_4^+, SO_4^{2-}, and NO_3^- mass concentrations into a "combined" soluble mass (Figure 16). Using the STP corrected OPC volume for $D_p < 1.3$ μm that corresponds to the PILS cut size and removing the refractory component (volume remaining after heating to 350°C), we are left with the volatile fraction generally associated with sulfate, nitrate, and ammonium concentrations. Finally, we assumed a dry aerosol density of 1.8 g cm^{-3} to estimate the resulting OPC volatile mass. Figure 16a shows the P3-B and C-130 PILS combined soluble masses and the OPC volatile mass that reveal agreement between the three measurements within 15% for the entire comparison time period over an order of magnitude of values.

[101] We also calculated the DC-8 combined soluble mass (bulk filters) and its fine component (MC/IC sulfate utilized in lieu of bulk sulfate). The DC-8 and PILS combined and OPC volatile masses are plotted again in Figure 16b for comparison flight 5, and the fine data agreed to within 25% during the MBL leg (~19.0–19.5 hours). The bulk filter data were significantly higher by approximately a factor of 2, suggesting that some of these soluble components were associated with the larger aerosol present (dust and sea salt). This is further illustrated in Figure 16c, where the difference (Δmass) between the DC-8 total combined mass and the P3-B masses (OPC volatile and PILS combined) is plotted versus OPC coarse mode surface area. We could plot this quantity versus OPC coarse mode volume (directly relatable to mass) but have decided to plot versus the surface area since it is the dust surface that is the location for heterogeneous chemistry with volatile aerosol components and gases. Figure 16c has considerable scatter in the data points but does suggest that Δmass increases with coarse mode surface area. Figure 16d shows the same DC-8/P3-B Δmasses for comparison flight 2. The DC-8 fine and P3-B PILS combined masses showed agreement to within a factor of 3 for this flight, with the OPC "volatile" mass being intermediate between them. The DC-8 MC/IC fine sulfate cut size is believed to be higher than 1.3 μm and might be responsible for the DC-8 fine mass having been higher on this flight. The Δmass derived from the bulk DC-8 data and the P3-B PILS and OPC measurements are plotted against the OPC coarse mode surface area in Figure 16e and show a much stronger relationship than Figure 16c. Figures 16c and 16d support that a significant fraction of the sulfate, nitrate, and ammonium were associated with the coarse aerosol during these flights.

10.5. Aerosol Optical Properties Revisited: A Regional Perspective

[102] The comparison of aerosol scattering and absorption revealed significant differences between the DC-8 and P3-B during individual comparison flights, depending on a variety of parameters including altitude, ambient RH, and aerosol composition. Two of the three flights were remote from the primary geographical focus of the TRACE-P experiment, the marine atmosphere close to the Asian coast. In the following, we assess the performance of the DC-8 optical instruments for flights near the Asian continent.

[103] Figure 17 plots scattering (Figure 17a), absorption (Figure 17b), and ω_0 (Figure 17c) versus altitude for the P3-B/DC-8 flights closest to Asia and most affected by Asian

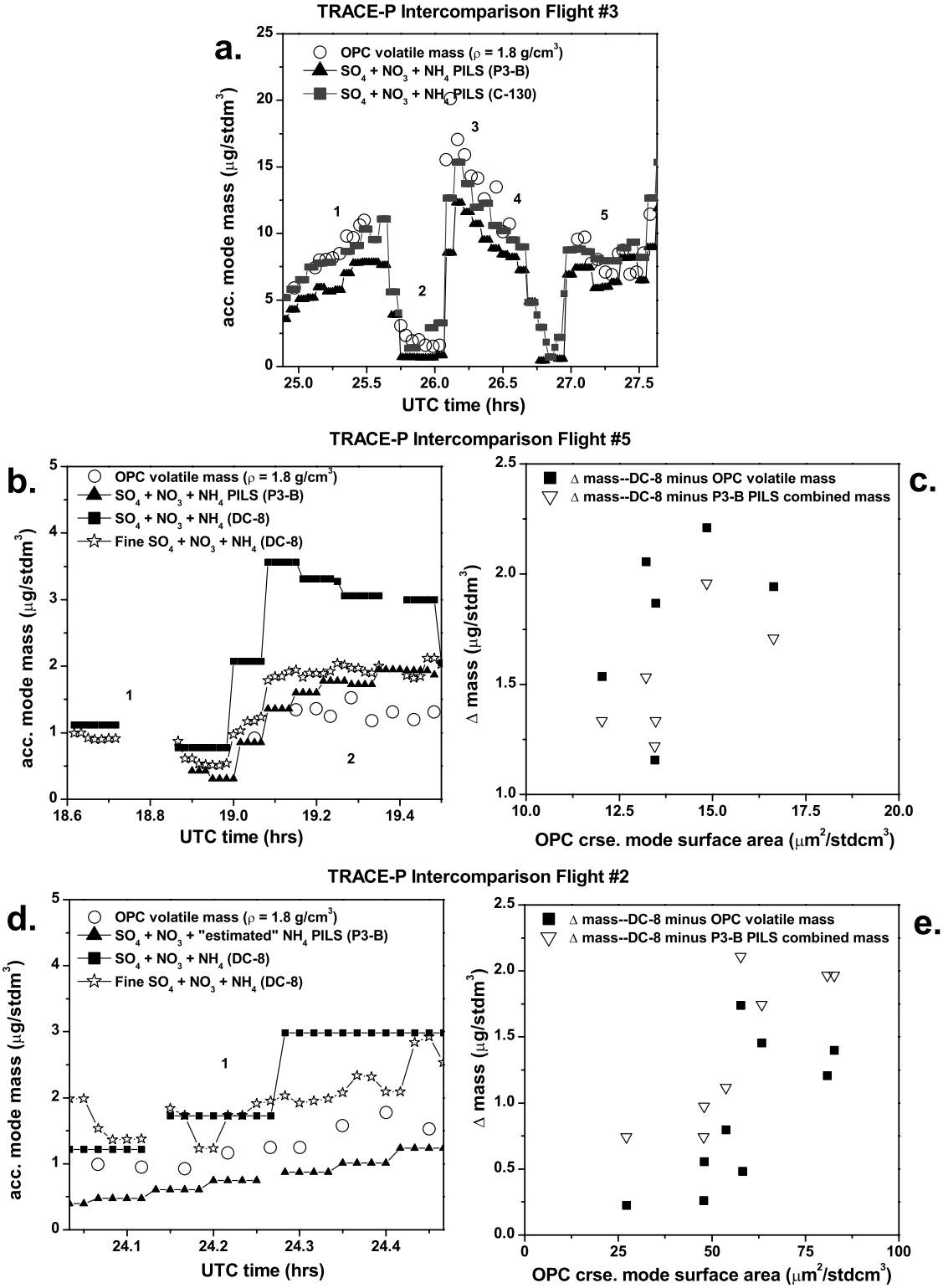

Figure 16. All data STP corrected. (a) Time series of PILS combined mass and OPC volatile mass (see text for description) for flight 3 (ACE-Asia C-130/TRACE-P P3-B). (b) Same as Figure 16a, but for flight 5 (TRACE-P DC-8/P3-B). The combined masses from the DC-8 utilizing the bulk filter data and the MC/IC fine sulfate are also shown. (c) Scatterplot of the difference between the DC-8 bulk filter combined mass and the PILS combined mass and the OPC volatile mass (Δmass) versus the OPC coarse mode surface area for the same flight as in Figure 16b. (d) Same as Figure 16b, but for flight 2 (TRACE-P DC-8/P3-B). (e) Same as Figure 16c, but for flight 2.

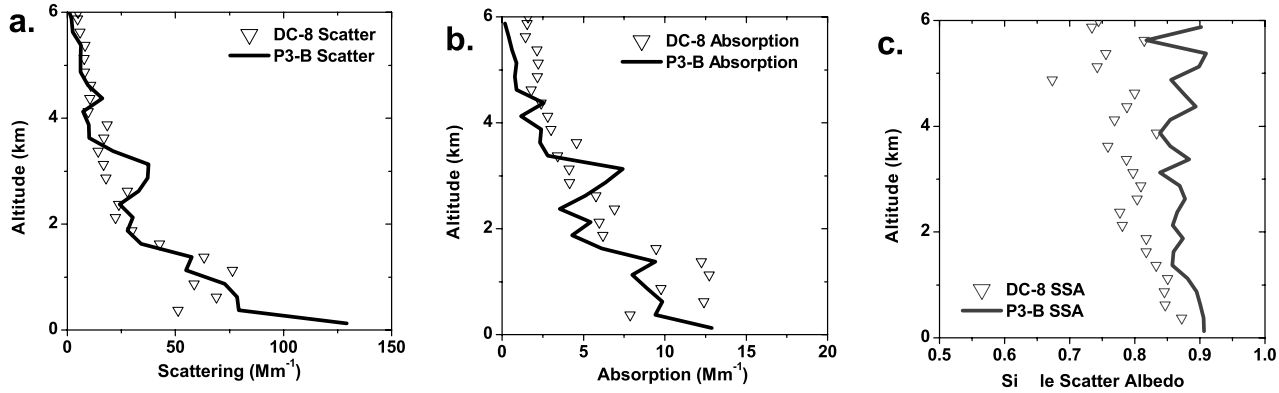

Figure 17. Vertical profiles of regional optical properties (no STP correction) measured on the DC-8 and P3-B for the intensive portion of the TRACE-P experiment near the Asian continent. (a) Vertical profile of altitude-averaged (0.25 km altitude bins) total scattering coefficients for DC-8/P3-B flights near the Asian continent below 6 km. (b) Same as Figure 17a, but for the altitude-averaged total absorption coefficients. (c) Same as Figure 17a, but for the altitude-averaged total single scatter albedo.

outflow (P3-B flights 8–19, DC-8 flights 6–17) and shows regional aerosol optical characteristics. In contrast to the MBL individual comparisons presented previously (comparison flights 1 and 5), the regional scattering profile (Figure 17a) reveals that the discrepancy between DC-8 and P3-B total scattering values was small, even at the lowest altitudes. This is probably due to the fact that near the continent, scattering values were dominated by the submicrometer component due to pollution aerosols and there was relatively less sea salt in the MBL near the continent than in the clean MBL in the central Pacific (flights 1 and 5), where supermicron and submicrometer scattering was nearly equal. From Figure 17a, it appears that for flights near Asia, the DC-8 scattering values were generally consistent with those on the P3-B.

[104] The absorption measurements (Figure 17b) on the DC-8 were systematically higher than those on the P3-B. At the highest altitudes, this difference was as much as a factor of 2. This behavior affected the derived values of ω_0 (Figure 17c). The P3-B measured ω_0 was nearly constant with altitude at $\sim$0.9, while the DC-8 ω_0 values were near 0.85 at the surface and generally decreased to $\sim$0.75 above 3 km. These low values of ω_0 were driven by the higher DC-8 absorption. The results from this comparison of aerosol optical properties suggest that the DC-8 scattering values provide representative values aloft near the continent in dry dusty conditions. For values at the lowest altitudes in wet, salty conditions, the DC-8 scattering appears to be more representative of submicrometer values. The measured DC-8 absorption coefficients (and the corresponding ω_0 and estimated BC concentrations) are problematic and should be considered qualitative, not quantitative.

11. Conclusions

[105] Five intercomparison flights were flown between the P3-B and DC-8 and C-130. These flights provided an opportunity to compare similar, simultaneous measurements made on the three aircraft. Results from these comparisons of aerosol optical properties, concentrations, size distributions and integrals, and chemical constituents were sometimes within or near the reported instrument uncertainties and other times were not. Discrepancies in the data were discussed and explained when possible.

[106] We conclude the following with confidence:

[107] 1. After allowing for the enhanced passing efficiency for the largest particles on the C-130 due to the LTI and losses in the P3-B SDI, aerosol optical properties (absorption and scattering) agreed within experimental uncertainty between the P3-B and C-130 aircraft.

[108] 2. The DC-8 scattering coefficients in the FT agree with those on the P3-B. However, in the clean MBL remote from the continents, DC-8 scattering values underestimated total scattering and appears to be related to poor inlet performance in the wet MBL in the presence of higher relative concentrations of sea salt.

[109] 3. DC-8 absorption values appeared unrealistically high for most of the comparisons with the P3-B. Resulting values of DC-8 ω_0 were too low for realistic atmospheric aerosols.

[110] 4. RCN, total CN, and UCN counters showed occasional poor instrument performance on several of the ACE-Asia/TRACE-P intercomparison legs (due to problems that were corrected after the two comparison flights). The modifications to the P3-B UCN counter [*Weber et al.*, 2003] resulted in undercounting when concentrations exceeded several thousand numbers per cubic centimeter compared to an unmodified UCN counter. The difference between cut sizes for the CN counters resulted in some discrepancies that appeared most significant at altitude in clean air with large concentrations of small particles but not for most of the experiment.

[111] 5. DMA and OPC/PCASP accumulation mode size distributions and integral properties agreed with each other within the stated uncertainties on the three platforms and accurately measured submicrometer aerosol size distributions.

[112] 6. OPC coarse mode measurements on the C-130 and P3-B produced integral properties that were within 10–20%, consistent with expected inlet performance and instrument uncertainties.

[113] 7. The PILS instrument appears to have been within stated uncertainties measuring soluble aerosol chemistry for particle sizes less than 1.3 μm. We expected small differ-

ences between the PILS (C-130/P3-B) measurements and bulk filter data (DC-8) for the aerosol normally associated with the accumulation mode (sulfate, nitrate, and ammonium), but the data presented, including OPC estimates of volatile accumulation mode mass, suggested that this difference was at least partially due to the association of some of these species with sizes larger than the PILS cut size.

[114] We also tentatively conclude the following:

[115] 8. Plots of regional optical properties showed that, when compared to the P3-B data, the DC-8 nephelometer measured total scattering more accurately near the Asian continent than over remote regions. This was probably due to the higher contribution of submicrometer to total scattering and decreased relative concentrations of wet sea salt found near the continent.

[116] 9. P3-B and C-130 FSSP measurements were consistent with each other within experimental uncertainties. DC-8 FSSP measurements appeared to overestimate concentrations in the wet MBL and underestimate concentrations in the dry FT relative to the P3-B measurements. The observed discrepancies greatly exceed the stated uncertainties.

[117] Most of the above conclusions were tested in the recently completed DC-8 Inlet Characterization Experiment (DICE, June 2003) that evaluated the SDI, DC-8 SDI, and the University of New Hampshire Inlet (NHI in Table 1) performance under a variety of conditions, including wet sea salt, dry dust, and pollution dominated air masses. For this experiment, all three inlets were flown simultaneously on the DC-8 aircraft with identical sets of instrumentation. Each instrumentation module could be switched to sample from different inlets to assess if discrepancies in measurements were due to instrumental/plumbing problems versus inlet performance. Additionally, a number of flight legs were devoted to intercomparing the DC-8 data with ground station measurements, including aerosol optical properties, CN concentrations, chemistry, and size distributions. The preliminary results of this experiment confirm the findings presented here and in the PELTI experiment, although there was no LTI during DICE. That is, all three compared inlets were found to effectively pass submicrometer aerosol and that the SDI and NHI inlets efficiently passed coarse mode aerosol, at least for the optically relevant measurements. The DC-8 SDI performed poorly during DICE, especially during the wet sea salt conditions (e.g., aerosol scattering coefficients were systematically lower). During periods of dust and/or pollution sampling, its performance was more comparable to the other inlets. During DICE, the PILS instrument did not have the 1.3 μm impactor in front of it, and the comparison of chemical concentrations of sulfate, nitrate, and ammonia between it and the bulk filter measurements were typically within the stated uncertainties, supporting the assertion that disparity between the two methods observed during the TRACE-P/ACE-Asia intercomparison flights was due to the association of these species with coarse mode particles.

[118] **Acknowledgments.** This research was sponsored by NASA's Global Tropospheric Experiment and the National Science Foundation under grants NCC-1-416 and ATM00-02070, respectively. We particularly appreciate the support of Vickie Connors, Anne Schmoltner, Jim Raper, Krista Laursen, Dick Bradford, Al Schanot, Dick Friesen, and the GTE Project Office. A special thanks is also extended to the people of the NASA Wallops Island facility, the NASA Ames facility, the NCAR JEFFCO facility, and the crews of the P3-B, DC-8, and C-130 aircraft for their repeated assistance in accommodating our needs throughout the TRACE-P and ACE-Asia experiments. We would like to thank the anonymous reviewers who have suggested many improvements. In addition, we would like to thank Steve Owens for his help with data processing issues.

References

Ackerman, A. S., O. B. Toon, D. E. Stevens, A. J. Heymsfield, V. Ramanathan, and E. J. Welton (2000), Reduction of tropical cloudiness by soot, *Science*, *288*, 1042–1047.

Anderson, T. L., et al. (1996), Performance characteristics of a high sensitivity, three-wavelength, total scatter/backscatter nephelometer, *J. Atmos. Oceanic Technol.*, *13*, 967–986.

Andreae, M. O. (1995), Climatic effects of changing atmospheric aerosol levels, in *World Survey of Climatology*, vol. 16, *Future Climates of the World*, edited by A. Henderson-Sellers, pp. 341–392, Elsevier Sci., New York.

Bates, T. S., B. J. Huebert, J. L. Gras, F. B. Griffiths, and P. A. Durkee (1998), The International Global Atmospheric Chemistry (IGAC) Project's First Aerosol Characterization Experiment (ACE 1), Overview, *J. Geophys. Res.*, *103*, 16,297–16,318.

Bond, T. C., T. L. Anderson, and D. Campbell (1999), Calibration and intercomparison of filter-based measurements of visible light absorption by aerosols, *Aerosol Sci. Technol.*, *30*, 582–600.

Charlson, R. J., and J. Heintzenberg (Eds.) (1995), *Dahlem Workshop Report on Aerosol Forcing of Climate*, 416 pp., John Wiley, Hoboken, N. J.

Charlson, R. J., J. Langner, H. Rodhe, C. B. Leovy, and S. G. Warren (1991), Perturbation of the northern hemisphere radiative balance by backscattering from anthropogenic sulfate aerosols, *Tellus, Ser. AB*, *43*, 152–163.

Chylek, P., G. Lesins, G. Videen, J. Wong, R. Pinnick, D. Ngo, and J. Klett (1996), Black carbon and absorption of solar radiation by clouds, *J. Geophys. Res.*, *101*, 23,365–23,371.

Clarke, A. D. (1991), A thermo-optic technique for in situ analysis of size-resolved aerosol physicochemistry, *Atmos. Environ.*, *25*, 635–644.

Clarke, A. D., T. Uehara, and J. N. Porter (1997), Atmospheric nuclei and related aerosol fields over the Atlantic: Clean subsiding air and continental pollution during ASTEX, *J. Geophys. Res.*, *102*, 25,281–25,292.

Clarke, A. D., W. G. Collins, P. J. Rasch, V. N. Kapustin, K. Moore, S. Howell, and H. E. Fuelberg (2001), Dust and pollution transport on global scales: Aerosol measurements and model predictions, *J. Geophys. Res.*, *106*, 32,555–32,569.

Clarke, A. D., et al. (2002), INDOEX aerosol: A comparison and summary of chemical, microphysical, and optical properties observed from land, ship, and aircraft, *J. Geophys. Res.*, *107*(D19), 8033, doi:10.1029/2001JD000572.

Clarke, A. D., et al. (2004), Size distributions and mixtures of dust and black carbon aerosol in Asian outflow: Physiochemistry and optical properties, *J. Geophys. Res.*, *109*, D15S09, doi:10.1029/2003JD004378.

Dentener, F. J., G. R. Carmichael, Y. Zhang, J. Lelieveld, and P. J. Crutzen (1996), Role of mineral aerosol as a reactive surface in the global troposphere, *J. Geophys. Res.*, *101*, 22,869–22,889.

Dibb, J. E., R. W. Talbot, E. M. Scheuer, G. Seid, M. A. Avery, and H. B. Singh (2003), Aerosol chemical composition in Asian continental outflow during the TRACE-P campaign: Comparison with PEM-West B, *J. Geophys. Res.*, *108*(D21), 8815, doi:10.1029/2002JD003111.

Dubovik, O., B. Holben, T. F. Eck, A. Smirnov, Y. J. Kaufman, M. D. King, D. Tanre, and I. Slutsker (2002), Variability of absorption and optical properties of key aerosol types observed in worldwide locations, *J. Atmos. Sci.*, *59*, 590–608.

Duce, R. A., and N. W. Tindale (1991), Atmospheric transport of iron and its deposition in the ocean, *Limnol. Oceanogr.*, *36*(8), 1715–1726.

Eisele, F. L., et al. (2003), Summary of measurement intercomparisons during TRACE-P, *J. Geophys. Res.*, *108*(D20), 8791, doi:10.1029/2002JD003167.

Fuller, K. A., W. C. Malm, and S. M. Kreidenweis (1999), Effects of mixing on extinction by carbonaceous particles, *J. Geophys. Res.*, *104*, 15,941–15,954.

Galloway, J. N., R. J. Charlson, M. O. Andreae, and H. Rodhe (Eds.) (1984), *The Biogeochemical Cycling of Sulfur and Nitrogen in the Remote Atmosphere*, *ASI Ser., Ser. C, Math. Phys. Sci.*, vol. 159. D. Riedel, Norwell, Mass.

Hagen, D. E., M. B. Trueblood, and D. R. White (1989), Hydration properties of combustion aerosols, *Aerosol Sci. Technol.*, *10*, 63–69.

Heintzenberg, J. (1982), Size segregated measurements of particulate elemental carbon and light absorption at remote Arctic locations, *Atmos. Environ.*, *16*, 2461–2469.

Hermann, M., and A. Wiedensohler (2001), Counting efficiency of condensation particle counters at low-pressures with illustrative data from the upper troposphere, *J. Aerosol Sci.*, *32*(8), 975–991.

Hoell, J., D. Davis, D. Jacob, M. Rodgers, R. Newell, H. Fuelberg, R. McNeal, J. Raper, and R. Bendura (1999), Pacific Exploratory Mission in the tropical Pacific: PEM-Tropics A, August–September 1996, *J. Geophys. Res.*, *104*, 5567–5584.

Huebert, B. J., T. Bates, P. B. Russell, G. Shi, Y. J. Kim, K. Kawamura, G. Carmichael, and T. Nakajima (2003), An overview of ACE-Asia: Strategies for quantifying the relationships between Asian aerosols and their climatic impacts, *J. Geophys. Res.*, *108*(D23), 8633, doi:10.1029/2003JD003550, [was 2002].

Jacob, D. J., J. H. Crawford, M. M. Kleb, V. S. Connors, R. J. Bendura, J. L. Raper, G. W. Sachse, J. C. Gille, L. Emmons, and C. L. Heald (2003), Transport and Chemical Evolution over the Pacific (TRACE-P) aircraft mission: Design, execution, and first results, *J. Geophys. Res.*, *108*(D20), 9000, doi:10.1029/2002JD003276.

Kaufmann, Y. J., D. Tanre, H. R. Gordon, T. Nakajima, J. Lenoble, R. Frouin, H. Grassl, B. M. Herman, M. D. King, and P. M. Teillet (1997), Passive remote sensing of tropospheric aerosol and atmospheric correction for the aerosol effect, *J. Geophys. Res.*, *102*, 16,815–16,830.

Lee, Y.-N., et al. (2003), Airborne measurement of inorganic ionic components of fine aerosol particles using the particle-into-liquid sampler coupled to ion chromatography technique during ACE-Asia and TRACE-P, *J. Geophys. Res.*, *108*(D23), 8646, doi:10.1029/2002JD003265.

McNeal, R. J., D. J. Jacob, D. D. Davis, and S. C. Liu (1998), The NASA Global Tropospheric Experiment: Recent accomplishments and future plans, *IGACtivities Newsl.*, *13*, 2–18.

Merrill, J. T. (1989), Atmospheric long range transport to the Pacific Ocean, *Chem. Oceanogr.*, *10*, 15–50.

Moore, K. G., II, A. D. Clarke, V. N. Kapustin, and S. G. Howell (2003), Long-range transport of continental plumes over the Pacific Basin: Aerosol physiochemistry and optical properties during PEM-Tropics A and B, *J. Geophys. Res.*, *108*(D2), 8236, doi:10.1029/2001JD001451.

Orsini, D. A., Y. L. Ma, A. Sullivan, B. Sierau, K. Baumann, and R. J. Weber (2003), Refinements to the particle-into-liquid sampler (PILS) for ground and airborne measurements of water soluble aerosol composition, *Atmos. Environ.*, *37*(9–10), 1243–1259.

Penner, J. E., R. E. Dickinson, and C. A. O'Neill (1992), Effects of aerosol from biomass burning on the global radiation budget, *Science*, *256*, 1432–1434.

Reid, J. S., et al. (2003), Comparison of size and morphological measurements of coarse mode dust particles from Africa, *J. Geophys. Res.*, *108*(D19), 8593, doi:10.1029/2002JD002485.

Rosenfeld, D. (1999), TRMM Observed first direct evidence of smoke from forest fires inhibiting rainfall, *Science*, *26*, 3105–3108.

Russell, P. B., et al. (2002), Comparison of aerosol single scattering albedos derived by diverse techniques in two North Atlantic experiments, *J. Atmos. Sci.*, *59*, 609–619.

Smith, M. H., and C. D. O'Dowd (1996), Observations of accumulation mode aerosol composition and soot carbon concentrations by means of a high-temperature volatility technique, *J. Geophys. Res.*, *101*, 19,583–19,591.

Tang, I. N., and R. H. Munkelwitz (1993), Composition and temperature dependence of the deliquescence properties of hygroscopic aerosols, *Atmos. Environ., Part A*, *27*, 467–473.

Twomey, S., M. Piepgrass, and T. L. Wolfe (1984), An assessment of the impact of pollution on global cloud albedo, *Tellus, Ser. B.*, *36*, 356–366.

Weber, R. J., P. H. McMurry, T. S. Bates, D. S. Covert, F. J. Brechtel, and G. L. Kok (1999), Intercomparison of airborne and surface-based measurements of condensation nuclei in the remote marine troposphere measured during ACE 1, *J. Geophys. Res.*, *104*, 21,673–21,683.

Weber, R. J., D. Orsini, Y. Daun, Y.-N. Lee, P. Klotz, and F. Brechtel (2001), A particle-into-liquid collector for rapid measurements of aerosol chemical composition, *Aerosol Sci. Technol.*, *35*, 718–727.

Weber, R. J., et al. (2003), New particle formation in anthropogenic plumes advecting from Asia observed during TRACE-P, *J. Geophys. Res.*, *108*(D21), 8814, doi:10.1029/2002JD003112.

Zhang, S. H., Y. Akutsu, L. M. Russel, R. C. Flagan, and J. H. Seinfeld (1995), Radial Differential Mobility Analyzer, *Aerosol Sci. Technol.*, *23*, 357–371.

B. E. Anderson, Chemistry and Dynamics Branch, Atmospheric Sciences Division, Langley Research Center, NASA, Hampton, VA 23681, USA. (b.e.anderson@larc.nasa.gov)

T. Anderson, D. Covert, and S. Doherty, Department of Atmospheric Sciences, University of Washington, Seattle, WA 98195-1640, USA. (tadand@atmos.washington.edu; dcovert@u.washington.edu; sarahd@atmos.washington.edu)

A. D. Clarke, V. N. Kapustin, C. McNaughton, and K. G. Moore II, School of Ocean and Earth Science and Technology, 1000 Pope Road, University of Hawaii at Manoa, Honolulu, HI 96822, USA. (tclarke@soest.hawaii.edu; kapustin@soest.hawaii.edu; cameronm@soest.hawaii.edu; kmoore@soest.hawaii.edu)

J. Dibb and R. Talbot, Institute for the Study of Earth, Oceans, and Space, Morse Hall, University of New Hampshire, Durham, NH 03824, USA. (jack.dibb@unh.edu; robert.talbot@unh.edu)

Y.-N. Lee, Environmental Sciences Department, Brookhaven National Laboratory, Upton, NY 11973, USA. (ynlee@bnl.gov)

Y. Ma and R. Weber, School of the Earth and Atmospheric Sciences, Georgia Institute of Technology, 221 Boddy Dodd Way, Atlanta, GA 30332, USA. (yma@eas.gatech.edu; rweber@eas.gatech.edu)

D. Rogers, NCAR/RAF, 10802 Airport Ct., Broomfield, CO 80021, USA. (dcrogers@ucar.edu)

E. L. Winstead, GATS, Inc., NASA Langley Research Center, MS 483, Hampton, VA 23681, USA. (e.l.winstead@larc.nasa.gov)